الجمهورية الجزائرية الديمقراطية الشعبية

République Algérienne Démocratique et Populaire

Ministère de L'Enseignement Supérieur et de la Recherche Scientifique

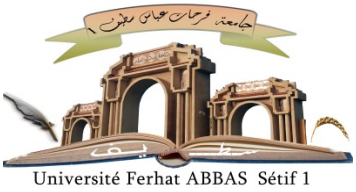

UNIVERSITÉ FERHAT ABBAS - SETIF1

FACULTÉ DE TECHNOLOGIE

THÈSE

Présentée au Département de Electronique

Pour l'obtention du diplôme de

DOCTORAT

Domaine : Sciences et Technologie

Filière : Electronique

Option : Electronique et Commande Industrielle

Par

Gherouat Oussama

THÈME

Commande robuste d'un système industriel

Soutenue le ……./……./…… devant le Jury:

ZEGADI Ameur	**Professeur**	**Univ. Ferhat Abbas Sétif 1**	**Président**
HASSAM Abdelouahab	**Professeur**	**Univ. Ferhat Abbas Sétif 1**	**Directeur de thèse**
KHEMLICHE Mabrouk	**Professeur**	**Univ. Ferhat Abbas Sétif 1**	**Examinateur**
BERRAH Smail	**Professeur**	**Univ . Béjaia**	**Examinateur**

Acknowledgements

Acknowledgements:

I thank Allah, the Almighty, the Merciful, for having taught me what I did not know, for having given me the health and everything I needed for the accomplishment of this doctoral thesis.

My thanks and appreciation to my thesis supervisor **Prof. Hassam Abdelouahab** for the guidance, encouragement and the advice provided throughout this yaers.

I would like to thank the members of the thesis jury:

Prof. ZEGADI Ameur from university of **Ferhat Abbas Setif 1.**

Prof. KHEMLICHE Mabrouk from university of **Ferhat Abbas Setif 1.**

Prof. BERRAH Smail from university of **Bejaia.**

Last but not least, my thanks and appreciation to **Prof. Fateh Krim** director of **L**aboratory **P**ower **E**lectronics and **I**ndustrial **C**ontrol **L**aboratory (**LEPCI**), Department of electronics, University of Setif-1, which allowed me to conduct experiments and provide all the equipment.

Dedications

Dedications:

This work is entirely dedicated to my respectful parents and brothers (**Walid, Okba, Ahmed**) whose constant support this thesis paper was not possible. They always inspire me at the same time, I also thank my caring friends Dr. **O.Aissa,** Dr**. B.Babes,** Dr**. K.Medani,** Dr**. F.Amrane ,** Dr**. H.Froura ,** Dr**. D .Matoug, F.Serdok** and **M.Felahi , I.BOURASSE** whose supported me in this thesis.

Gherouat Oussama

Abstract

Abstract:

The main objective of this thesis is to design a novel robust controller based on Artificial intelligence to improve the stability and robustness of system against matching disturbation and uncertainties. **SC-PSO** a **S**ynergetic **C**ontrol (**SC**) based on **P**article **S**warm **O**ptimization **(PSO)** algorithm is being presented to ensure the robustness of industrial systems. The **PSO** technique has been exploited to adjust the **SC** parameters.

This novel controller has been used for the first time to control the following two systems: one an **U**nmanned **A**erial **V**ehicle (**UAV**) Quadrotor for trajectory tracking which has a Six-**D**egree-**O**f-**F**reedom (6-**DOF**) and need six controllers for full control, the second is the **S**ingle-**P**hase **S**hunt **A**ctive **P**ower **F**ilter (**SP-SAPF**) to improv the power quality (**THD**<5% respect the IEEE519 Standard).

Although this proposed **SC-PSO** approach has not been previously applied for the quadrotor and the **SP-SAPF**, but it showed good robust characteristics similar to **S**liding **M**ode **C**ontrol (**SMC**) theory and without introducing steady state chattering effect which can cause wear and tear in actuating system, giving a significant advantage over conventional controller [**P**roportional **I**ntegrative **D**erivative (**PID**), **Hy**steresis **C**ontroller (**HC** or **HY**), **SMC**]

This thesis apparatus consists essentially of two parts: In section one, using MATLAB/Simulink® environment; a comparative study based on three control techniques: PID, SMC and SC-PSO, is proposed to illustrate the behaviors of the controllers against work hard conditions. The obtained results demonstrate the high performances of the quadrotor based on the **SC-PSO** controller in transient and steady states, a **H**ardware-**I**n-the-**L**oop (**HIL**)Real-Time testing method was used to prove results of the proposed technique SC-PSO. The teste has been proved by two **PC (MATLAB/Simulink® environment)** and two **dSPACE 1104 card** for several operating conditions. In the second section, a comparative study based on **HC**, **SMC** and **SC** controllers to demonstrate the outstanding performance of **SC-PSO** for single-phase active power filter (current control). The effectiveness of the suggested SC-PSO approach has been proved by simulation and finally real time experimental tests executed successfully using **PC (MATLAB/Simulink® environment)**, **dSPACE 1104 card** and electrical elements for several operating conditions.

Table of Contents

Table of contents:

List of Figures

List of figures:

List of Tables

List of tables :

General Introduction

0.1 Brief review:

The pace of development and adoption of new technologies in the industry has accelerated in recent decades. At 2020, the market size for industrial automation and control system worldwide was estimated at 146.79 billion USD. It is expected to expand from 2021-2028 at a **C**ompound **A**nnual **G**rowth **R**ate (**CAGR**) of 8.90% [1], thus this increase will affect the global distributed energy generation market size, this market was valued in 2019 at 242.6 billion USD and is expected to expand at a **CAGR** of 11.50% from 2020-2027 [2].

The COVID-19[1] crisis has changed the way companies operate in all sectors and regions. So that the number of jobs has been reduced to the maximum in order to achieve physical distancing, to avoid transmission of the virus, which prompted the world to use many Automatics machines (robot, drone, unmanned vehicles … etc.) [3].

In the same context, automation (control system) is an essential part of the industrial field, because industrial systems need a robust controller to operate smoothly and make production processes easier as well as saving time and money for factory owners. It is an inter-disciplinary field of engineering and mathematics that focuses on the behavior of dynamic systems. One of the main goals of the automation engineer is to design a system, called a controller, which is able to control a physical system (also called a physical process), in other words, to influence it so that it behaves in a certain way. The

[1] *COVID-19: COronaVIrus Disease appeared in 2019. Disease caused by the coronavirus SARS-CoV-2.*

idea is to obtain auto-regulated processes that require a minimum of human intervention to function [4].

In practice, the automation engineer is faced with two problems:

• The problem of evaluating whether a corrector ensures the desired behavior of the system: this is the analysis problem.

• The problem of designing a corrector ensuring the desired behavior of the system: this is the synthesis problem.

To solve these problems for a given system and properties, engineers use generic methods developed by scientists. The conventional control laws give good results in the case of linear systems with fixed parameters. Unlike systems that are non-linear or have non-stationary parameters, the results of these classical control laws can be unsatisfactory because they are not robust, especially when the requirements for accuracy and other dynamic properties of the system are stringent. It is necessary to demand control laws which are insensitive to changes in parameters for disturbances and non-linearities. Robust control solutions like the Backstepping method [5], robust **Linear** **M**atrix **I**nequality (**LMI)** switched controllers [6-7], **S**liding **M**ode **C**ontrol (**SMC**) [8-9] have been illustrated and designed to control such systems.

However, there are severe difficulties in the design of the **SMC** with respect to: (i) the vector synthesis procedure; (ii) chattering reducing or elimination problem and (iii) the closed-loop stability analysis. To overcome these difficulties, Professor A.A. Kolesnikov developed a new technique of control called **S**ynergistic **C**ontrol (**SC**) [10], it's technique solution for nonlinear uncertain systems. Indeed, **SC** is well known for its robustness against perturbations and uncertainties.

The principle of the synergistic control strategy is similar to the principle of **SMC** but it is devoid of the chattering problem. This robust approach is based on the concept of forcing a system under control to operate according to a preselected designer constraint. Based on a continuous control law and a macro-variable that can be a simple combination of state variables, synergistic control is more suitable to a real-time implementation. The main benefit of this approach is that once system states reach the attractor, the system dynamics remain insensitive to a class of parameter variation and external disturbances [11-12]. Thanks to the high performance of the synergistic control technique, several research articles were published in the literature. However, in much

of this research, the synergistic control law was designed on an asymptotic stability analysis where the trajectories of the studied system evolve towards a specified attractor reaching equilibrium in an infinite time [12-13].

The recently introduced synergistic control has been widely accepted by the control community as well as by the industrialists. The success of its implementation has been proven in several areas such as: the battery charging system [14].) have used the synergetic approach for the local control of the power converters; the flexible satellites with a desired attitude achievement have been presented in [15]; the output voltage control of the DC/DC buck converter system with an approximation of the unknown parameters has been studied by [16-17]; the speed control of the PMDC motor has been proposed [18]; the hydraulic turbine regulating system with a stable frequency for small and medium-size power stations has been treated by [19] present the design of Synergetic control theory scheme for asynchronous generator based dual-rotor wind power [20] presents a fast and accurate frequency tracking method for ultrasonic cutting system via the synergetic control of phase and current.

0.2 Thesis motivation:

This thesis consists of two main parts, which discuss both the control of aircraft and power filter system as follows:

- **Part one: Quadrotor**

The global commercial drone market size was valued at USD 13.44 billion in 2020. It is expected to expand at a compound annual growth rate (CAGR) of 57.5% from 2021 to 2028. In terms of volume, the demand was recorded at 689.4 thousand units in 2020 [21].

The drone is one of Emerging Technologies for Battling Covid-19 [22] ready to take to the skies to provide help. Some are able to quickly delivering essential, notify medical professionals to attend to those at risk, while energy companies use it to decrease the risk of serious injury or death [23] and to prevent outages electrical energy because Holding the power on is a dangerous business

The drone type quadrotor is an aircraft that has certain advantages compared to conventional helicopters. Because of its symmetry, this vehicle is dynamically sleek, easy

to model and build. Despite these advantages, the quadrotor is classified as one of the most complex flying systems since it is underactuated and highly nonlinear. This complexity induces a great difficulty in the design of the control.

The quadrotor has two sets of identical propellers powered by DC brushless motors to provide the necessary thrust and perform maneuvers while in flight. The quadrotor has the advantages of a lightweight configuration and inherent instability, which improves its maneuverability in flight compared to fixed-wing drones. Most importantly, quadrotors have the ability to perform VTOL and hover in mid-air.

We often have to generate trajectories to allow a drone to move from an initial state to a final state. Trajectory tracking is a subject that is often dealt with. There are many different algorithms to perform such a process as **PID** [24] and sliding mode control [25], **LQR** controller [26], **H1** [27]. The authors in [28-29] have developed controllers based on the linear dynamics model and neglected inherent nonlinearity of attitude dynamics. The synergetic control it is efficient for handling systems with large uncertainties, time-varying properties, and nonlinearities [30].

- **Part two: Shunt Active Power Filter (SAPF)**

This crisis caused a disturbation in power quality (Harmonic currents) which would, in turn, create a systemwide blackout, this effect due to massive use of nonlinear loads connected to the distribution system [31], examples of non-linear loads include transistors, electrical motors, variable speed drives and the non-ideal transformer [32].

According to the publisher's latest market study on “Power Quality Equipment Market Forecast to 2028 - COVID-19 Impact and Global Analysis - by Equipment, Phase, and End User,” the market is expected to reach US$ 45,531.9 million by 2028 from US$ 28,499.6 million in 2021; it is estimated to grow at a **CAGR** of 6.8% from 2021 to 2028 [33].

Harmonic currents have adverse consequences for the proper functioning of electrical devices and have immediate and long-term effects. It is therefore important for a given facility to know how to identify, analyze and measure harmonics, and given the seriousness of the problems caused by propagation of harmonics, research has focused on developing techniques to reduce these disturbances. Therefore, several solutions exist and others are still being tested. Use of filtering devices this solution consists of installing a filter between the nonlinear load and the electrical network in order to filter the

harmonics generated by the nonlinear load globally or by selective action, we will present three filter structures, which they are the passive filter, active filter and the hybrid filter which combines the active filter with the passive filter [34].

Nowadays, **S**ingle-**P**hase **P**ulse **W**idth **M**odulation (**SP-PWM**) inverter-based **S**hunt **A**ctive **P**ower **F**ilter (**SAPF**) plays a vitally important role to generate the required harmonic components to minimize harmonic distortion currents and compensate reactive power in low or medium voltage distribution networks [35]. **S**ingle-**P**hase **S**hunt **A**ctive **P**ower **F**ilter **SAPF** (**SP-SAPF**) is characterized by simple control design, small size, high energy efficiency, stable output voltage, improved safety, energy security and great ability to adapt with various forms of linear and non-linear loads. Moreover, the standard SP-SAPFs do not need high-voltage components that are typically required in specially designed three-phase **SAPFs** [36-37].

These **SAPF** systems can be used not only as **S**tatic **V**ar **G**enerator**s** (**SVGs**) to stabilize and improve the voltage profile in power systems, but also to compensate the harmonic contents, reactive power and unbalanced load current with a fast-dynamic behavior and flexibility during load variations [38-40]. One of the key factors for the establishment of the **SP-SAPF** system is the control mechanism. Faced with the variability over time of **SP-SAPF** systems, conventional deterministic strategies are not sufficiently resistant to ensure better performance required at the same time in the dynamic and permanent conditions [41], the control of the DC link voltage and the harmonic current of **SP-SAPF**, voltage and current controllers of the **P**roportional-**I**ntegral (**PI**) type have been used. However, this kind of controller requires exact linear mathematical model of the **SP-SAPF** system, hardly achievable under nonlinearity, parameter variations, and load disturbances [42-43].

Hysteresis controllers have been introduced in the published works and generated a great deal of interest [44] in **SP-SAPF** applications [45-46]. This type of controllers provides over-current protection capability for versatility and simplicity of practical implementation. To validate practically the hysteresis controller, the digital signal processor guarantees a good and fast dynamic response compared to other types of digital controllers [47]. Despite the excellent performance of the hysteresis controller, the latter suffers from the problem of the switching frequency which is variable and high. This phenomenon increases power losses and produces severe **E**lectro-Magnetic

Compatibility (**EMC**) noise in the single-phase APF and also complicates the selection of the coupling inductor in hysteresis current controllers [48].

To fix the switching frequency of **SP-SAPF** system, in [49] the authors have proposed an adaptive feed-forward control scheme that varied the hysteresis band in the hysteresis modulator in the event of any change of the current error. The adaptive hysteresis modulator is an efficient method for adjusting the switching frequency. The disadvantage of this modulator lies in the extra input voltage feedback which can lead to an increase in the total cost and the complexity of the employed control system. For these reasons, the adaptive hysteresis modulator is not suitable for **SP-SAPF** system. In their turn, [50] the authors have limited the switching frequency of **SP-SAPF** with calculation of any time interval while maintaining the switching action.

The **F**inite **C**ontrol **S**et **M**odel **P**redictive **C**ontrol (**FCS-MPC**) scheme is suggested in [51] for the harmonic current regulation of the SAPF system. The natural switching action of SP-SAPF is compatible with FCS-MPC feature. This strategy is well recognized for its stability, robustness, fast dynamic reaction, and good regulation properties in a wide range of operating conditions.

Furthermore, this method does not require the use of internal current loops, **P**ulse **W**idth **M**odulation (**PWM)** or **S**pace-**V**ector **P**ulse **w**idth **M**odulation (**SVPWM)** for the control of the single phase **APF**. According to the **FCS-MPC** theory, the main objective of the **SAPF** control is to predict the behavior of this system for all admissible switching states over the prediction horizon in order to solve the optimization problem and guarantee the filter current regulation with low **T**otal **H**armonic **D**istortion (**THD)** in different conditions. However, this control technique is more effective than the hysteresis controllers but its performances are dependent of the accurate prediction of the future behavior of the **SAPF** system [52]. Using incorrect parameters for the predictive controller may result in an inaccurate prediction of future behavior due to the incorrect system model. This situation can lead to the incorrect choice of switching states resulting in a deterioration of the performance of the applied control, even endangering the stability of the system. Building an exact system model with precise parameters is thus important to avoid these serious anomalies. To estimate the uncertain parameters, an FCS-MPC current control with model parameter mismatch and a fuzzy adaptive control law have been proposed for the governance of the SAPF system in [53-54].

0.3 The main objectives and contributions:

The main objective of this thesis is to design a robust controller to improve the stability and robustness of industrial systems against matching disturbances and uncertainties. To ensure the robustness of the controller, the proposed approach was tested on two different industrial systems as follows:

- **U**nmanned **A**erial **V**ehicle (**UAV**) Quadrotor.
- **S**ingle-**P**hase **S**hunt **A**ctive **P**ower **F**ilter (**SP-SAPF**).

Non-linearity, variable coupling and the parametric uncertainties and external disturbances of our industrial systems are the major challenges faced in this study. Therefore, our approach is being to be proposed in order to overcome these obstacles.

The core contributions of this thesis are as follow:

- Original research work based on a comparative study using conventional controllers such as: **PID**: **P**roportional-**I**ntegral-**D**erivate, **SMC**: **S**liding **M**ode **C**ontrol) for or **UAV** system in order to enhance the drone's tracking path.
- Original research work based on **H**ysteresis **C**ontroller (**HC**) and **S**liding **M**ode **C**ontroller (**SMC**) is applied for **SP-SAPF** system to improve the power quality (**THD**<5% respect the IEEE519 Standard).
- **S**ynergetic **C**ontrol (**SC**) technique has been applied for the both systems.
- Application of the **A**rtificial **I**ntelligence **(AI)** algorithm based on **P**article **S**warm **O**ptimization (**PSO**) has been proposed to adjust the various parameters of **SC** technique.
- Experimental validation for **SC-PSO** technique under **MATLAB/Simulink®** environment based on **H**ardware-**I**n-the-**L**oop (**HIL**)Real-Time testing method has been applied for the quadrotor, using two **dSPACE 1104** cards for many hard-operating conditions.
- Experimental investigation of the suggested **SC-PSO** approach under **MATLAB/Simulink®** environment for **SP-SAPF** using **dSPACE 1104** card for several operating conditions.

0.4 Thesis structure:

After a general introduction to the undertaken work, the main body of the thesis is structured as follows:

In the **first chapter**, some of the basic notions of the **SMC**, **SC** theories, and **PSO** algorithm are given.

The **second chapter** focuses on modeling of a quadrotor-type autonomous aircraft. A set of nonlinear equations representing the motion of the quadcopter vehicle are extracted.

In the **third chapter**, different control techniques namely **PID**, **SMC** and **SC-PSO** have been applied for a quadrotor, in order to improve accuracy tracking performance in the fully actuated subsystem, and under-actuated subsystem against difficult path. The obtained results of the suggested **SC-PSO** algorithm guarantee all system state variables converge to their desired values (trajectory tracking) in short time and demonstrate the high performances of **UAV** in transient and steady states. The **HIL** Real-Time testing method was used to prove the high robustness of the proposed technique **SC-PSO**.

In the **fourth chapter**, a brief introduction of power quality problems has been presented in the first part. Then, the second part is devoted a general presentation of power quality mitigation problems. Moreover, a literature research study is proposed for the **SP-SAPF** Control in the third part.

In the **fifth chapter**, several control techniques: **HC**, **SMC**, **SC**, and **SC-PSO** have been applied for the **SP-SAPF**. In the first part, a comparative study is presented to show the system behavior in transient and steady states. In the second part, **PSO** algorithm is proposed for the variables tuning of the **SC**. In the third part, to give more practical aspect to our research work, the suggested **SC-PSO** approach has been experimentally proved under **dSPACE1104** card.

0.5 Scientific production:

0.5.1 Scientific Articles

- **GHEROUAT, O.**, HASSAM, A., AISSA, O., *et al.* Experimental evaluation of single-phase shunt active power filter based on optimized synergetic control strategy for power quality enhancement. *J. Européen Systèmes Automatisés*, 2021, vol. 54, no 4, p. 649-659.
  Doi: 10.18280/jesa.540415
- AISSA, Oualid, **GHEROUAT, Oussama**, BABES, Badreddine, et al. Experimental validation of advanced SP-SAF based on intelligent controllers for power quality enhancement. Energy Reports, 2022, vol. 8, p. 3018-3029.
  Doi: 10.1016/j.egyr.2022.02.067

- MATOUK, Djihad, ABDESSEMED, Foudil, **GHEROUAT, Oussama**, et al. Second-order sliding mode for Position and Attitude tracking control of Quadcopter UAV: Super-Twisting Algorithm. In : International Journal of Innovative Computing, Information and Control ICIC 2020. 2020.

  Doi: 10.24507/ijicic.16.01.29

- **GHEROUAT, O.**, MATOUK, D., HASSAM, A., et al. Sliding mode control for a quadrotor unmanned aerial vehicle. Journal of Automation & System Engineering, 2007, vol. 10, no 3, p. 150-157.

  Doi :10.5281/zenodo.6369884

0.5.2 Conference papers

- **IEEE** , 8th International Conference on Modelling, Identification and Control (ICMIC), 2016 (Quadrotor position and attitude control via backstepping approach).
- **IEEE** , 2 International Conference On Electrical Sciences and Technologies October 26th - 28th, 2016 Marrakesh , Morocco (**Combined Backstepping and Enhanced PD Control Design for Position and Attitude Stabilization of an UAV Quadrotor**) .
- International Conference on Technological Advances in Electrical Engineering (ICTAEE'16.), October 2016 , Skikda , Algeria (**Robust Control of a Quadrotor Unmanned Aerial Vehicle**).
- NCEEE'16 : National Conference on Electronics and Electrical engineering, Bouira, Algeria. Sliding Mode Control for a Quadrotor Unmanned Aerial Vehicle

0.5.3 Book chapter

- Type-2 Fuzzy Logic Control for Quadrotor, Chapter 5, Advances in Engineering Research. Volume 30 , ISBN: 978-1-53616-092-5

Reference:

[1] Industrial Automation And Control Systems Market Size, Share & Trends Analysis Report By Component (Industrial Robots, Control Valves), By Control System (DCS, PLC, SCADA), By Vertical, By Region, And Segment Forecasts, 2021 – 2028 https://www.grandviewresearch.com/industry-analysis/industrial-automation-market.

[2] Distributed Energy Generation Market Size, Share & Trends Analysis Report By Application (Residential, Commercial & Industrial), By Technology (Fuel Cells, Solar PV), By Region, And Segment Forecasts, 2020 – 2027 https://www.grandviewresearch.com/industry-analysis/distributed-energy-generation-industry.

[3] https://blogs.worldbank.org/developmenttalk/how-did-covid-19-pandemic-influence-pace-new-business-formation

[4] Cederfeldt, Mikael. Planning Design Automation Systems: Criteria and Guidelines. Diss. Chalmers tekniska högskola, 2005. T. Madani and A. Benallegue, "Backstepping control for a quadrotor helicopter," in 2006 IEEE/RSJ International Conference on Intelligent Robots and Systems, pp. 3255–3260, IEEE, 2006. 14.

[5] D. Jabri, K. Guelton, N. Manamanni, A. Jaadari, and C.-D. Chinh, "Robust stabilization of nonlinear systems based on a switched fuzzy control law," vol. 14, no. 2, pp. 40–49, 2012. 14.

[6] B. Mansouri, N. Manamanni, K. Guelton, and M. Djemai, "Robust pole placement controller".

[7] Y. Shtessel, C. Edwards, L. Fridman, and A. Levant, Sliding mode control and observation. Springer, New York, USA, 2014. 14, 20.

[8] UTKIN, Vadim I. Sliding modes in control and optimization. Springer Science & Business Media, 2013.

[9] KOLESNIKOV, Anatoly A. et KUZMENKO, Andrew A. Synergetic synthesis of nonlinear interconnected control for turbogenerators. Citeseer, 2001.

[10] BOUCHAMA, Z., ESSOUNBOULI, Najib, HARMAS, M. N., et al. Reaching phase free adaptive fuzzy synergetic power system stabilizer. International Journal of Electrical Power & Energy Systems, 2016, vol. 77, p. 43-49.

[11] ZERROUG, Nadjat, HARMAS, Mohamed Naguib, BENAGGOUNE, Saïd, et al. DSP-based implementation of fast terminal synergetic control for a DC–DC Buck converter. Journal of the Franklin Institute, 2018, vol. 355, no 5, p. 2329-2343.

[12] ZHAO, Ping, YAO, Wei, WEN, Jinyu, et al. Improved synergetic excitation control for transient stability enhancement and voltage regulation of power systems. International Journal of Electrical Power & Energy Systems, 2015, vol. 68, p. 44-51.

[13] Eghtedarpour, N. (2019). A synergetic control architecture for the integration of photovoltaic generation and battery energy storage in DC microgrids. Sustainable Energy, Grids and Networks, 20, 100250. https://doi.org/10.1016/j.segan.2019.100250.

[14] Sabatini, M., Palmerini, G. B., & Gasbarri, P. (2020). Synergetic approach in attitude control of very flexible satellites by means of thrusters and PZT devices. Aerospace Science and Technology, 96, 105541. https://doi.org/10.1016/j.ast.2019.10554.

[15] Babes, B., Boutaghane, A., Hamouda, N., Mezaache, M., & Kahla, S. (2019, November). A robust adaptive fuzzy fast terminal synergetic voltage control scheme for DC/DC buck converter. 2019 International Conference on Advanced Electrical Engineering (ICAEE).https://doi.org/10.1109/icaee47123.2019.9014717.

[16] Hamouda, N., & Babes, B. (2020). A DC/DC buck converter voltage regulation using an adaptive fuzzy fast terminal synergetic control. In Lecture Notes in Electrical Engineering (pp. 711–721). Springer Singapore. https://doi.org/10.1007/978-981-15-6403-1_48.

[17] Hamouda, N., Babes, B., & Boutaghane, A. (2020). design and analysis of robust nonlinear synergetic controller for a PMDC motor driven wire-feeder system (WFS). In Lecture Notes in Electrical Engineering (pp. 373–387). Springer Singapore. https://doi.org/10.1007/978-981-15-6403-1_26

[18] Huang, S., Xiong, L., Wang, J., Li, P., Wang, Z., & Ma, M. (2020). Fixed-time synergetic controller for stabilization of hydraulic turbine regulating system. Renewable Energy, 157, 1233–1242. https://doi.org/10.1016/j.renene.2020.05.071.

[19] J. Zhang, K. Ma, J. Wang, P. Feng and S. Ahmad, "A Fast and Accurate Frequency Tracking Method for Ultrasonic Cutting System via the Synergetic Control of Phase and Current," in IEEE Transactions on Ultrasonics, Ferroelectrics, and Frequency Control, vol. 69, no. 2, pp. 902-910, Feb. 2022, doi: 10.1109/TUFFC.2021.3137391.

[20] Commercial Drone Market Size, Share & Trends Analysis Report By Product (Fixed-wing, Rotary Blade, Hybrid), By Application, By End-use, By Region, And Segment Forecasts, 2021 - 2028 AL-TURJMAN, Fadi, DEVI, Ajantha, et NAYYAR, Anand. Emerging Technologies for Battling Covid-19. Studies in Systems, Decision and Control, vol. 324. 2021. https://www.grandviewresearch.com/industry-analysis/global-commercial-drones-market

[21] JOHNSEN, S. O., BAKKEN, T., TRANSETH, A. A., et al. Safety and security of drones in the oil and gas industry. In : Proceedings of the 30th European Safety and Reliability Conference and the 15th Probabilistic Safety Assessment and Management Conference, ESREL2020-PSAM15 Organizers, Singapore. 2020.

[22] LI, Jun et LI, Yuntang. Dynamic analysis and PID control for a quadrotor. In : 2011 IEEE International Conference on Mechatronics and Automation. IEEE, 2011. p. 573-578.

[23] GHEROUAT, O., MATOUK, D., HASSAM, A., et al. Sliding mode control for a quadrotor unmanned aerial vehicle. Journal of Automation & System Engineering, 2016, vol. 10, no 3, p. 150-157.

[24] GHAFFAR, Alia Abdul et RICHARDSON, Tom. Model reference adaptive control and LQR control for quadrotor with parametric uncertainties. International Journal of Mechanical and Mechatronics Engineering, 2015, vol. 9, no 2, p. 244-250.

[25] P. Chen and J. Luo, Modeling and H1 of quadrotor and design of loop shaping controller, Nanjing University of Science and Technology, vol.33, no.1, pp.81-86, 2009.

[26] H. Liu, Y. Bai, G. Lu and Y. Zhong, Robust attitude control of uncertain quadrotors, IET Control Theory and Appl., vol.7, no.11, pp.1583-1589, 2013.

[27] ZHAO, Bo, XIAN, Bin, ZHANG, Yao, et al. Nonlinear robust adaptive tracking control of a quadrotor UAV via immersion and invariance methodology. IEEE Transactions on Industrial Electronics, 2014, vol. 62, no 5, p. 2891-2902.

[28] MOKHLISS, Hamza, EL-AMIRI, Asseya, et RAIS, Khalid. Estimation of five parameters of photovoltaic modules using a synergetic control theory approach. Journal of Computational Electronics, 2019, vol. 18, no 1, p. 241-250.

[29] ELAVARASAN, Rajvikram Madurai, SHAFIULLAH, G. M., RAJU, Kannadasan, et al. COVID-19: Impact analysis and recommendations for power sector operation. Applied energy, 2020, vol. 279, p. 115739.

[30] SINGH, Bhim, CHANDRA, Ambrish, et AL-HADDAD, Kamal. Power quality: problems and mitigation techniques. John Wiley & Sons, 2014.

[31] Power Quality Equipment Market Forecast to 2028 - COVID-19 Impact and Global Analysis by Equipment, Phase, and End User https://www.researchandmarkets.com/reports/5401848/power-quality-equipment-market-forecast-to-2028

[32] SINGH, Bhim, CHANDRA, Ambrish, et AL-HADDAD, Kamal. Power quality: problems and mitigation techniques. John Wiley & Sons, 2014.

[33] RAHMANI, S., AL-HADDAD, K., et KANAAN, H. Y. Two PWM techniques for single-phase shunt active power filters employing a direct current control strategy. IET Power Electronics, 2008, vol. 1, no 3, p. 376-385.

[34] LU, Dylan Dah-Chuan, IU, Herbert Ho-Ching, et PJEVALICA, Velibor. A single-stage AC/DC converter with high power factor, regulated bus voltage, and output voltage. IEEE Transactions on Power Electronics, 2008, vol. 23, no 1, p. 218-228.

[35] HAMOUDA, Noureddine, BABES, Badreddine, KAHLA, Sami, et al. Real time implementation of grid connected wind energy systems: Predictive current controller. In : 2019 1st International Conference on Sustainable Renewable Energy Systems and Applications (ICSRESA). IEEE, 2019. p. 1-6.

[36] KOMURCUGIL, Hasan et KUKRER, Osman. A new control strategy for single-phase shunt active power filters using a Lyapunov function. IEEE Transactions on Industrial Electronics, 2006, vol. 53, no 1, p. 305-312.

[37] ETXEBERRIA-OTADUI, Ion, DE HEREDIA, A. Lopez, GAZTAÑAGA, Haizea, et al. A single synchronous frame hybrid (SSFH) multifrequency controller for power active filters. IEEE Transactions on Industrial Electronics, 2006, vol. 53, no 5, p. 1640-1648.

[38] ROUTIMO, Mikko, SALO, M., et TUUSA, H. Current sensorless control of a voltage-source active power filter. In : Twentieth Annual IEEE Applied Power Electronics Conference and Exposition, 2005. APEC 2005. IEEE, 2005. p. 1696-1702.

[39] HONGJUAN, Fang, RONGFENG, Yang, YANNAN, Yu, et al. A study on the DC voltage control techniques of cascaded multilevel APF. In : Proceedings of The 7th International Power Electronics and Motion Control Conference. IEEE, 2012. p. 2727-2731.

[40] PATNAIK, Sushree Sangita et PANDA, Anup Kumar. Real-time performance analysis and comparison of various control schemes for particle swarm optimization-based shunt active power filters. International Journal of Electrical Power & Energy Systems, 2013, vol. 52, p. 185-197.

[41] AISSA, Oualid, MOULAHOUM, Samir, COLAK, Ilhami, et al. Analysis and experimental evaluation of shunt active power filter for power quality improvement based on predictive direct power control. Environmental Science and Pollution Research, 2018, vol. 25, no 25, p. 24548-24560.

[42] CHAITHANAKULWAT, Arckarakit. Optimization of Shunt Active Power Filtering with PI Control in a Three-Phase Three-Wire System. European Journal of Electrical Engineering, 2020, vol. 22, no 1, p. 39-47.

[43] RUKONUZZAMAN, M. et NAKAOKA, Mutsuo. Single-phase shunt active power filter with knowledge-based harmonic detection algorithm. In : Proceedings of the Power Conversion Conference-Osaka 2002 (Cat. No. 02TH8579). IEEE, 2002. p. 778-783.

[44] KOYA, Shameer A. et ALSUMIRI, Mohammed. A Modified Fuzzy Hysteresis Controller for Shunt Active Power Filter. In : 2018 Renewable Energies, Power Systems & Green Inclusive Economy (REPS-GIE). IEEE, 2018. p. 1-5.

[45] AKAGI, Hirofkni. Active and hybrid filters for power conditioning. In : ISIE'2000. Proceedings of the 2000 IEEE International Symposium on Industrial Electronics (Cat. No. 00TH8543). IEEE, 2000. p. TU26-TU36 vol. 1.

[46] CHELLI, Zoubir, TOUFOUTI, Riad, OMEIRI, Amar, et al. Hysteresis control for shunt active power filter under unbalanced three-phase load conditions. Journal of Electrical and computer Engineering, 2015, vol. 2015.

[47] Wang, L., Wong, M.-C., Lam, C.-S., Dai, N.-Y., Lao, K.- W., & Wong, C.-K. (2015). Non-linear adaptive hysteresis band pulse-width modulation control for hybrid active power filters to reduce switching loss. IET Power Electronics, 8(11), 2156–2167. https://doi.org/10.1049/iet-pel.2014.0824.

[48] Antchev, M. Hr., Petkova, M. P., Antchev, H. M., Gourgoulitsov, V. T., & Valtchev, S. S. (2011, October). Study of a single-phase series active power filter with hysteresis control. 11th International Conference on Electrical Power Quality and Utilisation. https://doi.org/10.1109/epqu.2011.6128921.

[49] Alhasheem, M., Mattavelli, P., & Davari, P. (2020). Harmonics mitigation and non-ideal voltage compensation utilising active power filter based on predictive current control. IET Power Electronics, 13(13), 2782–2793. https://doi.org/10.1049/iet-pel.2019.0985

[50] ZHAO, Ping, YAO, Wei, WEN, Jinyu, et al. Improved synergetic excitation control for transient stability enhancement and voltage regulation of power systems. International Journal of Electrical Power & Energy Systems, 2015, vol. 68, p. 44-51.

[51] Young, H. A., Perez, M. A., & Rodriguez, J. (2016). Analysis of finite-control-set model predictive current control with model parameter mismatch in a three-phase inverter. IEEE Transactions on Industrial Electronics,63(5),3100–3107. https://doi.org/10.1109/ tie.2016.2515072.

[52] Narongrit, T., Areerak, K., & Areerak, K. (2016). Adaptive fuzzy control for shunt active power filters. Electric Power Components and Systems, 44(6), 646–657. https://doi.org/10.1080/15325008.2015.1122111.

CHAPTER 1

Non-Linear Control Techniques and Artificial Intelligence

1.1 Introduction

The studied objects in control theory are systems (linear and nonlinear). A system is a set of elements connected to each other by information links within certain delimited system boundaries. Control theory has made considerable progress, with new mathematical techniques, as well as advances in power electronics and computer science, making it possible to control much more complex dynamic systems. Control methods applications have been useful in making space travel and communication satellites, safer and more efficient aircraft and cleaner car engines possible and electric power systems.

The conventional control laws give good results in the case of linear systems with fixed parameters. Unlike systems that are non-linear or have non-stationary parameters, the results of these classical control laws can be unsatisfactory because they are not robust, especially when the requirements for accuracy and other dynamic properties of

the system are stringent. It is necessary to demand control laws which are insensitive to changes in parameters for disturbances and non-linearities. Robust control solutions such as the backstepping technique [32] and robust **LMI** (**L**inear **M**atrix Inequalities) switched controllers [33-34], **S**liding **M**ode **C**ontrol **SMC** [35-36] have been designed to control such systems.

Another control solution for nonlinear uncertain systems is **S**ynergic **C**ontrol (**SC**). Indeed, **SC** is well known for its robustness against matching disturbation/uncertainties. It is also known for its finite time convergence and relative simplicity for application.

1.2 Sliding mode control

1.2.1 Principle of standard sliding mode Control

The concept of **SMC** is to forcing the system trajectory to achieve a domain, known as the sliding surface, in a finite time. As soon as the system's trajectory reaches the sliding surface, it will stay confined to it in spite of perturbations/uncertainties and need only be considered as sliding along this surface.

In summary, a sliding mode control law U_{smc} has two parts:

$$U_{smc} = U_{sw} + U_{eq} \tag{1.1}$$

a) The switching component control U_{sw} :

The discontinuous character of the control is due to the discontinuous component U_{sw} consisting of the sliding surface function $sign$ multiplied by a positive constant k which represents the gain of the switching control. It is determined in order to guarantee the attractiveness of the variable to be controlled towards the sliding surface and to satisfy the convergence condition. In non-linear control, its importance lies in its ability to eliminate the effects of model inaccuracies and to reject external disturbances.

b) The equivalent control U_{eq} :

It is the continuous component U_{eq}, its role is to maintain the state of the system on the sliding surface. It depends on the model of the system and is determined by considering that the derivative of the surface is zero.

The design of the stabilizing control is carried out in two stages:

- Sliding variable definition: the control objective is the basis for this step. The sliding variable is in general expressed as a function of the system output and eventually a finite number of its consecutive time derivatives. The sliding variable is defined such that, once it is equal to zero, the control objective will be reached, i.e. The output reaches the target.
- The system output function in general is an expression of the sliding variable the sliding variable and eventually a finite number of its consecutive time derivatives. The sliding variable is defined such that when it is equal to zero, the control objective will be achieved, i.e. The output reaches the target.
- Designing a discontinuous control law: The system is obliged to achieve the sliding surface at a finite time and to keep it there despite the uncertainties and perturbations due to the control law.

1.2.2 Sliding variable design

First of all, consider the following system

$$\begin{cases} \dot{x} = f(x,t) + g(x,t)u \\ y = h(x,t) \end{cases} \tag{1.2}$$

where $x \in X \subset \mathbb{R}^n$ is the state vector, $u \in U \subset \mathbb{R}$ the control input (X and U being bounded subsets of $\mathbb{R}^n$ and $\mathbb{R}$ respectively), f and g uncertain sufficiently smooth functions, and y the output function (sufficiently smooth). The control objective is to constrain the output y to track a sufficiently differentiable reference trajectory $y_{ref}(t)$, i.e. to force the tracking error $e_y = y - y_{ref}(t)$ to "0" in spite of uncertainties/perturbations.

Assumption 1.1.

"m" is the relative degree[1] of Eq(1.2) with respect to the tracking error e_y is constant and known i.e.[2]

$$e_y^{(m)} = a(x,t) + b(x,t)u \tag{1.3}$$

with $b(x,t) \neq 0$ and $t \geq 0$.

[1] The relative degree is an integer equal to the minimum number of times that *ey* should be differentiated with respect to time in order to make u appearing explicitly [6].

[2] $e_y^{(m)}$ denotes the m^{th} time derivative of e_y. This notation is used throughout the thesis for all the variables/functions.

Now, consider a smooth function $\sigma(x,t)$ as a virtual output for system Eq(1.2) and referred "sliding variable". The sliding surface ***S*** is given by

$$s = \{x \in X, t \geq 0 | \sigma(x,t) = 0\} \tag{1.4}$$

Definition 1.1. [37]. There exists an ideal sliding mode (or called sliding motion) on *S* if, after a finite time t_F , the solution of system (1.2) satisfies $\sigma(x,t) = 0$ for all $t \geq t_F$.

Now, a sliding surface can be viewed as a hypersurface in the state space. The dynamics of the system is determined by the definition of σ once the trajectories of the system Eq(1.2) evolve on S . Moreover, the choice of S and σ will ensure that the output y of the system converges to the control target. This is why σ must be defined such that, when $\sigma = 0$, then $e_y \to 0$. Then, a usual relationship between σ and e_y is defined in Eq(1.5):

$$\sigma(x,t) = {e_y}^{(m-1)} + \ldots + c_1 \dot{e}_y + c_0 e_y \tag{1.5}$$

Where the coefficients $c_i > 0$ $(1 \leq i \leq m-2)$ are chosen such that the polynomial is Hurwitz.

$$\Pi(\lambda) = \lambda^{m-1} + \sum_{i=0}^{m-2} c_i \lambda^i \tag{1.6}$$

Moreover, given Eq(1.3) and Assumption 1.1, the sliding variable has a relative degree equal to 1; it yields

$$\dot{\sigma} = \bar{a}(x,t) + \bar{b}(x,t)u \tag{1.7}$$

Assumption 1.2

$\bar{a}(x,t)$ and $\bar{b}(x,t)$ are unknown but bounded functions such that there exist positive constants a_M, b_m *and* b_M such that $\forall x \in X, t \geq 0$.

$$|\bar{a}(x,t)| \leq a_M \ , \quad 0 < b_m \leq \bar{b}(x,t) \leq b_M \tag{1.8}$$

The second step, once the sliding variable is selected, consists in designing the control input U_{sw} stabilizing the system Eq(1.7) in a finite time, and in spite of uncertainties and perturbations.

1.2.3 First order sliding mode control

V. Utkin [38] was the first to suggest the **SMC**, it can be applied to systems with relative degree equal to "1" with respect to the sliding variable as Eq.(1.7). Then, this controller can also be called a **F**irst **O**rder **S**liding **M**ode **C**ontrol (**FOSMC**).

Note that it is important to design the control input U_{sw} to force the system trajectories to achieve and evolve on the sliding surface S in spite of the uncertainties and perturbations. In other words, it must make the sliding surface locally attractive. Then, the design of the control law must verify a condition that ensures the stability of $\sigma(x,t)=0$. A solution is to use the Lyapunov approach to obtain a stabilizing controller.

A very popular approach to study the stability of an equilibrium point ($\sigma(x,t)=0$)is the Lyapunov function technique [39] and will therefore be used in the following.

Definition 1.2. A function $V:\mathbb{R}^n \to \mathbb{R}$ is a Lyapunov function candidate if

- $V(0)=0$;
- $\forall x \in X-\{0\}$, on a $V(x)>0$.

Given zero is the equilibrium point and the above definition, then the sign of the time derivative of the Lyapunov function candidate gives the information about the system stability. Considering the sliding variable σ Eq(1.5), a Lyapunov function candidate satisfying Definition 1.2 takes the form Eq(1.9)

$$V(\sigma)=\frac{1}{2}\sigma^2 \tag{1.9}$$

The time derivative of V must be defined negatively, i.e., in order to guarantee the asymptotic convergence of the sliding variable σ .

$$\dot{V}(\sigma)=\sigma\dot{\sigma}<0 \tag{1.10}$$

The inequality Eq(1.10) is referred the sliding condition in the context of **SMC**, it guarantees that the sliding surface σ is attractive i.e. once the system's trajectories reach σ, they remain on it despite the perturbations and uncertainties. Note that in order to obtain the finite time convergence of σ towards "0", a stricter condition called η - attractive condition [36] must be satisfied and reads as follows

$$\sigma\dot{\sigma}\le-\eta|\sigma|,\quad \eta>0 \tag{1.11}$$

It means that

$$\dot{V}\le-\eta\sqrt{2V} \tag{1.12}$$

Integrating of Eq(1.12) gives

$$\sqrt{2V(t)} - \sqrt{2V(0)} \leq -\eta t \tag{1.13}$$

Then,

$$\eta t \leq |\sigma(0)| - \|\sigma(t)\| \tag{1.14}$$

Consequently, σ reaches "0" in a finite time t_F with

$$t_F \leq \frac{|\sigma(0)|}{\eta} \tag{1.15}$$

Hence, a control U_{sw} satisfying Eq(1.11) drives the sliding variable to "0" in finite time. Such control U_{sw} takes the form

$$U_{sw} = -k \quad sign(\sigma) \tag{1.16}$$

The gain k of the controller U_{sw} must be chosen large enough to ensure the η-attractive condition Eq(1.11). It is the case if the gain k verifies

$$k \geq \frac{|\overline{a}(x,t)| + \eta}{\overline{b}(x,t)} \tag{1.17}$$

From Assumption 1.2, a sufficient condition reads as

$$k \geq \frac{a_M + \eta}{b_m} \tag{1.18}$$

Then, with the control input Eq(1.16) and the gain k checking Eq(1.18), the convergence of σ to "0" is ensured in a finite time t_F verifying Eq(1.15). The parameters of the definition of the sliding variable Eq(1.4) i.e determine the dynamics of the system once the trajectory of the system evolves on the sliding surface.

$$e_y^{(m-1)} + \ldots + c_1 \dot{e}_y + c_0 e_y = 0 \tag{1.19}$$

Then, the tracking error will asymptotically converge to "0" despite the perturbations and uncertainties, due to the characteristic Eq(1.6).

1.2.4 Summary of the controller

The behavior of the closed loop system Eq(1.2) controlled by Eq(1.16) with the satisfaction of Eq(1.18) can be split into 2 phases:

- Reaching phase: this phase corresponds to the time interval $[0, t_F[$ where the trajectories are not evolving on the sliding surface; nevertheless, they are converging towards it. Note that during this phase the system is still sensitive to

uncertainties and perturbations. Following Eq(1.15), the duration of this phase, t_F , can be reduced by increasing η ; this corresponds to increase the gain k .

- Sliding phase: this phase corresponds to the time interval $[t_F, +\infty[$ during which the trajectories are evolving on the sliding surface S. If the gain k is well tuned Eq.(1.18), the system is insensitive to uncertainties and perturbations, and the tracking error e_y converges to "0".

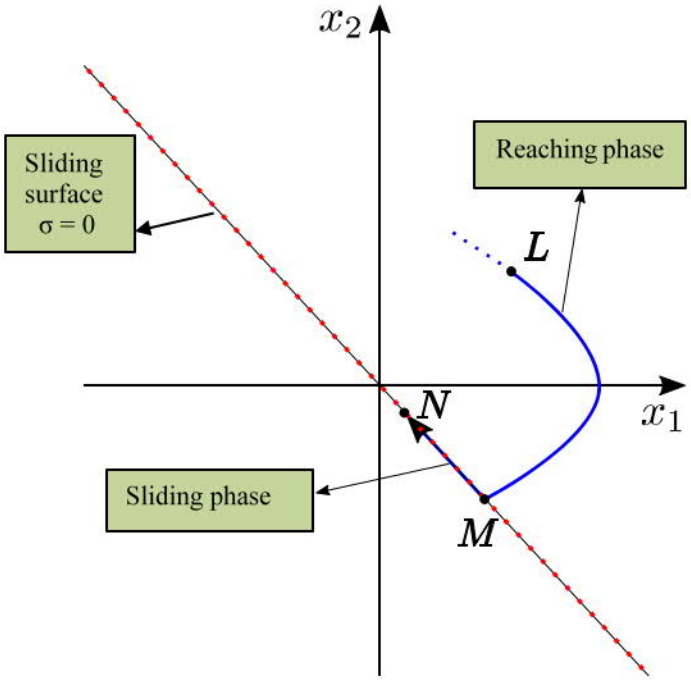

Figure.1. 1 : Example of system trajectory in the phase plane (x1, x2)

1.2.5 Phenomenon of chattering

An optimal sliding regime requires a controller that can switch at an infinite frequency. Obviously, for practical use, only switching at a finite frequency is possible, which causes a delay between the output measurement and the control calculation, which can be amplified if the system naturally has delays or neglected dynamics. This leads to the system leaving the sliding surface without the control being able to respond, and then, once the sign of the control has been reversed, to return to this surface and pass to the other side, and so on.

In practical applications of **SMC**, an undesirable phenomenon known as chattering can appear: high frequency oscillations that may lead to low control accuracy, high wear of moving mechanical parts, and high heat losses in power circuits [40]. There are two main reasons which can cause the chattering:

• neglected dynamics in the model of the system [41];

• the use of digital controllers with finite sampling rate [42]. Indeed, the "ideal" sliding motion $\sigma = 0$ requires the switching of the control input at an infinite frequency.

There are several methods that have been proposed to reduce the chattering effect. Notably, the **SMC** boundary layer method consists in replacing the sign function with an approximate continuous one, in a vicinity of the sliding surface S [43], The sliding mode is no longer confined to S, but to a vicinity of it. Then, the system is said to have a "pseudo" sliding motion [44]. Among the used continuous functions, one can cite.

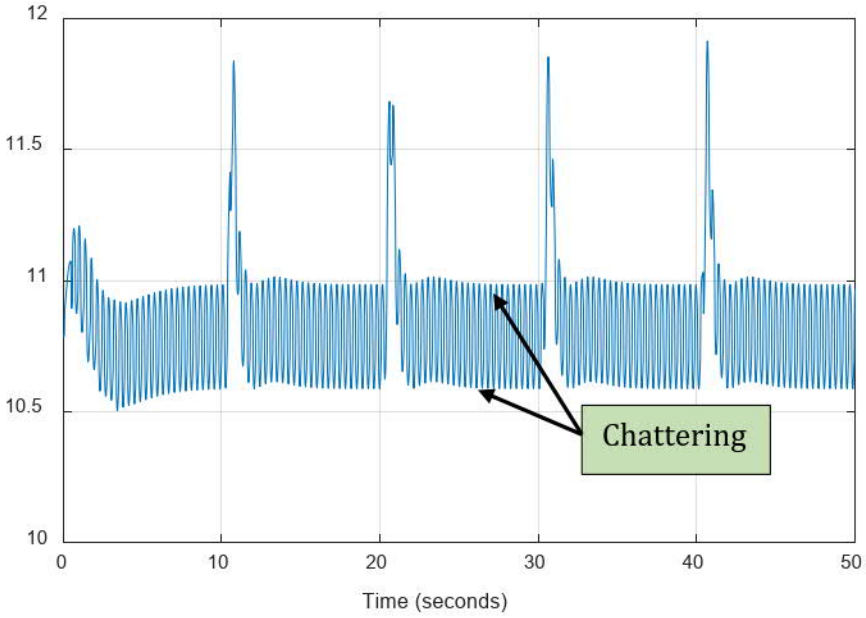

Figure.1. 2 : Phenomenon of chattering

1.2.5.1 The saturation fonction

a) The sign function : The function $sign(\sigma)$ (**Figure 1.3 (a)**) is replaced by a straight line with slope equal to $1/\delta (0 < \delta < 1)$ at a vicinity of the origin whose width is 2δ (**Figure 1.3 (b)**). Its expression is given by

$$sat(\sigma,\delta) = \begin{cases} sign(\sigma) & if \quad |\sigma| > \delta \\ \dfrac{\sigma}{\delta} & if \quad |\sigma| \le \delta \end{cases} \tag{1.20}$$

b) The atan function

It is given by

$$v(\sigma,\delta) = \frac{2}{\pi} atav\left(\frac{\sigma}{\delta}\right) \tag{1.21}$$

This function (see **Figure 1.3 (c)**) gives a good approximation of the sign function for sufficiently small δ .

c) The tanh function

Another solution is to use the hyperbolic tangent function (see **Figure 1.3 (d)**)

$$v(\sigma,\delta) = \tanh\left(\frac{\sigma}{\delta}\right) \tag{1.22}$$

With $0 < \delta < 1$.

Notice that, in the previous approximation approaches, δ strongly influences the slope of the function at a vicinity of S : the smaller the value of δ , the greater the slope. Notice that replacing the sign function by its continuous approximation reduces the chattering, but also reduces the robustness of the controller.

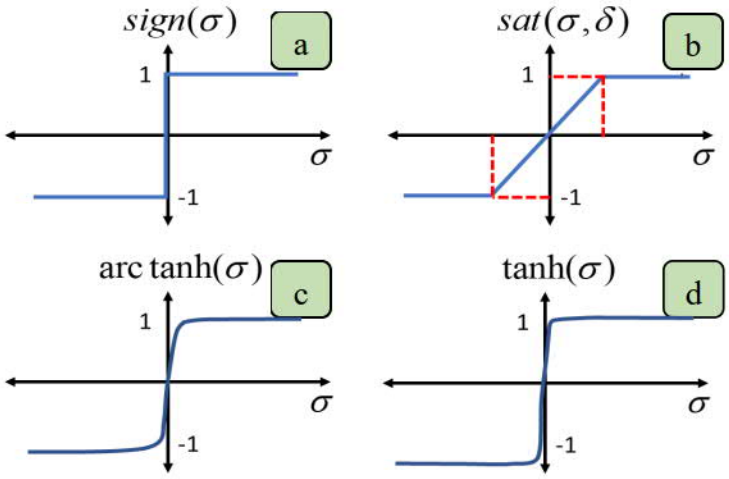

Figure.1. 3 : Sign function and some approximate functions

1.3 Synergetic control theory

Synergetic control theory was first introduced by a Russian researcher "Kolesnikov" in 2001 [45]. This approach has started to take its place in the field of control systems. This technique is often referred as " stabilization and control by system restriction and manifold invariance [46]. Confining motion or paths of a system onto the manifold (or hyperplane) in case it is not on the manifold already this is the main idea of the approach concept.

The problem of control discussed in this work is essentially stability (i.e., damping of any oscillation that may occur due to a disturbance in the system) and since the synergetic controller forces the system to take on the characteristics of the manifold, the manifold must be constructed in such a way as to ensure that the behavior of the system in closed loop is stable. Thus, the design approach can be described as consisting of two main steps: the construction of a stable manifold (or hyperplane); and the synthesis or

design of a controller so that the system's trajectories are forced onto the hyperplane and subsequently remain there. The controller objective can be considered as the one that makes the manifold stable and attractive.

The synergetic control technique is similar to sliding mode control (**SMC**) in the way the manifold is constructed [48-49]. However, this technique differs from the **SMC** technique in the way it forces the system to achieve the manifold. In the **SMC** case, there is a finite period of time in which the system is forced to reach the manifold, which introduces a certain form of discontinuity in the control action and thus creating chattering on the manifold. However, this chattering can cause wear and tear in the system's actuating components. But with synergistic control, the system is driven to the manifold exponentially, which eliminates the chattering effect and allows the system to reach the manifold in a more efficient manner.

1.3.1 Design of synergetic control law

Suppose that the system to be controlled is delineated by a set of non-linear Eq(1.2). The basic procedure of synergetic control synthesis for the system model Eq(1.2) is shown below. The choice of function of the system state variables (macro-variable) is the first step to design the synergetic controller's synthesis as shown in Eq(1.23).

$$\psi = \psi(x,t) \tag{1.23}$$

The main focus of the controller requires the system to have the attractor ψ=0. The characteristics of the macro-variable according to performance and control specifications can be selected by the designer. Also, the desired dynamic evolution of the macro variable is usually chosen by the Eq(1.24).

$$T\frac{d\psi}{dt} + \psi = 0, \quad T > 0 \tag{1.24}$$

T is a positive constant to be imposed by the designer. In our paper, its value is optimized by **P**article **S**warm **O**ptimization **PSO** algorithm.

The designer chooses speed convergence to the target equilibrium point. Equation (1.25) is given by the chain rule of differentiation as follows:

$$\frac{d\psi}{dt} = \frac{\partial\psi(x,t)}{\partial x}\frac{dx(t)}{dx} \tag{1.25}$$

By replacing the macro-variable from Eq(1.25) to Eq(1.24) leads:

$$T\frac{\partial\psi(x,t)}{\partial x} f(x,U_{sc},t) + \psi(x,t) = 0 \tag{1.26}$$

The law of the proposed **SC** can be found by solving Eq(1.26) as follows.

$$U_{SC} = U_d(x,t,\psi(x,t),T) \tag{1.27}$$

From Eq(1.27), it can be see that the control is not only dependent on the state variables of the system, but also on the macro-variable and the chosen time constant T. In other words, the designer can choose the characteristics of the controller by choosing an appropriate macro-variable and a specific time constant T. In synthesis of the controller, each domain introduces a new constraint on the state space field and reduces the order of the system by one degree, while going in the direction of global stability. In the synthesis of the synergetic controller shown above, it is clear that the synergetic controller operates on the nonlinear system and a linearization or simplification of the model is not necessary as when applying traditional control theory.

Through the appropriate choice of macro-variables, the designer can obtain the following interesting characteristics for the final form of the system such as [47]:

- Overall system stability
- Invariance to parameter changes
- Noise reduction

It is interesting to note that the law of synergetic control guarantees global stability on the selected domain. This means that once the hypersurface is reached the system is not supposed to leave it, even in case of quite large variations of the parameters. This property of invariance to perturbations is shared by the sliding mode control technique when sliding the trajectories on the sliding surface.

1.4 Particle swarm optimization

Particle Swarm Optimization is an evolutionary algorithm developed in 1995 by “J. Kennedy” & “R. Eberhart” [50] as a technique for solving non-linear continuous variable optimization problems. From social behavior and the movements of birds, insects or fish, this technique was inspired. The search algorithm relies on the two behaviors of (cooperation and disagreement) between members of the community. The objective is to get optimal regions of a complex search space by the interaction of singles in a group of particles. As a first step, the algorithm creates a "population" of random solutions (also called candidate solutions or particles). Every candidate solution has an adaptable velocity, based on which it moves through the search space. In addition, each candidate

has the ability to remember the best position (or fitness) in the search space that it has in fact never visited. Its movement is a conglomeration of acceleration toward its best previously visited position. The other best value followed by **PSO** is known as 'global best value', which is the best value or fitness that has been found so far via any of candidate in the neighborhood of the candidate. The main concept is that at each time step the position and velocity of each candidate is changed towards the local and global best locations. Consequently, after a certain number of time steps, it is found that the particle between populations has gathered around one or more of the optima and tends to locate the global optima among all.

The **PSO** has a good balanced and flexible mechanism to enhance the ability to locate the best local and global positions in contrast to other evolutionary algorithms such as the Genetic Algorithm (GA) [51-52].

Some of **PSO** advantages when compared to other optimization techniques are [53]:

- The quality of the solution obtained from this technique is independent of the initial population.
- It has more effective memory capability (local and neighboring best).
- It can overcome the untimely convergence problem and improve the search capability.
- It has less parameters to adjust.
- It is more flexible, robust and easy to implement.
- It is less vulnerable to getting trapped on local minimal.

1.4.1 The terminologies of PSO

The **PSO** is used throughout this study for a unmanned aerial vehicle (UAV) active power filter (APF) system to achieve the optimal parameter value of the synergistic controller. An illustration of the **PSO** terminologies is given below:

Particle $\Omega_i(t)$: A candidate solution (controllers' parameters) at iteration. Each particle's size is a summation of the controllers' parameters. In the case of the synergistic controller designed in chapter 3 the parameter number of the i^{th} controller is 12 and in chapter 5 $i^{th}=2$.

Population: A set of m particles $\{\Omega_1(t);\Omega_2(t);.....\Omega_m(t)\}$, where m is the number of candidate solutions.

Objective function $J_i(t)$: function use to determine the fitness of i^{th} controller at t^{th} iteration.

Individual best $\Omega_i^*(t)$: Also referred by local best. It' s the greatest value of fitness which this particle has achieved up to t^{th} iteration.

$$\Omega_i^*(t) = \{\Omega_i(t) : J_i(\Omega_i^*(t)) \le J_i(\Omega_i(\tau))\}, \quad \tau \le t \tag{1.28}$$

$$J_i^*(t) = J_i(\Omega_i^*(t)) \tag{1.29}$$

Global best $\Omega^{**}(t)$: The best position (or fitness) for all particles among all individual local best positions.

$$\Omega^{**}(t) = \{\Omega_i^*(t) : J(\Omega^{**}(t)) \le J_i(\Omega_i^*(\tau)), i = 1,.....,n\} \tag{1.30}$$

The **PSO** technique steps are described below:

- Initialization

1) Set the time counter t , performance evaluation counter c , and their maximum values , $t_{\max}, c_{\max}$.

2) Generate arbitrarily m particles and velocity for each of these particles. These values are generated from the following given information: the size of each particle p, the population size m, the admissible range for controller parameters $\phi_{j,jj}^{\min}, \phi_{j,jj}^{\max}$

$$\phi_{j,jj}^{\min} \le, \phi_{j,jj} \le \phi_{j,jj}^{\max} \qquad \text{j=1,2,.....,p,} \quad \text{jj=1,2,...,m} \tag{1.31}$$

and the admissible range of velocity

$$-v_{j,jj}^{\min} \le, v_{j,jj} \le v_{j,jj}^{\max} \tag{1.32}$$

Where

$$v_{j,jj}^{\max} = \frac{\phi_{j,jj}^{\max} - \phi_{j,jj}^{\min}}{\mu} \tag{1.33}$$

and μ is the number of interval in jj^{th} dimension.

3) Find the fitness for every particle, , then investigate for the best values among all the fitness values and define this value as the global best fitness $J^{**}(t)$ and the particle that offers this fitness value as the global best position $\Omega^{**}(t)$ i.e. $J_i^*(t) = J_i(t), \Omega_i^*(t) = \Omega_i(t)$ and $J^{**}(t,c) = \min[J^*_1(t), J^*_2(t), ..., J^*_n(t)]$

4) Set $t = t+1, c = c+1$

• Use the following equation to update the velocity

$$v_{j,jj}(t) = \psi(v_{j,jj}(t-1)) + c_1 r_1(\phi^*_{j,jj}(t-1) - \phi_{j,jj}(t-1)) + c_2 r_2(\phi^{**}_{j,jj}(t-1) - \phi_{j,jj}(t-1)) \quad (1.34)$$

$$\psi = \frac{2}{2 - x - \sqrt{x^2 - 4x}} \quad (1.35)$$

where

$x = c_1 + c_2, x > 4, \phi_{j,jj}{}^{*}(t)$ and $\phi_{j,jj}{}^{**}(t)$ are local best and global best parameters of controller.

➢ Updating the position

Due to the update of the velocities, every particle will change its positions according to the equation below:

$$\phi_{j,jj}(t) = \phi_{j,jj}(t-1) + v_{j,jj}(t) \quad (1.36)$$

Update the position $\Omega_i(t) = [\phi_{i,1}(t), \phi_{i,2}(t), \ldots\ldots\ldots, \phi_{i,m}(t)]$ for j=1,2,.....,p

➢ Individual and global best update

By using the updated position, every particle evaluates its objective function and new individual best $J_i^*(t)$ and associated $\Omega_i^*(t)$ for every i are defined from Eq(1.28) and Eq(1.29). Eq(1.30) is utilized to find the global best i.e. to find. $J^{**}(t,c) = J(\Omega^{**}(t,c))$ if

$$J^{**}(t,c) \le J^{**}(t-1, c-1) \quad (1.37)$$

then the fitness has enhanced, and the parameters are updated, defined $c = c+1$ and proceed to the next step. Otherwise, update $J^{**}(t,c), \Omega^{**}(t)$ and set $c = 0$. Then proceed to the second step.

➢ Stopping criteria

The scanning process will complete if one of the following conditions is meet:

1) If the counter has attained its maximum number, $c = c_{\max}$ and the best global solution $J^{**}(t,c)$ can no longer be improved. The optimal solution is considered to be the current $\Omega^{**}(t)$.

2) If the maximum allowable iteration is reached, $t = t_{\max}$.

The main optimization steps of the **SC-PSO** strategy are illustrated on the flowchart illustrated by **Figure (1.4).**

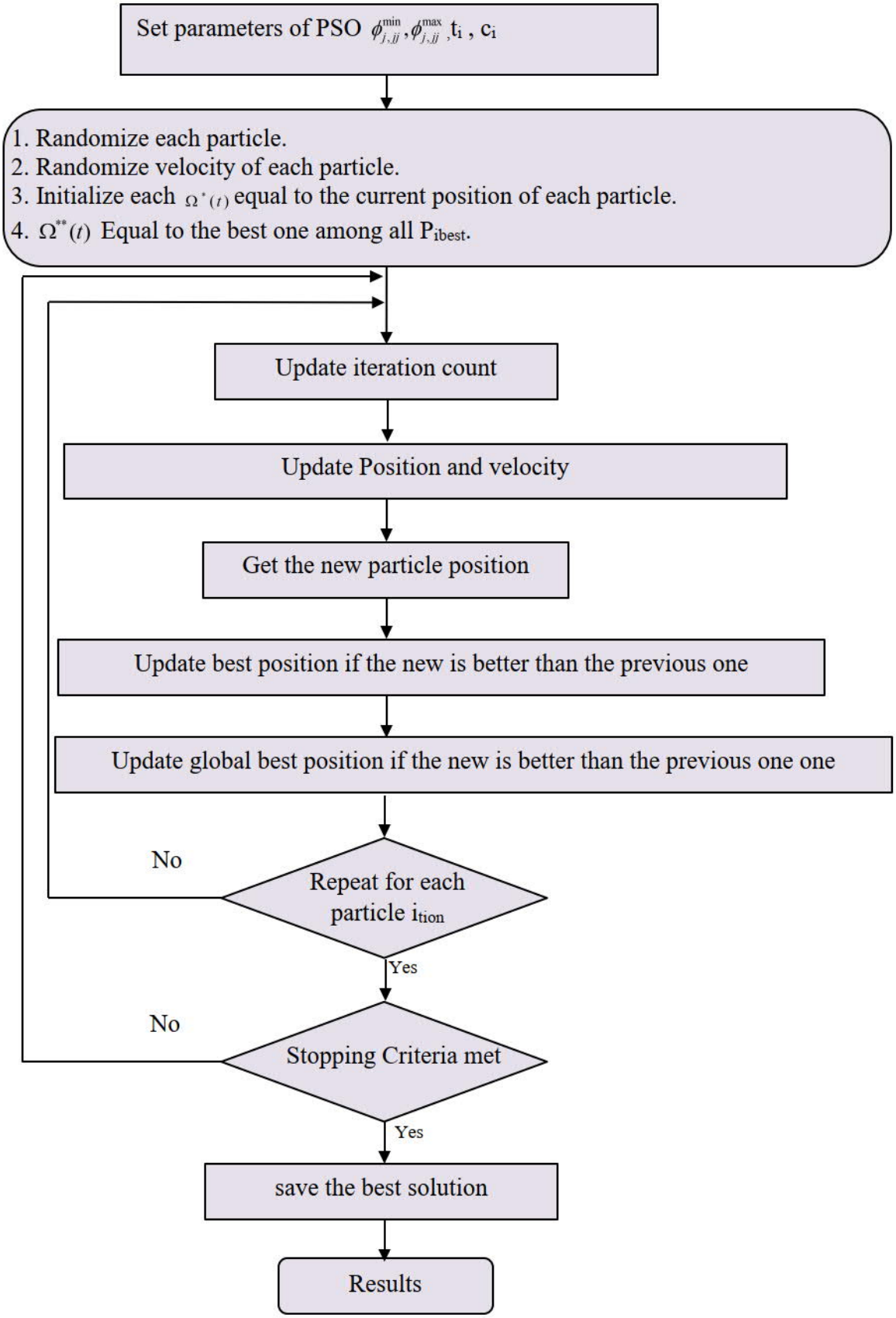

Figure.1. 4 : Flowchart of **SC** strategy optimized by **PSO**

1.5 Conclusion

The objective of the controller is to force the output system in order to track the reference signal. This follow-up is achieved by minimizing the approximation error on the one hand and by assuring the stability of the system on the other hand.

The application of the sliding mode control will cause oscillations with a switching frequency that tends to infinity (chattering phenomena) which may be unacceptable if the control signal has a physical meaning like force. Then, a new control technique adopted to solve the control problems of nonlinear systems was presented, it can be concluded from several scientific research that the synergistic control law shows a good tracking performance and guarantees the asymptotic stability of the system with a reduction of the interference problem. Also are proved that by using Particle Swarm Optimization to optimum tuning of the controller's parameters can obtain good results.

Reference:

[32] T. Madani and A. Benallegue, "Backstepping control for a quadrotor helicopter," in *2006 IEEE/RSJ International Conference on Intelligent Robots and Systems*, pp. 3255–3260, IEEE, 2006. 14

[33] D. Jabri, K. Guelton, N. Manamanni, A. Jaadari, and C.-D. Chinh, "Robust stabilization of nonlinear systems based on a switched fuzzy control law," vol. 14, no. 2, pp. 40–49, 2012. 14

[34] B. Mansouri, N. Manamanni, K. Guelton, and M. Djemai, "Robust pole placement controller

[35] Y. Shtessel, C. Edwards, L. Fridman, and A. Levant, *Sliding mode control and observation*. Springer, New York, USA, 2014. 14, 20

[36] V. I. Utkin, *Sliding modes in control and optimization*. Springer, Berlin, Germany, 1992. 14, 15, 16, 33, 34, 35

[37] A. Isidori, *Nonlinear control systems*. Springer, London, UK, 2013. 14

[38] V. Utkin, "Variable structure systems with sliding modes," *IEEE Transactions on Automatic control*, vol. 22, no. 2, pp. 212–222, 1977. 15

[39] H. K. Khalil, *Nonlinear Systems*. Pearson, 2001. 15

[40] V. Utkin and H. Lee, "Chattering problem in sliding mode control systems," in *9th International Workshop on Variable Structure Systems (VSS)*, Alghero, Italy, 2006. 18, 27, 33

[41] V. Utkin and J. Shi, "Integral sliding mode in systems operating under uncertainty conditions," in *IEEE Conference on Decision and Control (CDC)*, Kobe, Japan, 1996.18

[42] J. Guldner and V. Utkin, "The chattering problem in sliding mode systems," in *14th Intenational Symposium of Mathematical Theory of Networks and systems (MTNS)*, Perpignan, France, 2000. 18

[43] J. Burton and A. S. Zinober, "Continuous approximation of variable structure control," *International Journal of Systems Science*, vol. 17, no. 6, pp. 875–885, 1986. 19, 38

[44] X. Yu and R. B. Potts, "Analysis of discrete variable structure systems with pseudosliding

modes," *International Journal of Systems Science*, vol. 23, no. 4, pp. 503–516, 1992. 19

[45] Kolesnikov, A. A, Modern Applied control Theory: Synergetic Approach in Control Theory, TRTU, Moscow-Taganrog, 2000.

[46] Nusawardhana, Zak, S. H, Crossley, W. A., "Nonlinear Synergetic Optimal Controllers," *Journal of Guidance, Control and Dynamics*, Vol. 30, No. 4, July-August 2007.

[47] J. D. Li, K. Proddutur, E. Santi, and A. Monti, —Synergetic control of a boost converter: Theory and experimental verification,‖ in Proc. IEEE Southeast Conf., Apr. 2002, pp. 197–200.

[48] Hamouda, N., Babes, B., & Boutaghane, A. (2020). design and analysis of robust nonlinear synergetic controller for a PMDC motor driven wire-feeder system (WFS). In Lecture Notes in Electrical Engineering (pp. 373–387). Springer Singapore. https://doi.org/10.1007/978-981-15-6403-1_26

[49] Eghtedarpour, N. (2019). A synergetic control architecture for the integration of photovoltaic generation and battery energy storage in DC microgrids. Sustainable Energy, Grids and Networks, 20, 100250. https://doi.org/10.1016/j.segan.2019.100250

[50] Eberhart, R. C., and Kennedy J.,(1995) " A New Optimizer Using Particle swarm Theory," *Proceedings of the Sixth International Symposium on Micro Machine and Human Science*, Nagoya, Japan, 39-43. Piscataway, NJ: IEEE Service Center

[51] A. Iqbal and G. K. Singh, "PSO based controlled six-phase grid connected induction generator for wind energy generation," in *CES Transactions on Electrical Machines and Systems*, vol. 5, no. 1, pp. 41-49, March 2021, doi: 10.30941/CESTEMS.2021.00006.

[52] J. Song, W. X. Zheng and Y. Niu, "Self-Triggered Sliding Mode Control for Networked PMSM Speed Regulation System: A PSO-Optimized Super-Twisting Algorithm," in *IEEE Transactions on Industrial Electronics*, vol. 69, no. 1, pp. 763-773, Jan. 2022, doi: 10.1109/TIE.2021.3050348.

[53] B. Panigrahi, A. Abraham, and S. Das Eds., *Computational Intelligence in Power Engineering*.Berlin, Germany: Springer-Verlag, 2010.

CHAPTER 2

Modeling of an UAV Type Quadrotor

2.1 Introduction

Modeling is an important step for any design work on control law. It consists in finding a representation of the state of the physical system, more or less precise. This representation in the form of mathematical equations makes it possible to describe the behavior of the system according to its inputs. Thanks to these equations, it is possible to define and predict the attitude and position of the quadrotor reached in space, by studying only the control inputs.

In general, constant parameters appear in the equations of state (such as the mass or moment of inertia of a body, the coefficient of viscous friction, the capacitance of a capacitor, etc.). In such cases, an identification step may be necessary. Nevertheless, we will assume that all the parameters are known and we invite the reader to consult [54] for a panoply of identification methods.

A quadrotor is a rotary-wing drone consisting of four fixed-pitch propellers mounted at the ends of four cross-shaped arms. The propellers are coupled to DC or brushless motors.

Different formalisms are presented in the literature to model the dynamics of a 6 DOF aircraft, such as the quadrotor vehicle. The Euler-Lagrange and Newton-Euler formalisms are common methods used extensively for this purpose.

In this chapter, the notations and the frames used in the quadrotor model will be defined, and the transformations between the different frames will be discussed. Then, the kinematics and dynamics of the quadrotor are presented, and then the nonlinear equations of its motion are extracted based on the kinematics and force-moment dynamics. Next, the overall structure of the quadrotor model is described and discussed. Finally, the quadrotor model used in this work is presented with its state representation. Like any modeling, we make use of assumptions as follows:

- The structure of the quadrotor is rigid, with constant kinetic parameters, and perfectly symmetrical;
- The center of mass of the system and the center of symmetry coincide;
- The ground effect is neglected;
- The terrestrial frame is considered inertial.

The notations and the frames used in the quadrotor model will be defined in this chapter, and the transformations between the different frames will be discussed. In the following, the kinematics and dynamics of the quadrotor are presented, then the nonlinear equations of motion are extracted. In the last sections, the overall structure of the quadrotor model is described and discussed, and finally the quadrotor model used in this work is presented with its state representation.

Figure.2.1: The quadrotor (drone).

2.2 Preliminary and general considerations

2.2.1 Solid concept

Among the set of physical bodies, we consider as a rigid solid anybody which does not deform during its evolution in space, i.e. the distances between any two points M_1 and M_2 of this body are independent of the time variable.

$$d(M_1(t), M_2(t)) = \left\| \overrightarrow{M_1(t)M_2(t)} \right\|^2 = Cte \qquad (2.1)$$

The bases of classical mechanics present separately the study of the motion of rigid solids and that of deformable solids. The actual motion of any solid of course involves deformations, but in a number of cases these deformations can be considered negligible. Under the assumptions that we mentioned previously, the dynamics of the quadrotor can be considered as being the dynamics of a rigid body.

2.2.2. Identification and parameterization of a solid

We are interested in the movement of a solid S in space in relation to a reference frame of inertia $E = (O, x_e, y_e, z_e)$ related to the earth. In order to characterize the location of the solid S in relation to the reference frame E, it is necessary to know in the general case:

- The position of a particular point of the solid S relative to E.
- The orientation of the solid S with respect to E.

To do this, we first attach to the solid S a reference frame $\mathrm{B} = (O', x_b, y_b, z_b)$, said to be related to S. In the need to limit the associated calculations, the origin and orientation of the axes of this coordinate system must be chosen judiciously. It is often the reference of the main axes of inertia that causes the inertia matrix to be diagonal. The study of the movement of the solid S with respect to the earth, will therefore amount to studying the movement of the reference frame B in relation to the reference frame E **figure (2.2)**.

a) Position study

The position of $_{\mathrm{B}}$ with respect to E, at each moment, is defined by the position vector $\overrightarrow{OO'}$: coordinates (x, y, z) of the point O' in the dihedron (O, x_e, y_e, z_e).

$$\overrightarrow{OO'} = \begin{pmatrix} x \\ y \\ z \end{pmatrix}_E \tag{2.2}$$

These are the translation parameters of the solid that also represent its degrees of freedom in translation.

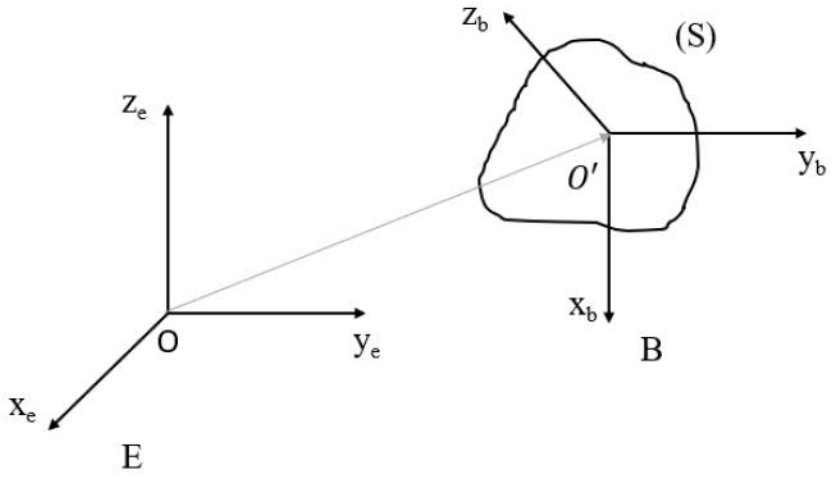

Figure.2.2: Solid in motion.

b) **Orientation study**

The orientation of the solid S does not depend on the choice of O' origin. By analogy to translation, rotational parameters or degrees of rotational freedoms, depending on time, are necessary to determine the orientation of the solid. In analytical mechanics, the use of Euler angles is the most common technique for parameterizing this orientation. It is based on the use of three angles defining three successive rotations from the fixed coordinate system when arriving at the moving coordinate system, and respecting the rule of the right hand. In the case of the ZYX convention that we adopt here, a first rotation around the axis z_e, of angle called yaw angle ψ transforms the coordinate system (O, x_e, y_e, z_e) into a temporary coordinate system (O, x_1, y_1, z_1). The corresponding rotation matrix is:

$$\begin{aligned} x_1 &= \mathrm{c}_\psi\, x_e + s_\psi y_e \\ y_1 &= -s_\psi x_e + c_\psi y_e \\ z_1 &= z_e \end{aligned} \quad \Rightarrow R_z(\psi) = \begin{bmatrix} \mathrm{c}_\psi & -\mathrm{s}_\psi & 0 \\ \mathrm{s}_\psi & \mathrm{c}_\psi & 0 \\ 0 & 0 & 1 \end{bmatrix} \tag{2.3}$$

It is customary to note: and $\cos(x) = c_x$ $\sin(x) = s_x$

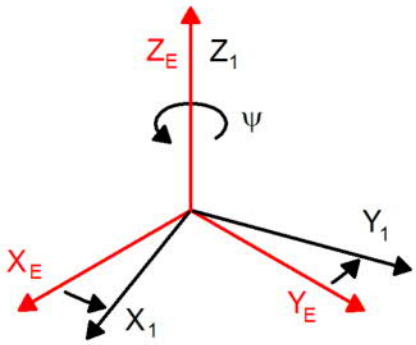

Figure.2.3: Rotation about the Z_E axis of the angle ψ (yaw)

A second rotation around the axis y_1, of an angle θ called the pitch angle turns the base (x_1, y_1, z_1) into a temporary base (x_2, y_2, z_2). The corresponding rotation matrix is:

$$\begin{aligned} x_2 &= c_\theta x_1 - s_\theta z_1 \\ y_2 &= y_1 \\ z_2 &= s_\theta x_1 + c_\theta z_1 \end{aligned} \quad \Rightarrow \quad R_y(\theta) = \begin{bmatrix} c_\theta & 0 & s_\theta \\ 0 & 1 & 0 \\ -s_\theta & 0 & c_\theta \end{bmatrix} \tag{2.4}$$

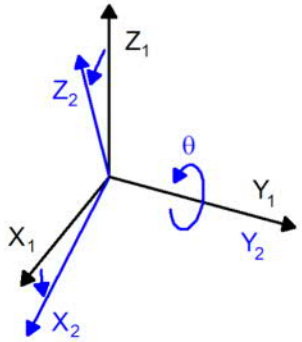

Figure.2.4: Rotation about the Y_1 axis of the angle θ (pitch)

A third rotation around the axis x_2, of angle called roll angle ϕ transforms the base (x_2, y_2, z_2) into a base (x_b, y_b, z_b). The corresponding rotation matrix is:

$$\begin{aligned} x_b &= x_2 \\ y_b &= c_\phi y_2 + s_\phi z_2 \\ z_b &= -s_\phi y_2 + c_\phi z_2 \end{aligned} \quad \Rightarrow \quad R_x(\phi) = \begin{bmatrix} 1 & 0 & 0 \\ 0 & c_\phi & -s_\phi \\ 0 & s_\phi & c_\phi \end{bmatrix} \tag{2.5}$$

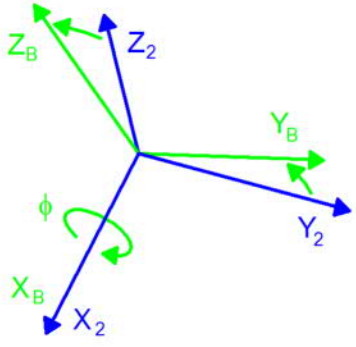

Figure.2.5: Rotation about the X_2 axis of the angle φ (roll)

The three successive coordinate system changes and in ZYX order lead to the coordinate system change matrix R that allows the passage from B (mobile) to E (fixed).

$$R(\eta) = R_z(\psi) \cdot R_y(\theta) \cdot R_x(\phi) \tag{2.6}$$

$$R(\eta) = \begin{bmatrix} c_\theta c_\psi & s_\phi s_\theta c_\psi - c_\phi s_\psi & c_\phi s_\theta c_\psi + s_\phi s_\psi \\ c_\theta s_\psi & s_\phi s_\theta s_\psi + c_\phi c_\psi & c_\phi s_\theta s_\psi - s_\phi c_\psi \\ -s_\theta & s_\phi c_\theta & c_\phi c_\theta \end{bmatrix} \tag{2.7}$$

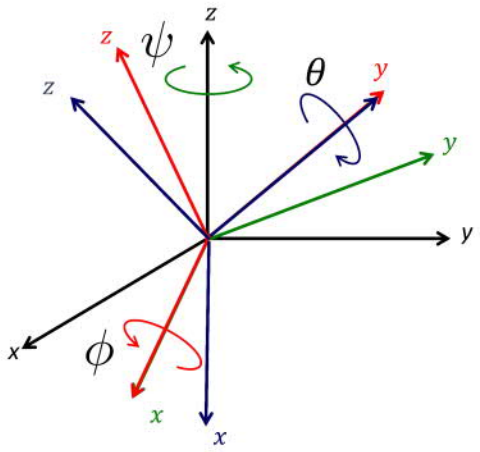

Figure.2.6: Euler Angles

with: $-\frac{\pi}{2} < \phi < \frac{\pi}{2}$ $-\frac{\pi}{2} < \theta < \frac{\pi}{2}$ $-\pi \le \psi \le \pi$

Rotation matrices belong to the *special orthogonal* group $SO(3)$. They check the following properties:

$$SO(3) = \left\{ R \in \mathbb{R}^{3\times 3} \,\middle|\, R^T R = R R^T = I_d, \det(R) = 1 \right\} \tag{2.8}$$

Thus, the matrix $R(\eta)$ having as inverse its transposed $R(\eta)^{-1} = R(\eta)^T$ and I_d is the identity matrix.

Like any three-parameter representation, Euler angles can show singularities of orientations. In order to counter the singularity problem, it is important to restrict roll and pitch angles such as: $|\phi| < \frac{\pi}{2}$ and $|\theta| < \frac{\pi}{2}$. This avoids extreme values $\pm\frac{\pi}{2}$ for which the behavior of the quadrotor is upset.

2.3 Quadrotor mathematical model

Before describing the mathematical model of a quadrotor, it is necessary to introduce the reference coordinates in which the structure and its location are described. For the quadrotor, it is possible to use two reference systems. The first $\{\Im = O; X, Y, Z\}$ is fixed and the second $\{\mathcal{B} = G; x_B, y_B, z_B\}$ is mobile. The fixed coordinate system, also called inertial, is a system where Newton's first law is considered valid.

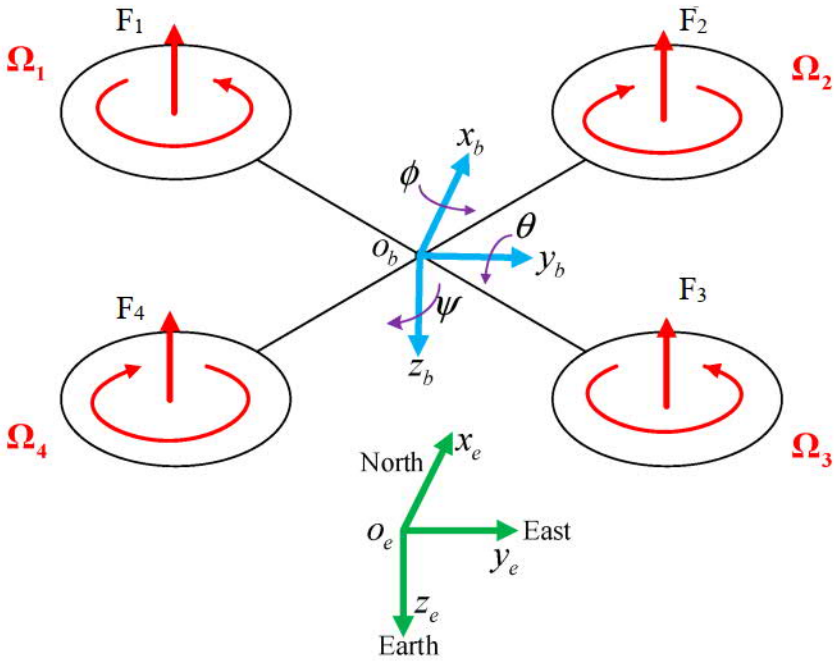

Figure.2.7: Structure of the quadrotor.

2.3.1 Kinematic modeling of the quadrotor

Kinematics is the part of mechanics that aims to mathematically describe the movements of different physical systems. Nevertheless, the causes of these movements are not taken into account. These causes are included as part of the dynamic.

The present modeling of the kinematics of the quadrotor vehicle consists in establishing the kinematic vectors of its translation as well as its rotation. Since the sensors are installed on the vehicle, the measurements provided are expressed in the moving coordinate system. For this purpose, it is convenient to give the vectors expressed in the inertial frame of reference according to those expressed in the local coordinate system.

Either:

$\dot{\xi} = (\dot{x}\ \dot{y}\ \dot{z})^T$: the linear speed of the quadrotor expressed in E

$V = (V_x\ V_y\ V_z)^T$: the linear speed of the quadrotor expressed in B

$\dot{\eta} = (\dot{\phi}\ \dot{\theta}\ \dot{\psi})^T$: the angular velocity of the quadrotor expressed in E

$\Omega = (\Omega_x\ \Omega_y\ \Omega_z)^T$: the angular velocity of the quadrotor expressed in B

A vector ${}^{\mathrm{B}}\mathrm{A}$ expressed in the coordinate B linked to the vehicle can be expressed in the inertia frame E , by a vector ${}^{E}\mathrm{A}$, using the rotation matrix R as follows :

$$ {}^{E}\mathrm{A} = R(\eta) \cdot {}^{\mathrm{B}}\mathrm{A} \tag{2.9} $$

However, the relationship between angular velocities is much less clear than the relationship between linear velocities and difficult to perceive. The derivatives of the vector $\eta = (\phi\ \theta\ \psi)^T$ are all expressed in different coordinate systems. Using the passage matrices, everything will be brought back to the local coordinate system.

$$ \begin{bmatrix} \Omega_x \\ \Omega_y \\ \Omega_z \end{bmatrix} = \begin{bmatrix} \dot{\phi} \\ 0 \\ 0 \end{bmatrix} + \begin{bmatrix} 1 & 0 & 0 \\ 0 & \mathrm{c}\phi & \mathrm{s}\phi \\ 0 & -\mathrm{s}\phi & \mathrm{c}\phi \end{bmatrix} \begin{bmatrix} 0 \\ \dot{\theta} \\ 0 \end{bmatrix} + \begin{bmatrix} \mathrm{c}\theta & 0 & -\mathrm{s}\theta \\ 0 & 1 & 0 \\ \mathrm{s}\theta & 0 & \mathrm{c}\theta \end{bmatrix} \begin{bmatrix} 1 & 0 & 0 \\ 0 & \mathrm{c}\phi & \mathrm{s}\phi \\ 0 & -\mathrm{s}\phi & \mathrm{c}\phi \end{bmatrix} \begin{bmatrix} 0 \\ 0 \\ \dot{\psi} \end{bmatrix} \tag{2.10} $$

Thus, the relationship between the angular velocities Ω and $\dot{\eta}$ can be expressed using the matrix $Q(\eta)$ given by:

$$ Q(\eta) = \begin{bmatrix} 1 & 0 & -\mathrm{s}\theta \\ 0 & \mathrm{c}\phi & \mathrm{s}\phi\mathrm{c}\theta \\ 0 & -\mathrm{s}\phi & \mathrm{c}\phi\mathrm{c}\theta \end{bmatrix} \tag{2.11} $$

Using matrices $R(\eta)$ and $Q(\eta)$, the motion of the quadrotor in space with respect to a fixed reference frame and thus characterized by the kinetic equations of translation and rotation

$$ \begin{aligned} \dot{\xi} &= R(\eta) \cdot V \\ \dot{\eta} &= Q^{-1}(\eta) \cdot \Omega \end{aligned} \tag{2.12} $$

It should be noted that for small values of angles, the matrix $Q(\eta)$ can be approximately simplified to the identity matrix. Thus, the Euler angle velocities are identical to the angular velocities in the moving coordinate $\Omega \approx \dot{\eta}$.

2.3.2 Dynamic modeling of the quadrotor

Dynamics is the other major part of mechanics that is interested in describing the causes of motion based on kinematic study.

The movement of the quadrotor having been characterized previously, it now remains the analysis of the mechanical actions likely to be exercised on the latter in order to produce this or that movement. This step makes it possible to establish the mathematical equations linking the accelerations of the quadrotor to the forces and moments exercised.

2.3.3 Mechanical actions

The **figure (2.8)** illustrates the diagram of a quadrotor. Despite the possibility of the plus shape $(+)$, the remainder-shaped configuration $(\times)$ is preferred [55] **Figure (2.8)**. The control of the rotational speeds of the blades allows the manipulation of movements of the quadrotor. It can be set in vertical motion (ascending/descending), propelled horizontally or laterally. Hover position control is achieved by maintaining a constant value of the total thrust force. The direction of rotation of each rotor is very unique. Two rotors of the same arm rotate in one direction while the other two rotate in the opposite direction. This involves cancelling the reactive moments and creating the desired yaw movement.

The maintenance in equilibrium or the production of the movement of a solid are mechanical phenomena that result from the mechanical actions exercised. In order to study the dynamics of the quadrotor, these actions acting on the structure of the machine will be classified into forces and torques.

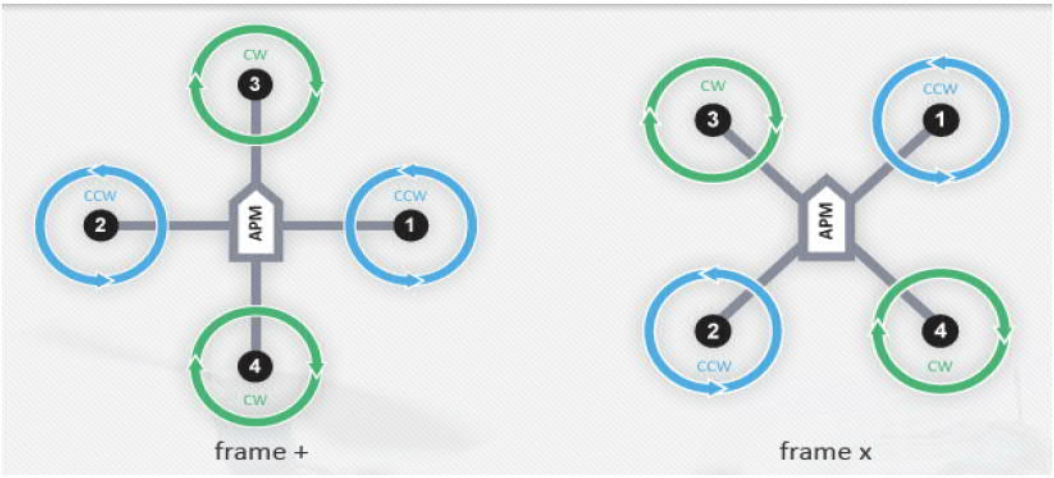

Figure.2.8: Quadrotor (+) Configuration and (x) Configuration.

a) Force of gravity

The weight of the quadrotor is the force having as its point of application its center of gravity, carried on the axis z_e and points towards the center of the earth. It is proportional to the value of the weight as follows:

$$P = -mgz_e \tag{2.13}$$

Where: m is the total mass and g is the intensity of gravity.

b) Lift force

Each of the four actuators produces a lift force proportional F_i to the square of its angular velocity ω_i. This force is perpendicular to the plane of the appropriate i propeller, and oriented in the direction of z_b. The **figure (2.7)** shows the four lift forces generated by the actuators of the quadrotor. According to Hamel and Mahony [56], F_i is given by:

$$F_i = k_f \omega_i^2 z_b \tag{2.14}$$

with: : $k_f > 0$ coefficient of lift.

ω_i: the rotational speed of the rotor $r_i (i = 1,2,3,4)$.

The total lift T, responsible for the movement of the quadrotor according to the different axes, is the sum of the four lift forces produced by each rotor. Taking into account the assumption that all actuators are identical, this force T is given by:

$$T = k_f \sum_{i=1}^{4} \omega_i^2 \; z_b \tag{2.15}$$

c) Drag force

It is a coupling between two forces acting on the system:

- The drag according to the three axes which is a force of aerodynamic resistance to the translation of the quadrotor:

$$F_D = -k_{da} \dot{\xi} \quad , (a = x, y, z) \quad , k_{da} > 0 \tag{2.16}$$

- The air resistance on the blades produces a drag force in the propellers. It opposes the rotation of the blades and parallels their plane of rotation. To this drag force correspond a moment of drag M_i. This anti-rotating moment therefore causes the

quadrotor to rotate around the axis z_b in the opposite direction to ω_i . The sign of M_i therefore depends on the direction of rotation of the actuator i.

$$M_i = -k_m \omega_i |\omega_i| z_b \tag{2.17}$$

With:

$k_d > 0$: the aerodynamic coefficient of drag in translation.

$k_m > 0$: the aerodynamic coefficient of drag depending, mainly, on the aerodynamic properties of the propellers and the geometry of the blade.

d) Active couples

The vector of the active torques results from the sum of the moments of lift and drag generated by the rotors by the action of the area on the blades. It is therefore expressed as follows:

$$\tau_a = \sum_{i=1}^{4} \left(\vec{l}_i \wedge \vec{F}_i \right) + \sum_{i=1}^{4} M_i \Rightarrow \tau_a = \begin{pmatrix} \tau_x \\ \tau_y \\ \tau_z \end{pmatrix} = \begin{pmatrix} l(F_2 - F_4) \\ l(F_3 - F_1) \\ \sum_{i=1}^{4} M_i \end{pmatrix} \tag{2.18}$$

$\vec{l}_i$ being the position of the center of the rotor r_i in the coordinate B and l are the arm of a rotor.

The active roll τ_x and pitch torques τ_y are responsible for rotating the quadrotor around the axes x_b and y_b, respectively. They result from the difference between two lift forces of the same arm (F_2, F_4) and (F_1, F_3), respectively. Thus,

$$\tau_x = l(F_2 - F_4) = l k_f (\omega_2^2 - \omega_4^2) \tag{2.19}$$

$$\tau_y = l(F_3 - F_1) = l k_f (\omega_3^2 - \omega_1^2) \tag{2.20}$$

The active yaw torque τ_z makes it possible to rotate the quadrotor around the axis z_b. This torque results from the combination of drag moments of the four rotors. We have chosen a counter-clockwise direction of rotation for the rotors r_1 and r_3, therefore they produce moments M_1 and M_3 negatives resistant to yaw movement. On the other hand, the rotors r_2 and r_4 rotate in the opposite direction which is the negative direction of yaw

$(-\psi)$ and produce moments M_2 and M_4 positive drive the quadrotor in rotation in the positive direction of yaw $(+\psi)$. According to the positive direction of the yaw chosen on the **figure (2.7),** the couple τ_ψ is written as follows:

$$\tau_z = \sum_{i=1}^{4} M_i = k_m \left(\sum_{i=1}^{2} \omega_{2i}^2 - \sum_{i=1}^{2} \omega_{2i-1}^2\right) \tag{2.21}$$

Which is like writing:

$$\tau_z = k_m \sum_{i=1}^{4} (-1)^i \omega_i^2 \tag{2.22}$$

e) Aerodynamic resistance torque to rotation:

When it comes to rotary motion, rotational resistance torque τ_D is the analogue of aerodynamic resistance in translation. It is given by:

$$\tau_D = -k_{db}\Omega^2 \quad ,(b = \phi, \theta, \psi) \tag{2.23}$$

with, k_{db} is the coefficient of aerodynamic friction.

f) Gyroscopic couples

Each rotor r_i is considered to be a rigid disk rotating at speed ω_i around its vertical axis $z_{ri} = z_b$. The rotor undergoes the rotations of the fuselage which induces the change in the direction of its axis of rotation. To resist this change, the rotor exerts a torque called gyroscopic torque. The sum of these four gyroscopic couples gives the torque τ_{gr} exerted on the quadrotor. It has the expression [57]:

$$\tau_{gr} = \sum_{i=1}^{4} I_r (\Omega \wedge z_b)(-1)^{i+1} \omega_i \tag{2.24}$$

with: I_r the inertia of the rotor.

Indeed, there is also another gyro torque applied to the quadrotor. This second type of gyroscopic effect is due to the angular movements of the vehicle body τ_{gq}.

$$\tau_{gq} = \Omega \wedge I\Omega \tag{2.25}$$

2.3.3.1 The dynamics of translation and rotation

As detailed in [58] the dynamics of a rigid body subjected to external forces and couples can be expressed by applying the Newton-Euler formalism.

$$\begin{aligned} m\dot{V} + \Omega \wedge mV &= F \\ I\dot{\Omega} + \Omega \wedge I\Omega &= \tau \\ \dot{R}(\eta) &= R(\eta) \cdot sk(\Omega) \end{aligned} \tag{2.26}$$

F and τ are respectively the forces and torques applied to the center of mass of the quadrotor and expressed in its local coordinate system B. $I \in \Re^{3\times3}$ is the inertia matrix around the center of mass and also given in the local coordinate system B. It characterizes the difficulty of putting the body in rotational movements.

The first equation in Eq(2.26) represents the dynamics of translation. This dynamic equation of Newton is independent of the rotational motion of the quadrotor because we use its center of mass to determine its position.

By deriving the first kinematic equation in Eq(2.12) and replacing the expression of the derivative of the rotation matrix $\dot{R}(\eta)$ from (2.26), the vector of linear accelerations $\ddot{\xi}$ is written as:

$$\ddot{\xi} = R(\eta) \cdot sk(\Omega) \cdot V + R(\eta) \cdot \dot{V} \tag{2.27}$$

By replacing $\dot{V}$ with its expression deduced from Newton's equation in (2.26), we obtain:

$$m\ddot{\xi} = R(\eta)F \tag{2.28}$$

The term $R(\eta)F$ transforms the forces expressed in the moving coordinate system into forces expressed in the inertial frame of reference. What amounts to writing

$$m\ddot{\xi} = R(\eta)T + P + F_D \tag{2.29}$$

By replacing the forces with their expressions (2.13), (2.15) and (2.16), the translation dynamics of the quadrotor expressed in the reference frame is given by the following differential equations: I

$$\begin{bmatrix} \ddot{x} \\ \ddot{y} \\ \ddot{z} \end{bmatrix} = \frac{1}{m} \begin{bmatrix} c_\phi s_\theta c_\psi + s_\phi s_\psi \\ c_\phi s_\theta s_\psi - s_\phi c_\psi \\ c_\phi c_\theta \end{bmatrix} U_z - \begin{bmatrix} 0 \\ 0 \\ g \end{bmatrix} - \frac{1}{m} \begin{bmatrix} k_{dx}\dot{x} \\ k_{dy}\dot{y} \\ k_{dz}\dot{z} \end{bmatrix} \tag{2.30}$$

Similarly, equations describing the dynamics of rotational motion can be derived using the second equation given by Eq(2.26). One of the main characteristics of the quadrotor is its symmetry, therefore, the inertia matrix is diagonal with. $I_x = I_y$

$$I = \begin{bmatrix} I_x & 0 & 0 \\ 0 & I_y & 0 \\ 0 & 0 & I_z \end{bmatrix} \tag{2.31}$$

Note that the gyroscopic moment due to the rotational movement of the quadrotor is included in the Euler equation describing this dynamic. By replacing the given moments with their expressions Eq(2.18), Eq(2.23) and Eq(2.24) in this same equation, the rotation dynamics is formulated as follows:

$$\begin{bmatrix} \dot{\Omega}_x \\ \dot{\Omega}_y \\ \dot{\Omega}_z \end{bmatrix} = \frac{1}{I}\begin{bmatrix} (I_y - I_z)\Omega_y\Omega_z \\ (I_z - I_x)\Omega_x\Omega_z \\ (I_x - I_y)\Omega_x\Omega_y \end{bmatrix} - \frac{1}{I}\begin{bmatrix} I_r\Omega_y\varpi \\ -I_r\Omega_x\varpi \\ 0 \end{bmatrix} + \frac{1}{I}\begin{bmatrix} U_\phi \\ U_\theta \\ U_\psi \end{bmatrix} - \frac{1}{I}\begin{bmatrix} k_{d\phi}\Omega_x^{\,2} \\ k_{d\theta}\Omega_y^{\,2} \\ k_{d\psi}\Omega_z^{\,2} \end{bmatrix} \tag{2.32}$$

Where:

$$\begin{aligned} \varpi &= \sum_{i=1}^{4}(-1)^{i+1}\omega_i \\ U_\phi &= \tau_x \\ U_\theta &= \tau_y \\ U_\psi &= \tau_z \end{aligned} \tag{2.33}$$

It is also worth noting:

$$\begin{aligned} u_x &= c_\phi s_\theta c_\psi + s_\phi s_\psi \\ u_y &= c_\phi s_\theta s_\psi - s_\phi c_\psi \end{aligned} \tag{2.34}$$

These two equations represent the coupling between longitudinal/lateral displacement and quadrotor orientation.

After calculation of the vector $\dot{\Omega}_{x,y,z}$, it can be written in the form:

$$\dot{\Omega}_{x,y,z} = \begin{bmatrix} \dot{\Omega}_x \\ \dot{\Omega}_y \\ \dot{\Omega}_z \end{bmatrix} = \begin{bmatrix} \ddot{\phi} \\ \ddot{\theta} \\ \ddot{\psi} \end{bmatrix} \tag{2.35}$$

By combining the dynamic relationships Eq(2.30) and Eq(2.32) previously established and applying the approximation of small angles, we derive the complete

dynamic model at 6 DDL from a quadrotor with configuration (+) having two planes of symmetry (x_b, z_b) and (y_b, z_b).

$$\begin{cases} \ddot{x} = \frac{1}{m}\left(u_x U_z - k_{dx}\dot{x}\right) \\ \ddot{y} = \frac{1}{m}\left(u_y U_z - k_{dy}\dot{y}\right) \\ \ddot{z} = \frac{1}{m}\left(c_\phi c_\theta U_z - k_{dz}\dot{z} - mg\right) \\ \ddot{\phi} = \frac{1}{I_x}\left[(I_y - I_z)\dot{\theta}\dot{\psi} - I_r\varpi\dot{\theta} + U_\phi - k_{d\phi}\dot{\phi}^2\right] \\ \ddot{\theta} = \frac{1}{I_y}\left[(I_z - I_x)\dot{\phi}\dot{\psi} + I_r\varpi\dot{\phi} + U_\theta - k_{d\theta}\dot{\theta}^2\right] \\ \ddot{\psi} = \frac{1}{I_z}\left[(I_x - I_y)\dot{\phi}\dot{\theta} + U_\psi - k_{d\psi}\dot{\psi}^2\right] \end{cases} \tag{2.36}$$

2.4 State representation

Considering the n quadrotor state variables collected in the vector $X = [x_1\ x_2\ x_3\ \ldots\ x_{12}]^T$, $X \in \mathbb{R}^n$.

Either:

$$X = [x\ \dot{x}\ y\ \dot{y}\ z\ \dot{z}\ \phi\ \dot{\phi}\ \theta\ \dot{\theta}\ \psi\ \dot{\psi}]^T \tag{2.37}$$

Therefore, model Eq(2.36) can be represented in the state space $\dot{X} = f(X,t) + g(X,t)U(t)$ as follows:

$$\begin{cases} \dot{x}_1 = x_2 \\ \dot{x}_2 = f_2(X,t) + g_2(X,t)u_x \\ \dot{x}_3 = x_4 \\ \dot{x}_4 = f_4(X,t) + g_4(X,t)u_y \\ \dot{x}_5 = x_6 \\ \dot{x}_6 = f_6(X,t) + g_6(X,t)U_z \\ \dot{x}_7 = x_8 \\ \dot{x}_8 = f_8(X,t) + g_8(X,t)U_\phi \\ \dot{x}_9 = x_{10} \\ \dot{x}_{10} = f_{10}(X,t) + g_{10}(X,t)U_\theta \\ \dot{x}_{11} = x_{12} \\ \dot{x}_{12} = f_{12}(X,t) + g_{12}(X,t)U_\psi \end{cases} \tag{2.38}$$

Where functions $f_i(X,t)$ and $g_i(X,t)$, $i \in (2,4,6,8,10,12)$ can be easily identified from (2.36). $U \in \mathbb{R}^p$ is the vector that represents the control. We come back to this control vector in the next chapter.

$$
\begin{aligned}
f_2(X,t) &= -\frac{1}{m} k_{dx} x_2 & g_2(X,t) &= \frac{1}{m} U_z \\
f_4(X,t) &= -\frac{1}{m} k_{dy} x_4 & g_4(X,t) &= \frac{1}{m} U_z \\
f_6(X,t) &= -\frac{1}{m} (k_{dz} x_6 + mg) & g_6(X,t) &= \frac{1}{m} c_\phi c_\theta \\
f_8(X,t) &= \frac{1}{I_x} \left[(I_y - I_z) x_{10} x_{12} - I_r \varpi x_{10} - k_{d\phi} x_8^2 \right] & g_8(X,t) &= \frac{1}{I_x} \\
f_{10}(X,t) &= \frac{1}{I_y} \left[(I_z - I_x) x_8 x_{12} + I_r \varpi x_8 - k_{d\theta} x_{10}^2 \right] & g_{10}(X,t) &= \frac{1}{I_y} \\
f_{12}(X,t) &= \frac{1}{I_z} \left[(I_x - I_y) x_8 x_{10} - k_{d\psi} x_{12}^2 \right] & g_{12}(X,t) &= \frac{1}{I_z}
\end{aligned}
\qquad (2.39)
$$

2.5 Conclusion

In this chapter, two main parts have been discussed. Firstly, an overall description of the operation principle of the quadrotor was presented. Also, the physical phenomena acting on his behavior were studied. Next, the Euler-Newton formalism was used for the purpose of establishing a complete dynamic model of the quadrotor. This model showed a non-linear, coupled and under-actuated nature. The main objective is to give a mathematical description concepts to obtain the dynamic model of the quadrotor vehicle, in the last decade most research's in robotics, especially in drones, have rely on the convention of Euler Angles. Moreover, this modeling of the quadrotor dynamics will enable us to design a controller, the synthesis of control laws will be discussed in the next chapter.

Reference :

[54] E. Walter, L. Pronzato, Identification de modèles paramétriques à partir de données exprimentales, édition Elsevier/Masson, 1994.
[55] H. L. Chan and K. T. Woo, Design and control of small quadcopter system with motor closed loop speed control, *International Journal of Mechanical Engineering and Robotics Research*, vol.4, no.4, pp.287-292, 2015.
[56] R. Mahony and T. Hamel, Adaptive compensation of aerodynamic effects during takeoff and landing maneuvers for a scale model autonomous helicopter, *European Journal of Control*, vol.7, no.1, pp. 43-57, 2001.

[57] F. Guerrero Castellanos, Estimation de l'attitude et commande bornée en attitude d'un corps rigide : Application à un mini hélicoptère à quatre rotors. Thèse doctorat, Université Joseph Fourier - Grenoble I, 2008.
[58] T. Hamel, R. Mahony, R. Lozano, et al., Dynamic modelling and configuration stabilization for an X4-flyer, *IFAC Proceedings Volumes*, vol. 35, no. 1, p. 217-222, , 2002.

CHAPTER 3

Unmanned Aerial Vehicle (UAV) Quadrotor Based On SC-PSO Technique

3.1 Introduction

There is always a difference between the mathematical process model and reality. This difference is due to neglected environmental phenomena during modeling and errors in the precision of model parameter values. With the complexity of new industrial installations, conventional controllers become powerless and usually give less efficient results. To overcome this problem, the current research trend is towards robust nonlinear controls that give acceptable results in large operating domains. Among these techniques, we find sliding mode control, which has long been the subject of several research works, alone or in hybridization with other control techniques. Sliding mode control contains a discontinuous term that can cause chattering. The main reasons for this phenomenon are actuator limitations or switching delays at the control. This drawback theoretically does not affect performance in any way, but it can be harmful to certain system components (actuator, mechanical elements, etc.) such as drone quadrotor. Thus, the main

contributions on sliding mode controls in recent years concern the reduction of chattering. Control by synergetic, is another non-linear control technique which is also considered robust, the stability of the synthesis control is done based on the approach of Lyapunov. To further enhance the performance of the system, a particle swarm optimization (PSO) technique is used to optimally tune the controller's parameters.

In this chapter a comparative study between non-linear controller strategies the PID, SMC and the proposed method **SC-PSO**) to overcome the quadrotor plane tracking path problem in the workspace (Empty three-dimensional 3D room). the comparisons about these control strategies are done by MATLAB/Simulink environment to evaluate the results of **PID**, **SMC** and **SC-PSO** controllers against each other, The effectiveness of the suggested **SC-PSO** approach has been proved by a **H**ardware-In-the-**L**oop (**HIL**) Simulink Real-Time testing method using two PC (**MATLAB/Simulink®** environment) equipped with two dSPACE 1104 card for several operating conditions.

3.2 Control design of quadrotor

The X4-flyer is an under actuated system with four inputs vs six outputs, and strongly coupled. So, the control of the position and the attitude is achieved through two cascade loops and a correction block. The inner loop is designed in order to ensure the asymptotic convergence of the attitude and altitude motions to their desired values ϕ^*, θ^*, ψ^* and z^*. On the other hand, the outer loop is devoted to the control of the longitudinal and lateral motions. The outer loop has as inputs the desired positions x^* and y^*chosen directly by the user as well as the altitude controller **Uz**. It provides the corresponding desired controllers **Ux** and **Uy**. These latter serve as inputs for the correction block that adjusts the desired roll and pitch rotations ϕ^* and θ^* according to the desired yaw ψ^* (**Figure (3.1)**). The obtained values of the desired roll and pitch angles are used as inputs for the inner loop where the desired yaw and desired altitude remain as assigned.

Let us define **Ux** and **Uy** as virtual inputs **Eq(3.1).**

$$\begin{cases} U_x = \left(c\phi s\theta c\psi + s\phi s\psi\right) \\ U_y = \left(c\phi s\theta s\psi - s\phi c\psi\right) \end{cases} \tag{3.1}$$

Then, the correction block aims at finding $\boldsymbol{\phi}^*$ and $\boldsymbol{\theta}^*$ corresponding to **Ux** and **Uy** by using **Eq(3.1)** as follow:

$$\begin{cases} \phi^d = arcsin\left(U_x \sin\left(\psi^d\right) - U_y \cos\left(\psi^d\right)\right) \\ \theta^d = arcsin\left(\dfrac{U_x \cos\left(\psi^d\right) + U_y \, sin\left(\psi^d\right)}{\cos\left(\phi^d\right)}\right) \end{cases} \tag{3.2}$$

The scheme in **Figure (3.1)** shows the control strategy for $(U_x, U_y, U_z, U_\phi, U_\theta, U_\psi)$ and **Figure (3.2)** demonstration the correction block in simulink**.**

The differential equations form of nonlinear dynamic for quadrotor (UAV) system is given by the **Eq(3.3).** Considering the ***n*** quadrotor state variables collected in the vector $X = [x_1\ x_2\ x_3\ \ldots\ x_{12}]^T \Leftrightarrow X = [x\ \dot{x}\ y\ \dot{y}\ z\ \dot{z}\ \phi\ \dot{\phi}\ \theta\ \dot{\theta}\ \psi\ \dot{\psi}]^T$, $X \in \mathbb{R}^n$.

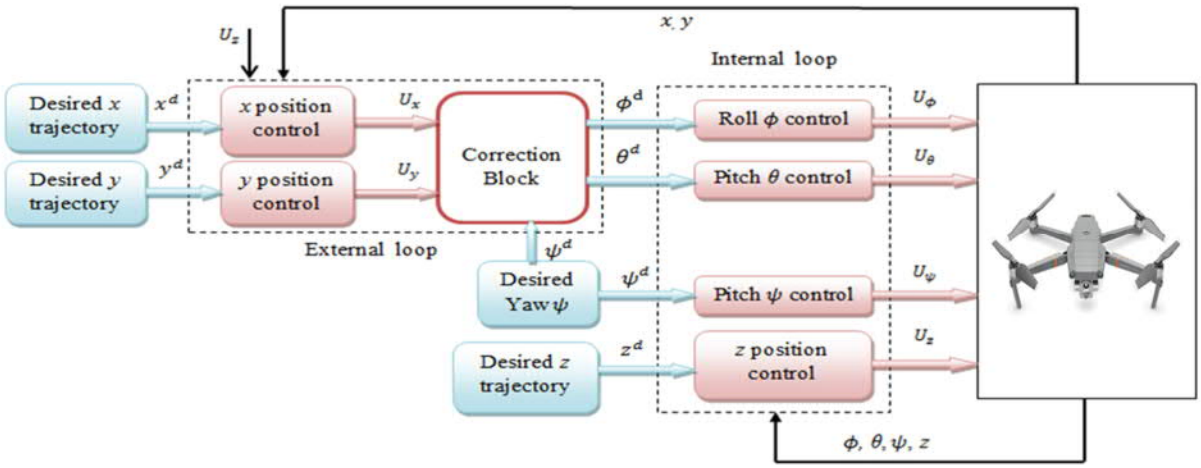

Figure.3. 1: Synoptic scheme of the adopted control system.

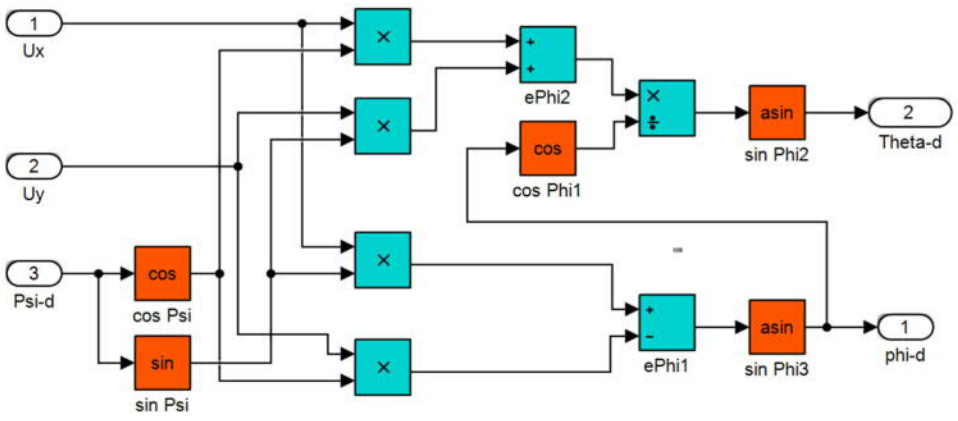

Figure.3. 2: The correction block

$$\begin{cases} \dot{x}_1 = x_2 \\ \dot{x}_2 = f_2(X,t) + g_2(X,t)u_x \\ \dot{x}_3 = x_4 \\ \dot{x}_4 = f_4(X,t) + g_4(X,t)u_y \\ \dot{x}_5 = x_6 \\ \dot{x}_6 = f_6(X,t) + g_6(X,t)U_z \\ \dot{x}_7 = x_8 \\ \dot{x}_8 = f_8(X,t) + g_8(X,t)U_\phi \\ \dot{x}_9 = x_{10} \\ \dot{x}_{10} = f_{10}(X,t) + g_{10}(X,t)U_\theta \\ \dot{x}_{11} = x_{12} \\ \dot{x}_{12} = f_{12}(X,t) + g_{12}(X,t)U_\psi \end{cases} \tag{3.3}$$

$$f_2(X,t) = -\frac{1}{m}k_{dx}x_2 \qquad g_2(X,t) = \frac{1}{m}U_z$$

$$f_4(X,t) = -\frac{1}{m}k_{dy}x_4 \qquad g_4(X,t) = \frac{1}{m}U_z$$

$$f_6(X,t) = -\frac{1}{m}(k_{dz}x_6 + mg) \qquad g_6(X,t) = \frac{1}{m}c_\phi c_\theta$$

$$f_8(X,t) = \frac{1}{I_x}\left[(I_y - I_z)x_{10}x_{12} - I_r\varpi x_{10} - k_{d\phi}x_8^2\right] \qquad g_8(X,t) = \frac{1}{I_x}$$

$$f_{10}(X,t) = \frac{1}{I_y}\left[(I_z - I_x)x_8x_{12} + I_r\varpi x_8 - k_{d\theta}x_{10}^2\right] \qquad g_{10}(X,t) = \frac{1}{I_y}$$

$$f_{12}(X,t) = \frac{1}{I_z}\left[(I_x - I_y)x_8x_{10} - k_{d\psi}x_{12}^2\right] \qquad g_{12}(X,t) = \frac{1}{I_z}$$

3.2.1 Classic control by PID

In robotics, the PID regulator represents the basis of control, even if other algorithms offer better performance. The reasons for this success are mainly the simple structure, the good performance for a wide range of processes and the fact that it is adjustable even without a specific model of the controlled system. Due to its simplicity, PID controllers can be manufactured with a variety of technologies: electronic, mechanical, pneumatic, hydraulic, analog and digital. This implies high commercial

availability, which enables the realization of complex control schemes in a short time and at low cost.

3.2.1.1 PID Regulator Model

PID is a linear system control method. Traditionally, its structure is introduced on the basis of empirical considerations that the control variable ***u*** should be generated as the sum of three control terms which are: the proportional, integral and derivative component. Each controller has a different task to improve the dynamic response of the controlled system.

The relationship between the control law u and the deviation e is as follow

$$u(t) = k_P e(t) + k_I \int_0^t e(\tau) d\tau + k_D \frac{de(t)}{dt} \tag{3.4}$$

Where ***e*** is the error between the reference value and the output of the process. ***u*** is the control signal. $\mathbf{k_p}$, $\mathbf{k_i}$ and $\mathbf{k_D}$ are positive or zero constants. The coefficient $\mathbf{k_p}$ is called the coefficient of the proportional action, while $\mathbf{k_i}$ and $\mathbf{k_D}$ are respectively the coefficient of the integral action and the coefficient of the derivative action.

Using the PID controller requires the parameters to achieve the desired response. Some tuning methods can be used, such as: Trial-Error and Ziegler-Nichols. Optimization methods are also developed to obtain the optimal value of the PID constants: fuzzy logic, genetic algorithm and optimization by particle swarm.

The first contribution (P) of the PID structure, intuitive in meaning, operates the system proportionally to the error between the actual operation (process variable) and the desired setpoint. In fact, the relative simplicity of control is not without flaws. If the relative gain is set too low, the system response becomes slow. Conversely, if the gain is too high, the system will react quickly to errors, but will experience oscillations around the desired point. The introduction of two additional contributions, the integral action (I) and the derivative action (D), allows us to more completely define the desired properties of the control system. The integral part examines the global error in steady state. It varies with the integral of the error. Although this component increases overshoot and stabilization time, it has a unique property: it eliminates steady-state error. The derivative part (D) varies according to the derivative of the error. This component reduces overshoot and stabilization time. Together, these gains make up the extremely popular PID (Proportional, Integral, Derivative) controller.

By using the Laplace transform to the equation (3.1), we can easily determine the classic PID transfer function as follows[22]:

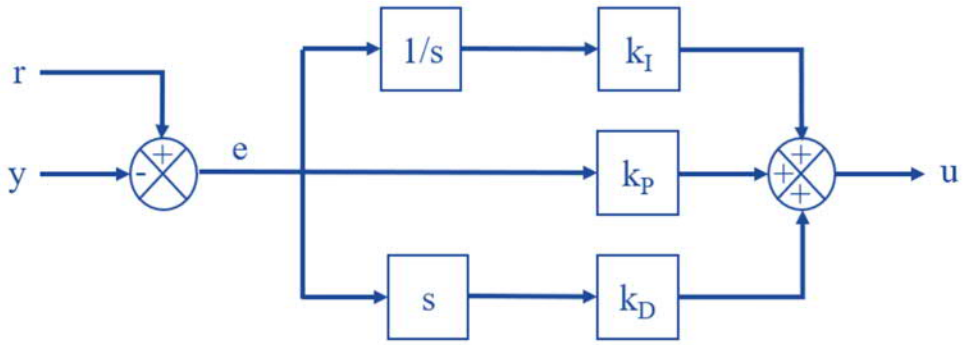

Figure.3. 3: Structure of the conventional PID

The noted reference **r** is in fact the desired value for the process variable **y** (system output). This reference signal is compared via negative feedback to the measured output.

The result of this comparison is the error signal **(e)**, which is the input to the controller. The controller takes care of forcing this error signal to zero by use of the proportional, integral, and derivative controls described earlier (or by other mechanisms if a different controller architecture is used). The controller then outputs an appropriate signal **u** as input to the system **u** with the idea that **y** will conduct more towards **r**, thus decreasing the amplitude of **e**.

A different representation of the PID than **eq(3.1)** can be more used

$$u(s) = k_P\left(1 + \frac{1}{T_I s} + T_D s\right)e(s) \tag{3.5}$$

and in winch, $T_I = {k_P}/{k_I}$ et $T_D = {k_D}/{k_P}$.

3.2.2 Synthesis of the sliding mode control law for the quadrotor

The basic idea of the SMC is first to attract the tracking errors of the system's state variables into a suitably selected region $\sigma(X,\ t) = 0$ [7,8], then design a control law $\mathbf{U_{sw}}$ that always maintains the system in that region. In summary, an **SMC** consists of two parts like in Eq(1.1). The equivalent control $\mathbf{U_{eq}}$ is determined by the model of the system. It is designed with the equivalent control method, whose principle is based on the determination of the system behavior when it is on the sliding surface S.

Take, for example, the altitude equation:

$$\dot{x}_5 = x_6$$
$$\dot{x}_6 = f_6(x,t) + g_6(x,t)U_z = -\frac{1}{m}(k_{dz}x_6 + mg) + \frac{1}{m}\cos\phi\ \cos\theta\ U_z \tag{3.6}$$

The control objective is to force the output **Z** towards a reference trajectory **Z*.** The relative degree with respect to the error $e_z = z - z^*$ is equal to 2, satisfying **Assumption 1.1**. Then, following Eq(1.5), define the sliding variable as:

$$\sigma_z = \dot{e}_z + c_z e_z \tag{3.7}$$

with $c_z > 0$. Then, the sliding surface is given by:

$$S = \left\{ x \in \mathrm{X} \mid \sigma_z = \dot{e}_z + c_z e_z = 0 \right\} \tag{3.8}$$

We start by determining the equivalent order U_{zeq}, it is calculated when:

$$\sigma_z = 0 \text{ and } \dot{\sigma}_z = 0 \tag{3.9}$$

The relative degree of the altitude equation Eq(3.6) with respect to σ is equal to 1 and has the following Equation

$$\dot{\sigma}_z = \ddot{e}_z + c_z\dot{e}_z = \dot{x}_6 - \ddot{x}_5^{\,*} + c_z\dot{e}_z \tag{3.10}$$

By replacing Eq(3.6) in Eq(3.10) we find

$$\begin{aligned} \dot{\sigma}_z &= f_6(x,t) - \ddot{x}_5^{\,*} + c_z\dot{e}_z + g_6(x,t)U_z \\ \dot{\sigma}_z &= \bar{a}(x,t) + \bar{b}(x,t)u \end{aligned} \tag{3.11}$$

which is of the form of Eq(1.7) satisfying **Assumption 1.2**.
From Eq(3.8) and Eq(3.9) we find

$$\dot{x}_6 - \ddot{x}_5^{\,*} + c_z\left(x_6 - \dot{x}_5^{\,*}\right) = 0 \tag{3.12}$$

U_{zeq} it is calculated when $\dot{\sigma}_z = 0$, From Eq(3.11) we obtain

$$U_{zeq} = \frac{1}{g_6(x,t)}\left[\ddot{x}_5^{\,*} - f_6(x,t) - c_z\left(x_6 - \dot{x}_5^{\,*}\right)\right] \tag{3.13}$$

$$U_{zeq} = \frac{m}{\cos x_7 \cos x_9}\left[\ddot{x}_5^{\,*} + \frac{k_{dz}}{m}x_6 + g_6 - c_z\left(x_6 - \dot{x}_5^{\,*}\right)\right] \tag{3.14}$$

As previously indicated Eq(1.1), the control law is formed by two terms, the equivalent control law and the switching control law:

$$U_z = U_{zsw} + U_{zeq} \tag{3.15}$$

The equivalent part is a continuous control law deduced from $\frac{\partial \sigma_z(e,t)}{\partial t} = \dot{\sigma}_z(e,t) = 0$ and the second control part us has a discontinuous U_{zsw} feature defined as in chapter 1:

$$U_{zsw} = -k_3 sign(\sigma_z) \tag{3.16}$$

where K_3 is a positive constant and sign is the sign function.

Consequently

$$\begin{aligned} U_z &= -k_3 sign(\sigma_z) + \frac{1}{g_6(x,t)}\left[\ddot{x}_5^{\,*} - f_6(x,t) - c_z\left(x_6 - \dot{x}_5^{\,*}\right)\right] \\ U_z &= -k_3 sign(\sigma_z) + \frac{m}{\cos x_7 \cos x_9}\left[\ddot{x}_5^{\,*} + \frac{k_{dz}}{m}x_6 + g - c_z\left(x_6 - \dot{x}_5^{\,*}\right)\right] \end{aligned} \tag{3.17}$$

Considering the sliding variable σ_z Eq(3.7), a Lyapunov function candidate satisfying **Definition 1.2** takes the following form

$$V(x,t) = \frac{1}{2}\sigma_z^2(x,t) \tag{3.18}$$

In order to ensure the asymptotic convergence of the sliding variable σ_z, the time derivative of **V** has to be negative definite i.e. Therefore, the derivative of the function **Eq(3.18)** is:

$$\dot{V}(x,t) = \sigma_z(x,t)\ \dot{\sigma}_z(x,t) \tag{3.19}$$

In order for the function $\dot{V}(x,t)$ to decrease, it is sufficient to ensure that its derivative is negative. This is only true if condition Eq(3.19) is satisfied.

$$\sigma_z(x,t)\ \dot{\sigma}_z(x,t) < 0 \tag{3.20}$$

By emplacing Eq(3.11) in Eq(3.19) we obtain

$$\dot{V}(x,t) = \sigma_z(x,t)\ \left[f_6(x,t) - \ddot{x}_5^{\,*} + c_z\dot{e}_z + g_6(x,t)U_z \right] \tag{3.21}$$

By emplacing Eq(3.17) in Eq(3.21) we obtain

$$\dot{V}(x,t) = \sigma_z(x,t) \begin{bmatrix} f_6(x,t) - \ddot{x}_5^{\,*} + c_z\dot{e}_z \\ +g_6(x,t)\left[-k_3 sign(\sigma_z) + \dfrac{1}{g_6(x,t)}\left[\ddot{x}_5^{\,*} - f_6(x,t) - c_z\dot{e} \right] \right] \end{bmatrix}$$

$$\dot{V}(x,t) = \sigma_z(x,t)\ \left[f_6(x,t) - \ddot{x}_5^{\,*} + c_z\dot{e}_z + \ddot{x}_5^{\,*} - f_6(x,t) - c_z\dot{e} - g_6(x,t)k_3 sign(\sigma_z) \right] \tag{3.22}$$

$$\dot{V}(x,t) = \sigma_z(x,t)\ \left[-g_6(x,t)k_3 sign(\sigma_z) \right]$$

$$-g_6(x,t)k_3 sign(\sigma_z) < 0 \quad \Rightarrow \dot{V}(x,t) < 0$$

Note that

$$g_6(x,t) = \frac{m}{\cos\phi\ \cos\theta} > 0, \quad m > 0 \quad and \quad 0 \le \phi,\theta \le \frac{\pi}{2} \Rightarrow \cos\phi\ \cos\theta\ > 0$$

$$and \quad k_3 > 0$$

$$-sign(\sigma_z) < 0 \Rightarrow -|\sigma_z| < 0$$

Therefore, under the controllers, the subsystem state trajectories can reach, and, thereafter, stay on the manifold S=0 in finite-time.

The equations Eq(3.18), explains that the square of the distance between a given point of the phase plane and the sliding surface expressed by $\sigma_z^2(x,t)$ decreases all the time, i.e. the state system will be attracted to the sliding surface, hence the name of attractivity.

Form Eq. (3.22) it can be found that $\dot{V}(x,t) < 0$. On the basis of Lyapunov theory, the stability of the quadrotor system is assured via the SMC control law. The same procedure must be followed in order to extract $u_x, u_y, U_\phi, U_\theta$ and U_ψ.

the errors of etch state variables are defined as below:

$$\begin{cases} e_x = x_1 - x_1^* = x - x^* \\ e_y = x_3 - x_3^* = y - y^* \\ e_\phi = x_7 - x_7^* = \phi - \phi^* \\ e_\theta = x_9 - x_9^* = \theta - \theta^* \\ e_\psi = x_{11} - x_{11}^* = \psi - \psi^* \end{cases} \tag{3.23}$$

the sliding variable are chosen as follows:

$$\begin{cases} \sigma_x = \dot{e}_x + c_x e_x \\ \sigma_y = \dot{e}_y + c_y e_y \\ \sigma_\phi = \dot{e}_\phi + c_\phi e_\phi \\ \sigma_\theta = \dot{e}_\theta + c_\theta e_\theta \\ \sigma_\psi = \dot{e}_\psi + c_\psi e_\psi \end{cases} \tag{3.24}$$

with $c_x, c_y, c_\phi, c_\theta, c_\psi > 0$. The controllers are designed as follows:

$$\begin{aligned} u_x &= -k_1 sign(\sigma_x) + \frac{m}{U_z}\left[\ddot{x}_1^* + \frac{k_{dx}}{m}x_2 + c_x\left(x_2 - \dot{x}_1^*\right)\right] \\ u_y &= -k_2 sign(\sigma_y) + \frac{m}{U_z}\left[\ddot{x}_3^* + \frac{k_{dy}}{m}x_4 + c_y\left(x_4 - \dot{x}_3^*\right)\right] \\ U_\phi &= -k_4 sign(\sigma_\phi) + I_x\left[\ddot{x}_7^* - \frac{\left(I_y - I_z\right)}{I_x}x_{10}x_{12} + \frac{I_r\bar{\omega}}{I_x}x_{10} + \frac{k_{d\phi}}{I_x}{x_8}^2 + c_\phi\left(x_8 - \dot{x}_7^*\right)\right] \\ U_\theta &= -k_5 sign(\sigma_\theta) + I_y\left[\ddot{x}_9^* - \frac{\left(I_z - I_x\right)}{I_y}x_8x_{12} - \frac{I_r\bar{\omega}}{I_y}x_8 + \frac{k_{d\theta}}{I_y}{x_{10}}^2 + c_\theta\left(x_{10} - \dot{x}_9^*\right)\right] \\ U_\psi &= -k_6 sign(\sigma_\psi) + I_z\left[\ddot{x}_{11}^* - \frac{\left(I_x - I_y\right)}{I_z}x_8x_{10} + \frac{k_{d\psi}}{I_z}{x_{12}}^2 + c_\psi\left(x_{12} - \dot{x}_{11}^*\right)\right] \end{aligned} \tag{3.25}$$

where K_1, k_2, k_4, k_5 and k_6 are a positive constants and **sign** is the sign function.

3.2.3 Design of synergetic control law for the quadrotor

The basic procedure of synergetic control synthesis for quadrotor is shown below. The choice of function of the system state variables (macro-variable) $\psi = \psi(x,t)$ is the first step to design the synergetic controller's synthesis.

$$\dot{x} = f(x,t) + g(x,t)u(x,t) \tag{3.26}$$

The main focus of the controller requires the system to have the attractor ξ=0. The characteristics of the macro-variable according to performance and control specifications can be selected by the designer. Also, the desired dynamic evolution of the macro variable is usually chosen by the Eq(3.27).

$$T\frac{d\xi}{dt} + \xi = 0, \quad T > 0 \tag{3.27}$$

T is a positive constant to be imposed by the designer. In our paper, its value is optimized by PSO algorithm.

The designer chooses speed convergence to the target equilibrium point. Equation Eq(3.28) is given by the chain rule of differentiation as follows:

$$\frac{d\xi}{dt} = \frac{\partial\xi(x,t)}{\partial x}\frac{dx(t)}{dx} \tag{3.28}$$

Take time derivative of the selected macro-variable ξ(x,t) with respect to the system variable **x**, take account of the chain rule of differentiation, and then substitute Eq(3.28) and Eq(3.26) into Eq(3.27), and we have

$$T\frac{\partial\xi(x,t)}{\partial x}\left[f(x,t) + g(x,t)u(x,t)\right] + \xi(x,t) = 0 \tag{3.29}$$

Subsequently, by defining a suitable macro-variable and selecting the control parameter **T**, the expression above Eq(3.29) can be directly solved to find the controller **u(x,t)** which can be written as follows.

$$U_{SC} = U_d(x,t,\xi(x,t),T) \tag{3.30}$$

The differential equations form of quadrotor is given by the Eq(3.3).

The synergetic control synthesis of the system that we have presented in Eq(3.29) started by demonstrating a designer that is been chosen as macro-variable and given in Eq(3.31).

$$\xi_Z = e_Z + \lambda \int e_Z = (x_5 - x_5^*) + \lambda_3 \int (x_5 - x_5^*) dx(t) \tag{3.31}$$

$$\begin{aligned} \dot{\xi}_Z &= \ddot{e}_Z + \lambda_3 e_Z \\ \dot{\xi}_Z &= (\ddot{x}_5 - \dot{x}_5^*) + \lambda_3 (x_5 - x_5^*) \end{aligned} \tag{3.32}$$

which λ_3 is a positive constant.

$$\dot{\xi}_Z = (\dot{x}_6 - x_6^*) + \lambda_3 (x_5 - x_5^*)$$

$\dot{x}_5$ and $\ddot{x}_5$ can be written according to Eq(3.3) as:

$$\dot{\xi}_Z = \left[\frac{1}{m} \left(\cos\phi \ \cos\theta \, U_z - k_{dz} \dot{z} - mg \right) - x_6^* \right] + \lambda_3 (x_5 - x_5^*) \tag{3.33}$$

Moreover, having Eq(3.29) and Eq(3.33), the resulting control law U_Z is given by Eq(3.34):

$$T_3 \left[\frac{1}{m} \left(\cos\phi \ \cos\theta \, U_z - k_{dz} \dot{z} - mg \right) - x_6^* \right] + \lambda (x_5 - x_5^*) + \xi_Z = 0$$

$$\frac{1}{m} \left(\cos\phi \ \cos\theta \, U_z - k_{dz} \dot{z} - mg \right) = -\frac{\xi_Z}{T_3} - \lambda_3 (x_5 - x_5^*) + x_6^*$$

$$U_z = \frac{m \left[-\frac{\xi_Z}{T_3} - \lambda_3 (x_5 - x_5^*) + x_6^* \right] + k_{dz} \dot{z} + mg}{\cos\phi \ \cos\theta}$$

$$U_z = \frac{m \left[-\frac{(x_5 - x_5^*) + \lambda_3 \int (x_5 - x_5^*) dx(t)}{T_3} - \lambda_3 (x_5 - x_5^*) + x_6^* \right] + k_{dz} \dot{z} + mg}{\cos\phi \ \cos\theta} \tag{3.34}$$

Stability analysis: In order to confirm the stability of the system, we use the following Lyapunov function candidate:

$$V = \frac{1}{2}\xi_z{}^T\xi_z \tag{3.35}$$

Therefore:

$$\dot{V} = \xi_z{}^T\dot{\xi}_z \tag{3.36}$$

The use of Eq(3.36) leads to:

$$\dot{V} = -\frac{1}{\mathrm{T}_3}(e_Z + \lambda_3\int e_Z)^2 \tag{3.37}$$

$$\dot{V} = \xi(\ddot{e}_z + \lambda_3 e_z) = \xi_z\left[\left[\frac{1}{m}\left(\cos\phi\ \cos\theta\, U_z - k_{dz}\dot{z} - mg\right) - x_6^*\right] + \lambda_3\left(x_5 - x_5^*\right)\right]$$

$$\dot{V} = \xi_z(\ddot{e}_z + \lambda_3 e_z) = \xi_z\left[\left[\frac{1}{m}\left(\cos\phi\ \cos\theta\, U_z - k_{dz}\dot{z} - mg\right) - x_6^*\right] + \lambda_3\left(x_5 - x_5^*\right)\right] \tag{3.38}$$

Using (3.33) in (3.38) results

$$\dot{V} = \xi_z\left(\frac{-\xi_z}{T_3}\right) = -\frac{1}{T_3}\xi_z^2 \tag{3.39}$$

Form Eq(3.39) it can be found that $\dot{V} < 0$, note $T_3>0$. The system Eq(3.3) under synergetic control law Eq(3.34) has an asymptotic stability and its trajectories converge theoretically to the equilibrium at an infinite time.

The same steps should be applied to defined the controller's equation $(u_x, u_y, U_z, U_\phi, U_\theta)$. The macro-variable of etch state variables are chosen as below:

$$\begin{aligned}
\xi_x &= e_x + \lambda_1\int e_x = (x_1 - x_1^*) + \lambda_1\int(x_1 - x_1^*)dx(t)\\
\xi_y &= e_y + \lambda_2\int e_y = (x_3 - x_3^*) + \lambda_2\int(x_3 - x_3^*)dx(t)\\
\xi_\phi &= e_\phi + \lambda_4\int e_\phi = (x_7 - x_7^*) + \lambda_4\int(x_7 - x_7^*)dx(t)\\
\xi_\theta &= e_\theta + \lambda_5\int e_\theta = (x_9 - x_9^*) + \lambda_5\int(x_9 - x_9^*)dx(t)\\
\xi_\psi &= e_\psi + \lambda_6\int e_\psi = (x_{11} - x_{11}^*) + \lambda_6\int(x_{11} - x_{11}^*)dx(t)
\end{aligned} \tag{3.40}$$

with $\lambda_1, \lambda_3, \lambda_7, \lambda_9, \lambda_{11} > 0$. The controllers are designed as follows:

$$
\begin{aligned}
u_x &= \frac{m}{U_z}\left[-\frac{\xi_x}{T_1} + x_2^* + \frac{k_{dx}}{m}x_2 + c_1\left(x_2 - x_2^*\right)\right] \\
u_y &= \frac{m}{U_z}\left[-\frac{\xi_y}{T_2} + x_4^* + \frac{k_{dy}}{m}x_4 + c_2\left(x_4 - x_4^*\right)\right] \\
U_z &= \frac{m\left[-\frac{\xi_z}{T_3} - \lambda_3(x_5 - x_5^*) + x_6^*\right] + k_{dz}\dot{z} + mg}{\cos\phi\ \cos\theta} \\
U_\phi &= I_x\left[-\frac{\xi_\phi}{T_4} + x_8^* - \frac{\left(I_y - I_z\right)}{I_x}x_{10}x_{12} + \frac{I_r\bar{\omega}}{I_x}x_{10} + \frac{k_{d\phi}}{I_x}x_8^{\,2} + c_4\left(x_8 - x_8^*\right)\right] \\
U_\theta &= I_y\left[-\frac{\xi_\theta}{T_5} + x_{10}^* - \frac{\left(I_z - I_x\right)}{I_y}x_8x_{12} - \frac{I_r\bar{\omega}}{I_y}x_8 + \frac{k_{d\theta}}{I_y}x_{10}^{\,2} + c_5\left(x_{10} - x_{10}^*\right)\right] \\
U_\psi &= I_z\left[-\frac{\xi_\psi}{T_6} + x_{12}^* - \frac{\left(I_x - I_y\right)}{I_z}x_8x_{10} + \frac{k_{d\psi}}{I_z}x_{12}^{\,2} + c_6\left(x_{12} - x_{12}^*\right)\right]
\end{aligned}
\tag{3.41}
$$

$$
\begin{aligned}
u_x &= \frac{m}{U_z}\left[-\frac{(x_1 - x_1^*) + \lambda_1\int(x_1 - x_1^*)dx(t)}{T_1} + x_2^* + \frac{k_{dx}}{m}x_2 + c_1\left(x_2 - x_2^*\right)\right] \\
u_y &= \frac{m}{U_z}\left[-\frac{(x_3 - x_3^*) + \lambda_2\int(x_3 - x_3^*)dx(t)}{T_2} + x_4^* + \frac{k_{dy}}{m}x_4 + c_2\left(x_4 - x_4^*\right)\right] \\
U_z &= \frac{m}{\cos\phi\ \cos\theta}\left[-\frac{(x_5 - x_5^*) + \lambda_2\int(x_5 - x_5^*)dx(t)}{T_3} - \lambda_3(x_5 - x_5^*) + x_6^*\right] + k_{dz}\dot{z} + mg \\
U_\phi &= I_x\left[-\frac{(x_7 - x_7^*) + \lambda_4\int(x_7 - x_7^*)dx(t)}{T_4} + x_8^* - \frac{\left(I_y - I_z\right)}{I_x}x_{10}x_{12} + \frac{I_r\bar{\omega}}{I_x}x_{10} + \frac{k_{d\phi}}{I_x}x_8^{\,2} + c_4\left(x_8 - x_8^*\right)\right] \\
U_\theta &= I_y\left[-\frac{(x_9 - x_9^*) + \lambda_5\int(x_9 - x_9^*)dx(t)}{T_5} + x_{10}^* - \frac{\left(I_z - I_x\right)}{I_y}x_8x_{12} - \frac{I_r\bar{\omega}}{I_y}x_8 + \frac{k_{d\theta}}{I_y}x_{10}^{\,2} + c_5\left(x_{10} - x_{10}^*\right)\right] \\
U_\psi &= I_z\left[-\frac{(x_{11} - x_{11}^*) + \lambda_6\int(x_{11} - x_{11}^*)dx(t)}{T_6} + x_{12}^* - \frac{\left(I_x - I_y\right)}{I_z}x_8x_{10} + \frac{k_{d\psi}}{I_z}x_{12}^{\,2} + c_6\left(x_{12} - x_{12}^*\right)\right]
\end{aligned}
\tag{3.42}
$$

3.2.3.1 Implementation of PSO for Synergetic controller (SC-PSO)

3.2.3.1.1 Formulation of the problem to be optimized

The formulation of the problem to be optimized is mainly concerned with minimizing the error $ERR_i = x_i - x_i^*$ where the objective function $F(X_i)$ can be written as fellow:

$$Min\, F(x) = Min_i(ERR) \qquad \text{i= 1,2,3,..... ,12} \tag{3.43}$$

With: X_i the control parameter set which can be written in the following form:

$$X = [T_i, \lambda_i] \tag{3.44}$$

The objective function is subjected to inequality constraints as shown below:

$$\begin{aligned} T_i^{\min} < T_i < T_i^{\max} \\ \lambda_i^{\min} < \lambda_i < \lambda_i^{\max} \end{aligned} \tag{3.45}$$

3.2.4 Simulation Results and Discussion

In order to validate the designed control laws and evaluate the results obtained, MATLAB/Simulink is used. We hold the same numerical values of the quadrotor parameters. These are summarized in **Table 3.1** In the present work, the values of the desired trajectories are fixed for the position and yaw angle. That is, the desired position (x^*, y^*, z^*) and desired yaw angle ψ^* come directly from the user. The corresponding values of the desired angles, ϕ^* and θ^* are calculated through the correction block. Finally, the control laws based on the proposed algorithms are applied for the six state variables (position and attitude).

In this simulation, the proposed controller's is examined for a fly tracking different types of trajectories, namely, square and horizontal flight trajectory. The quadrotor must fly with a yaw of 0.52 rad,(**ψ^* =0.52** rad).

For the purposes of comparison and validation of the proposed controller SC-PSO, the PID and SMC are performed for the same flight scenario.

Figures 3.4 represents the 3D trajectory of quadrotor aircraft for all of the controller SC-PSO, PID and SMC during the flight. The simulation results given by this figure shows a good performances and robustness towards stability and trajectory

tracking trajectory tracking even after a 90° lane change, which explains the efficiency of the proposed SC-PSO control strategy.

Table 3. 1 Quadrotor model parameters

Symbols	Values	Physical Significance
I_x	1.22	Quadrotor moment of inertia around X axis (Ns²/rad)
I_y	1.22	Quadrotor moment of inertia around Y axis (Ns²/rad)
I_z	2.2	Quadrotor moment of inertia around Z axis (Ns²/rad)
I_r	0.2	Total rotational moment of inertia around the rotor axis (Ns²/rad)
k_F	5	Lift factor (Ns²)
k_M	2	Drag factor (N/ms²)
l	0.21	Arm length (m)
m	1.1	Total mass of the quadrotor (Kg)
g	9.806	Acceleration due to gravity (m/s²)
k_{dx}	0.12	Translational drage coefficient according to X axies (Ns/m)
k_{dy}	0.12	Translational drage coefficient according to Y axies (Ns/m)
k_{dz}	0.12	Translational drage coefficient according to Z axies (Ns/m)
$k_{d\phi}$	0.1	Rotational drage coefficient, Roll movement (Ns/m)
$k_{d\theta}$	0.1	Rotational drage coefficient, Pitch movement (Ns/m)
$k_{d\psi}$	0.1	Rotational drage coefficient, Yaw movement (Ns/m)

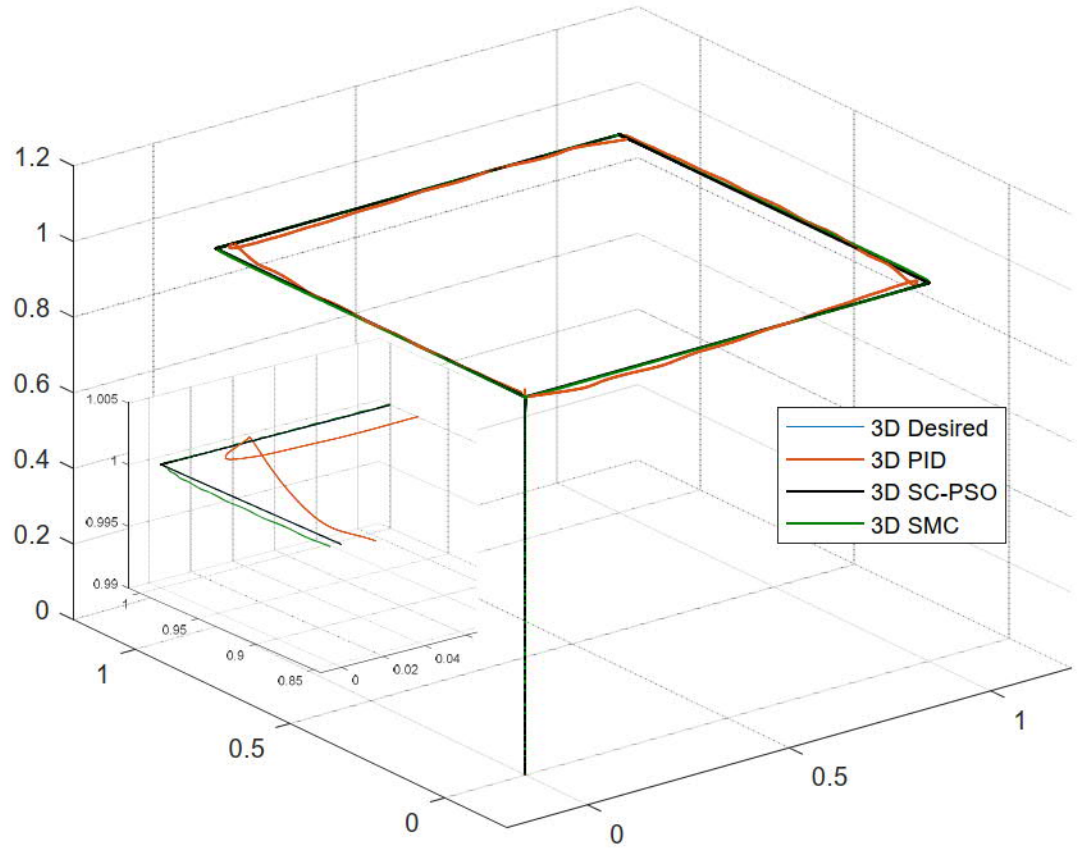

Figure.3. 4: 3D Path tracking with SC-PSO, PID and SMC control

Figures (3.5) and (3.7) shows the results of the correction block angles ϕ and θ of the controllers with the tracking errors **Figures (3.6) and (3.8),** Each controller generates its own angles as shows in **Figures (3.9),** also **Figure (3.10)** represent the response to stabilize the ψ angle at a desired value, and their tracking errors

Figures (3.11) (3.12) and **(3.13)** represent, respectively, the response of the proposed controller to stabilize the quadrotor aerial robot at a desired position along the axes (x, y, z) and the tracking errors in x, y, z directions. The different control strategies results allowed zero overshoot except the PID controller where the overshoot is clearly visible. In the steady state, the trajectories x, y, z and ψ conform to the desired trajectories. All the controllers demonstrated good results except the case of the PID controller which presents the most degraded performance in the transient state with the slowest response time, oscillations and the largest error in the steady state. Unlike the SMC controller demonstrated good results in terms of response time and static error compared or PID controller. However, it is necessary to point out the presence of chattering which affects the control signal as can be seen in **figure (3.16)** and **(3.17).**

Control by SC-PSO has proved the robustness and its ability to overcome the problems encountered by PID and SMC, the results obtained prove excellent transient performance with the fastest response time, absolutely no oscillation and the minimum steady-state error.

the different control strategies signals given by the figures **(3.14), (3.15), (3.16), (3.17), (3.18)** and **(3.19),** each controller has its own control signal form that is different from the others.

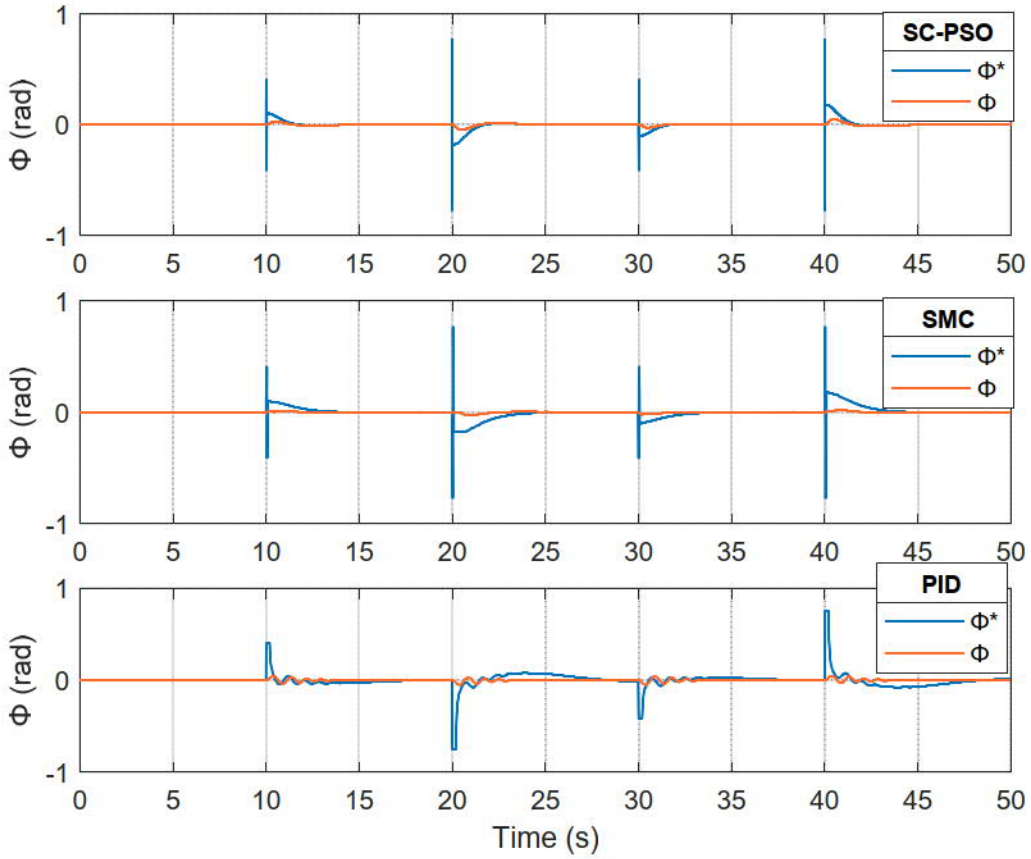

Figure.3. 5: Roll angle from the correction bloc using SC-PSO, SMC and PID controllers

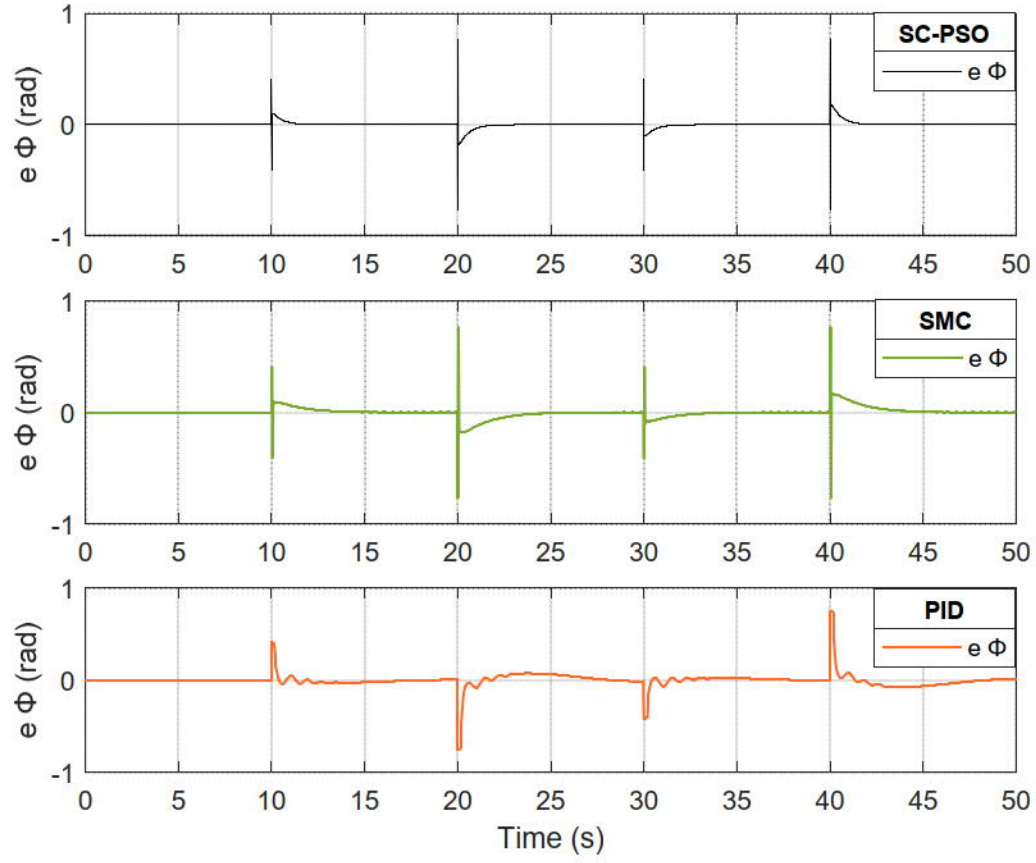

Figure.3. 6: Tracking error for roll angle

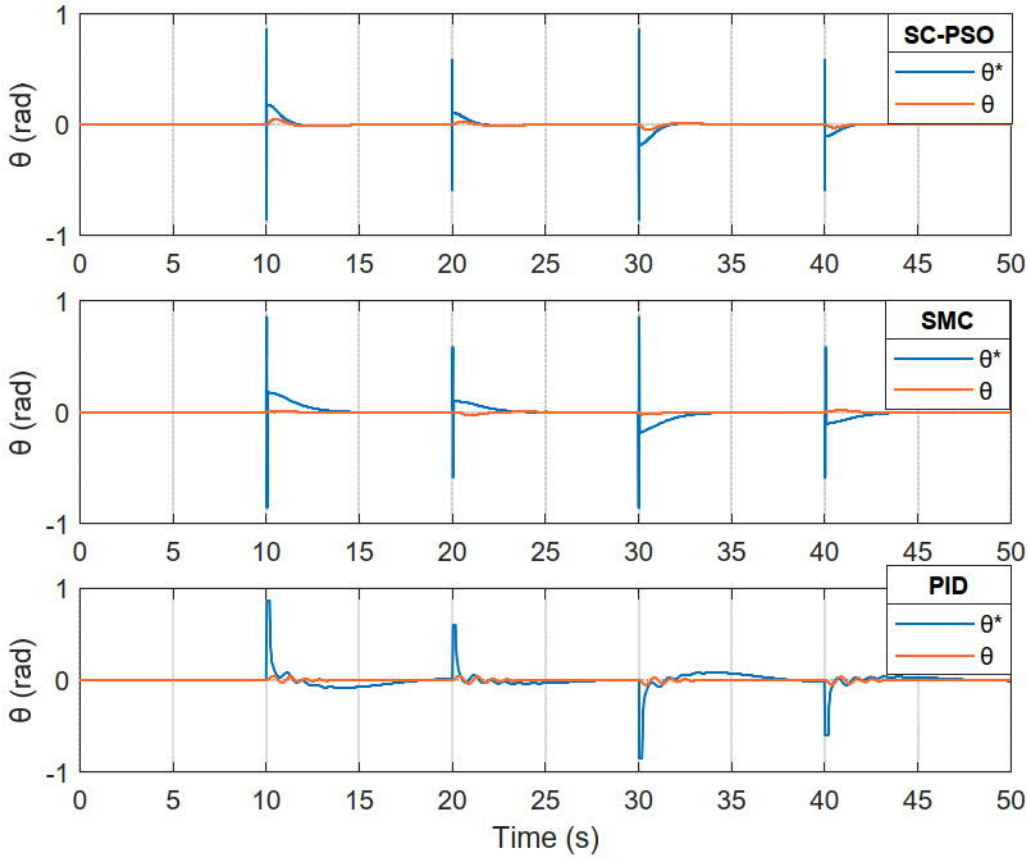

Figure.3. 7 : Pitch angle from the correction bloc using SC-PSO, SMC and controllers

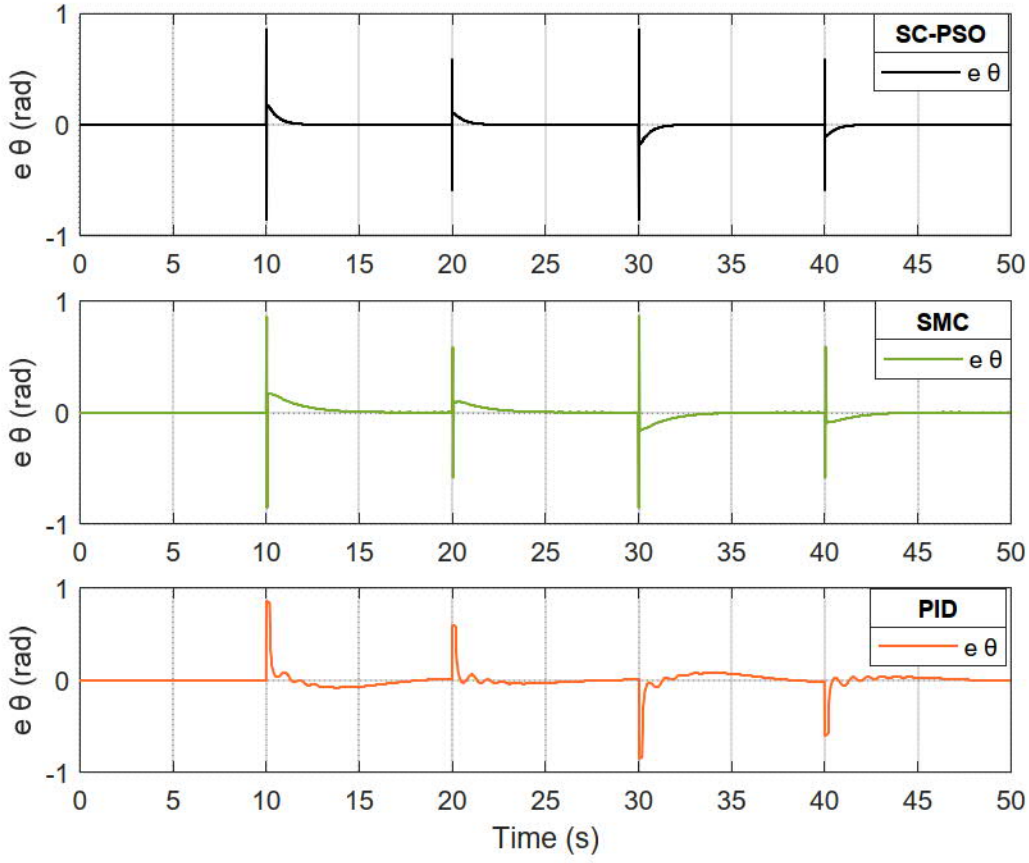

Figure.3. 8 : Tracking error for pitch angle

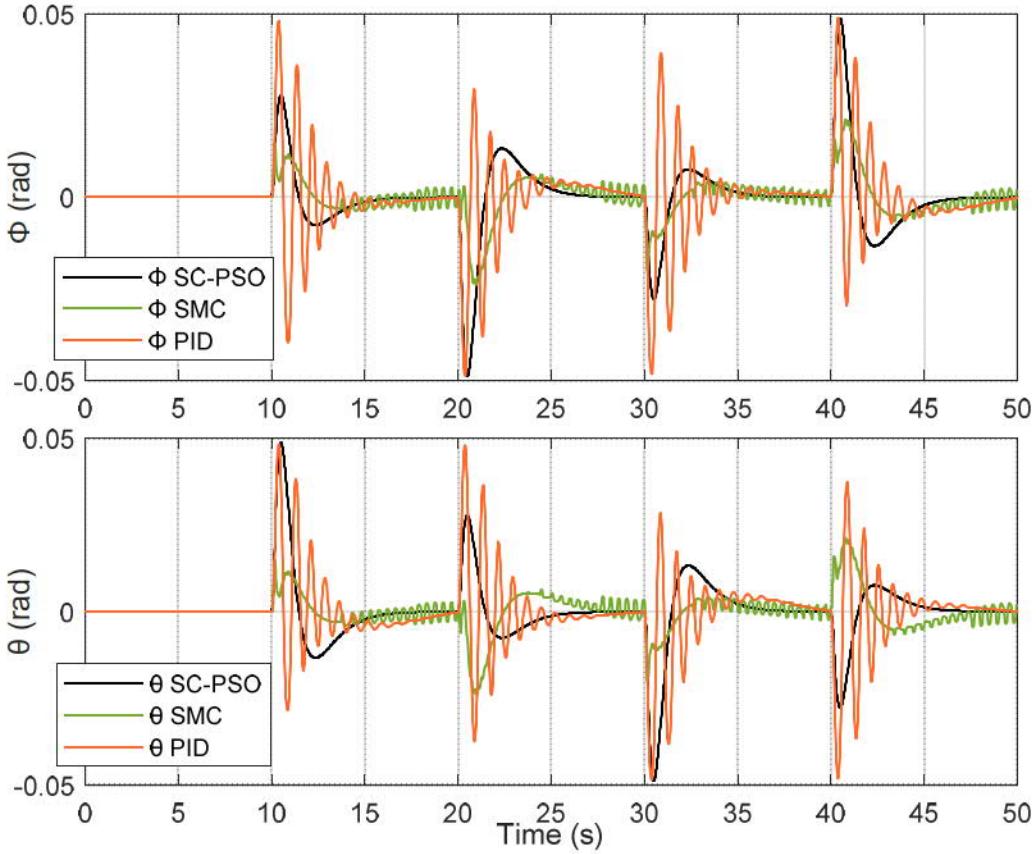

Figure.3. 9: Roll and Pitch angle using SC-PSO, SMC and controllers

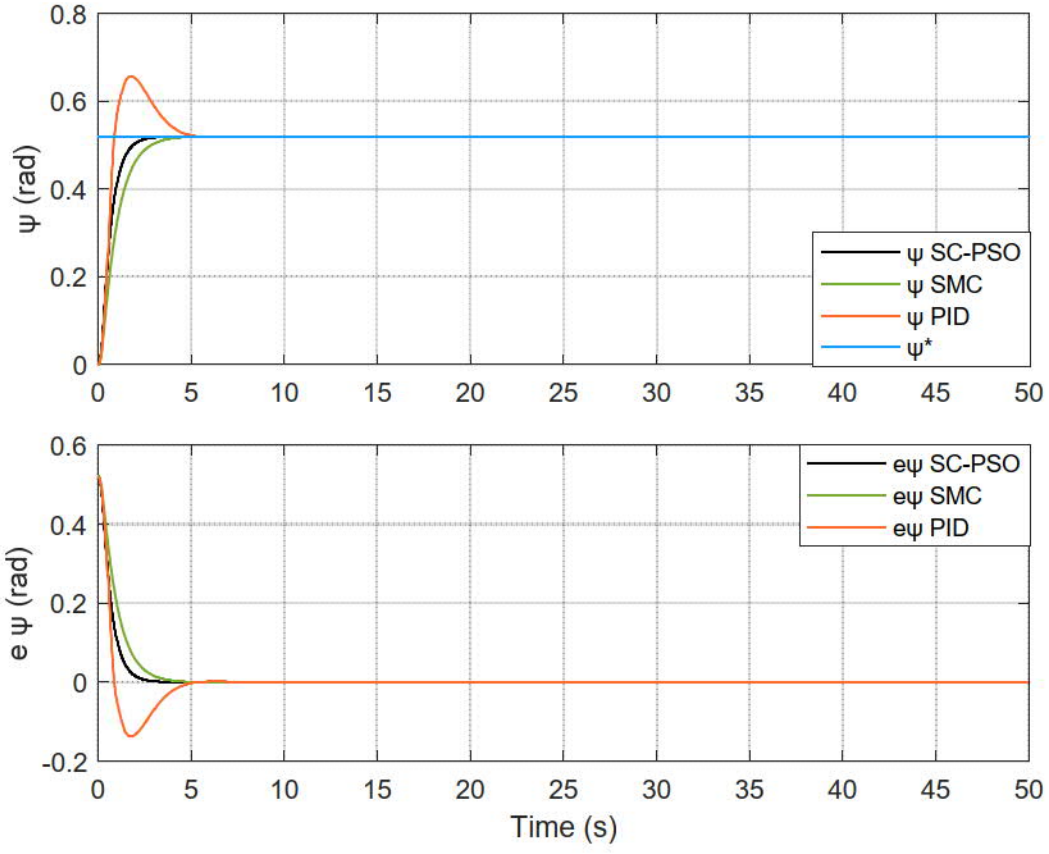

Figure.3. 10: Quadrotor yaw angle ψ and its tracking error

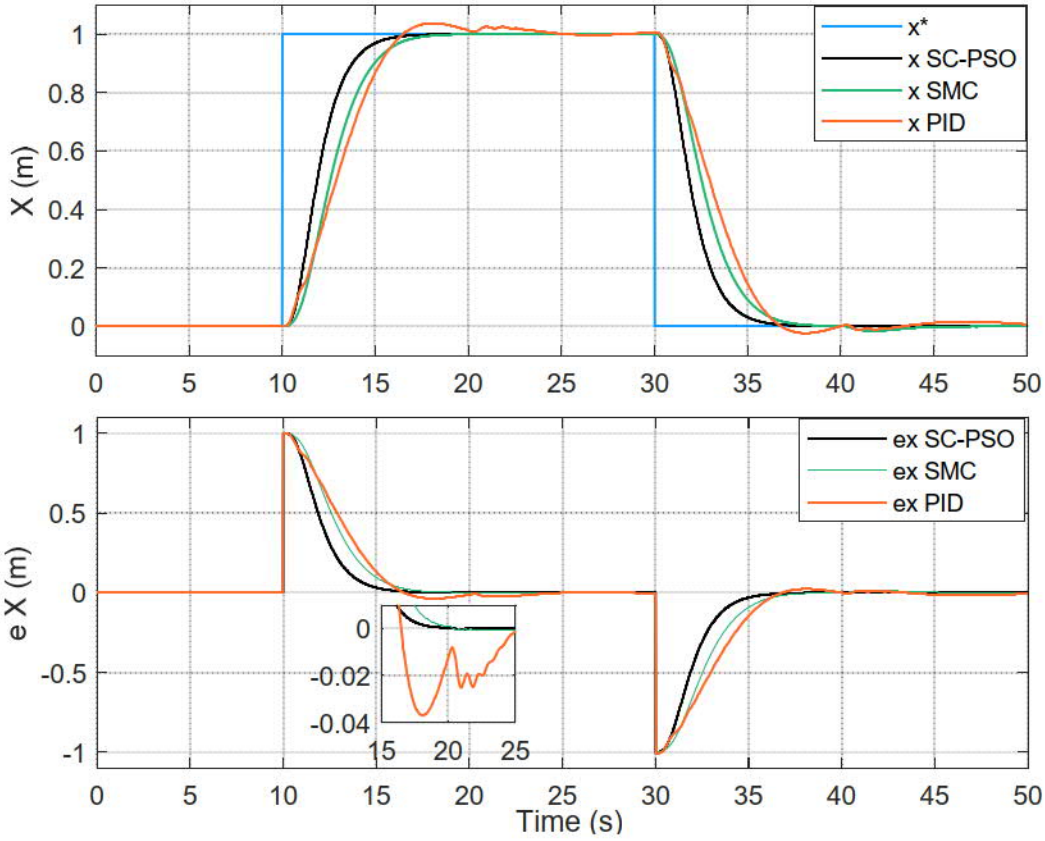

Figure.3. 11: Quadrotor position along x and its tracking error

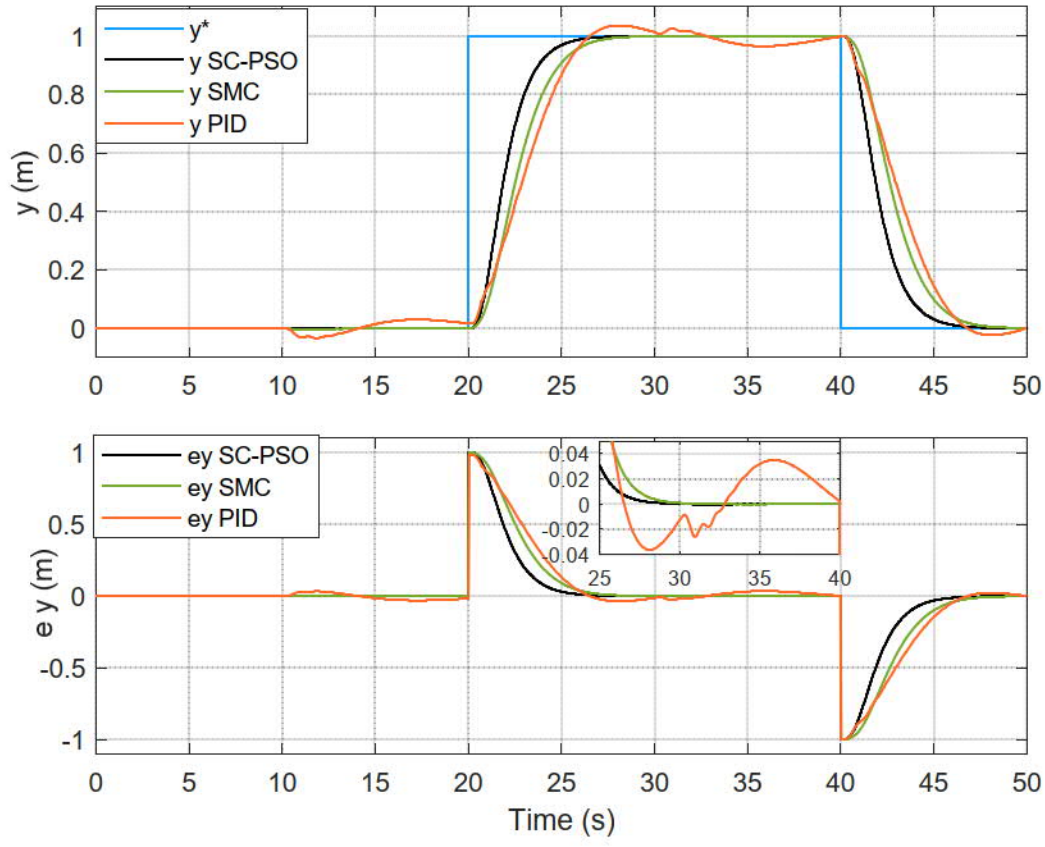

Figure.3. 12: Quadrotor position along y and its tracking error

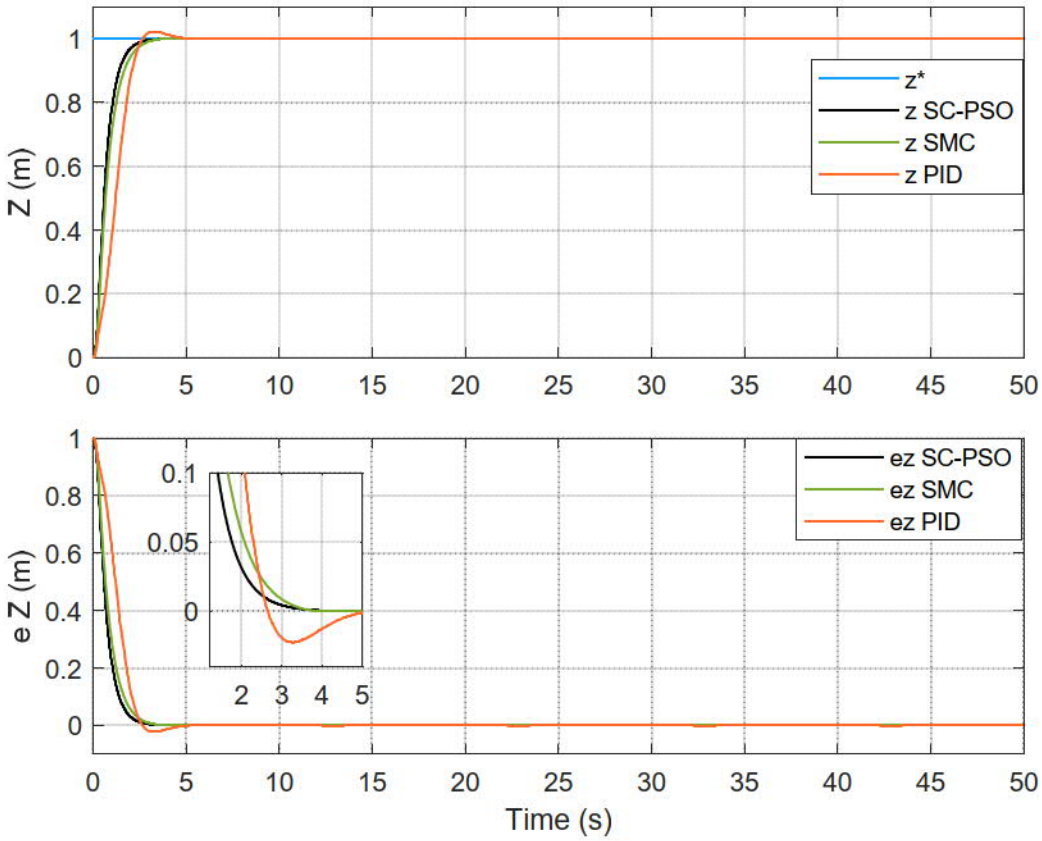

Figure.3. 13: Quadrotor position along Z and its tracking error

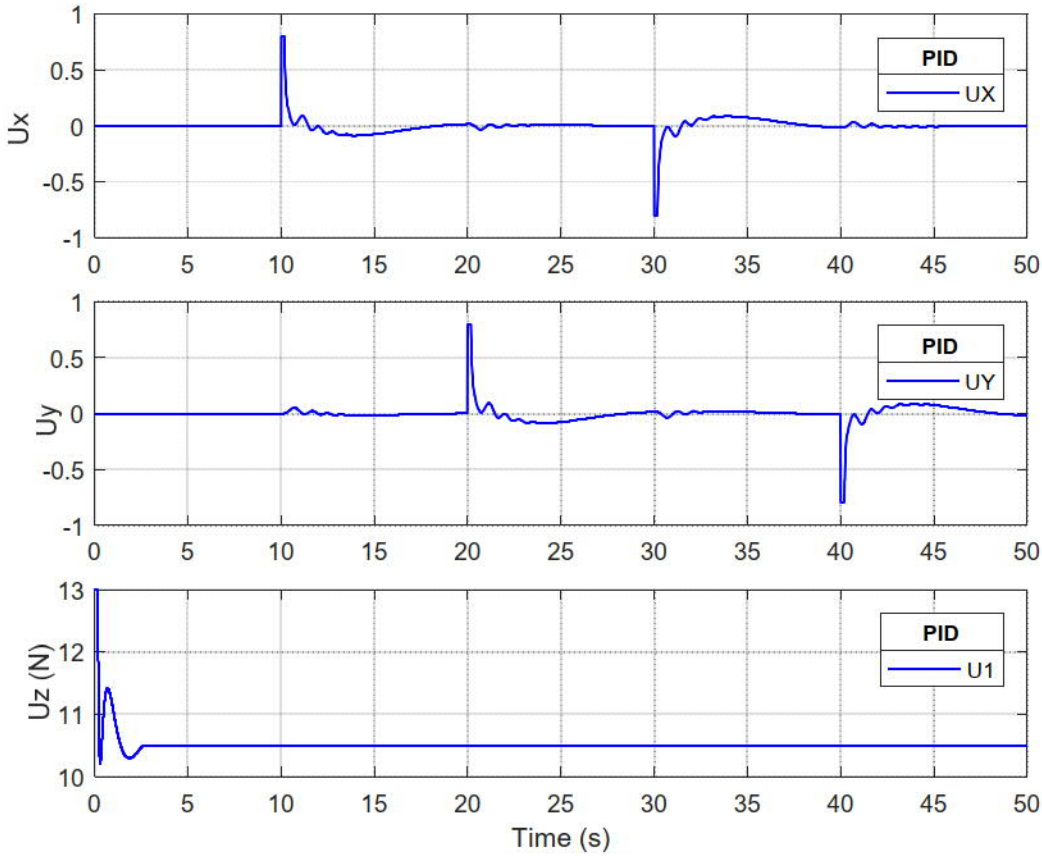

Figure.3. 14: The outputs U_x, U_y, U_z of the PID controller

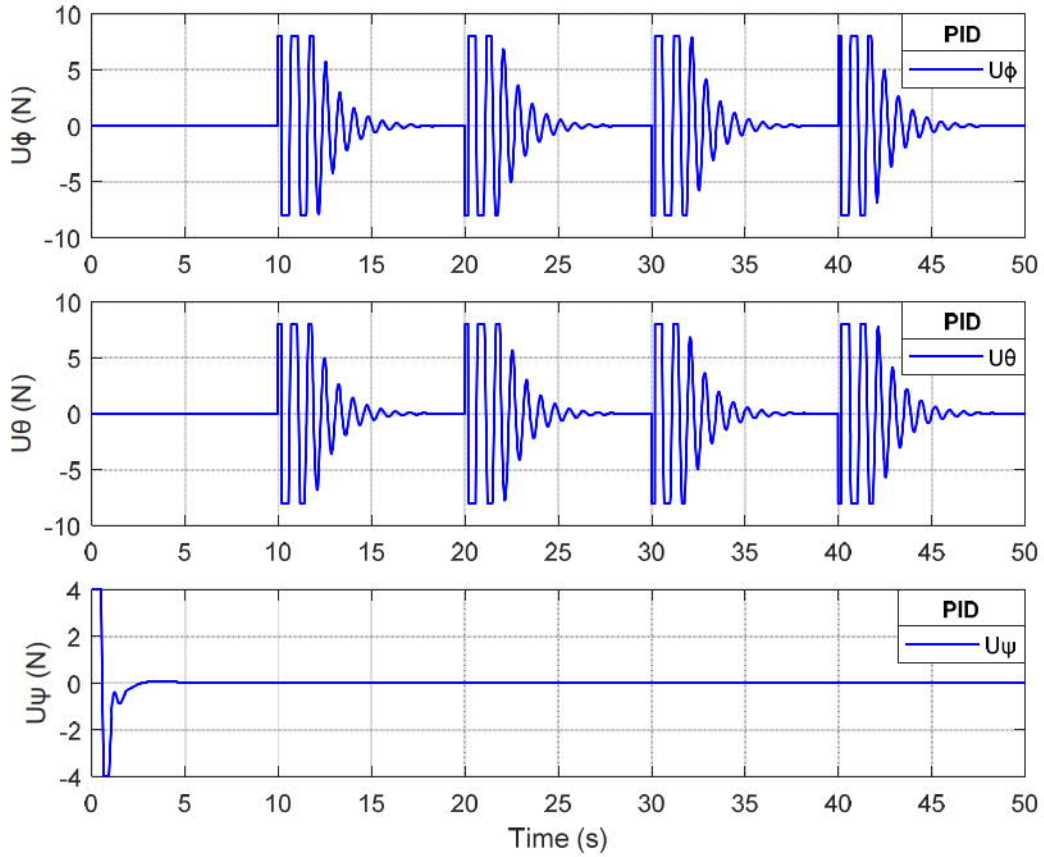

Figure.3. 15: The outputs U_ϕ, U_θ, U_ψ of the PID controller

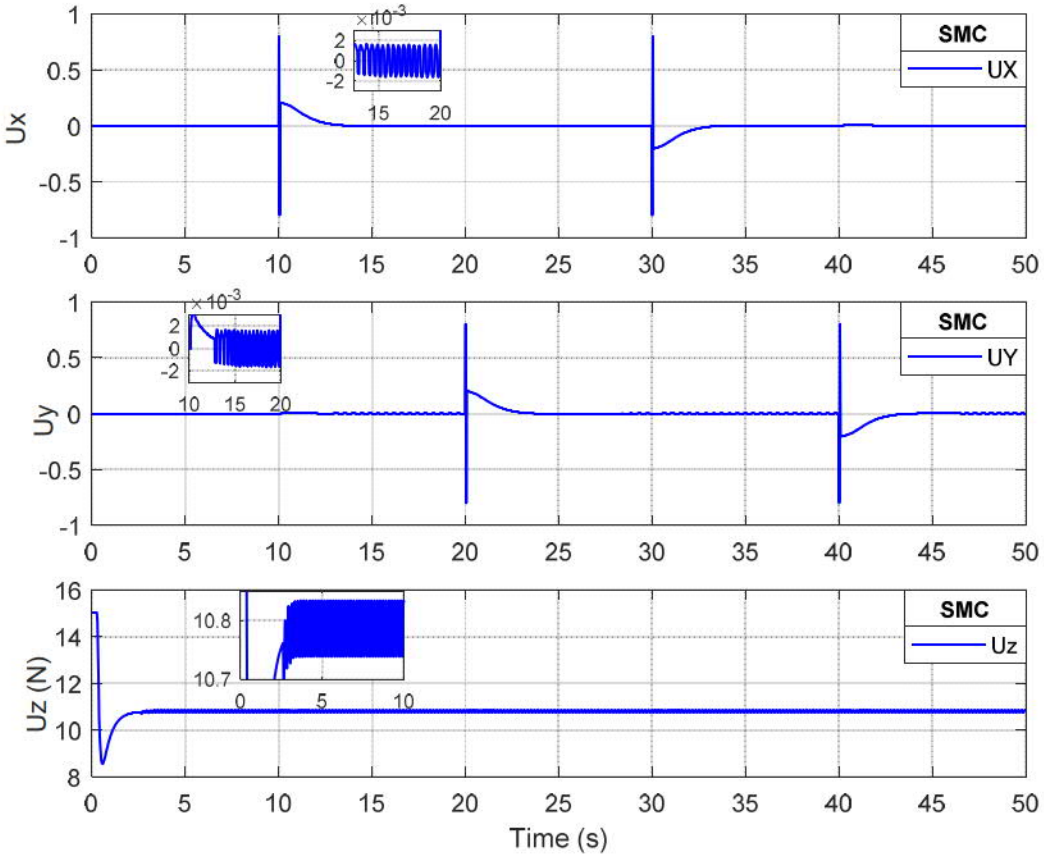

Figure.3. 16: The outputs U_x, U_y, U_z of the SMC controller

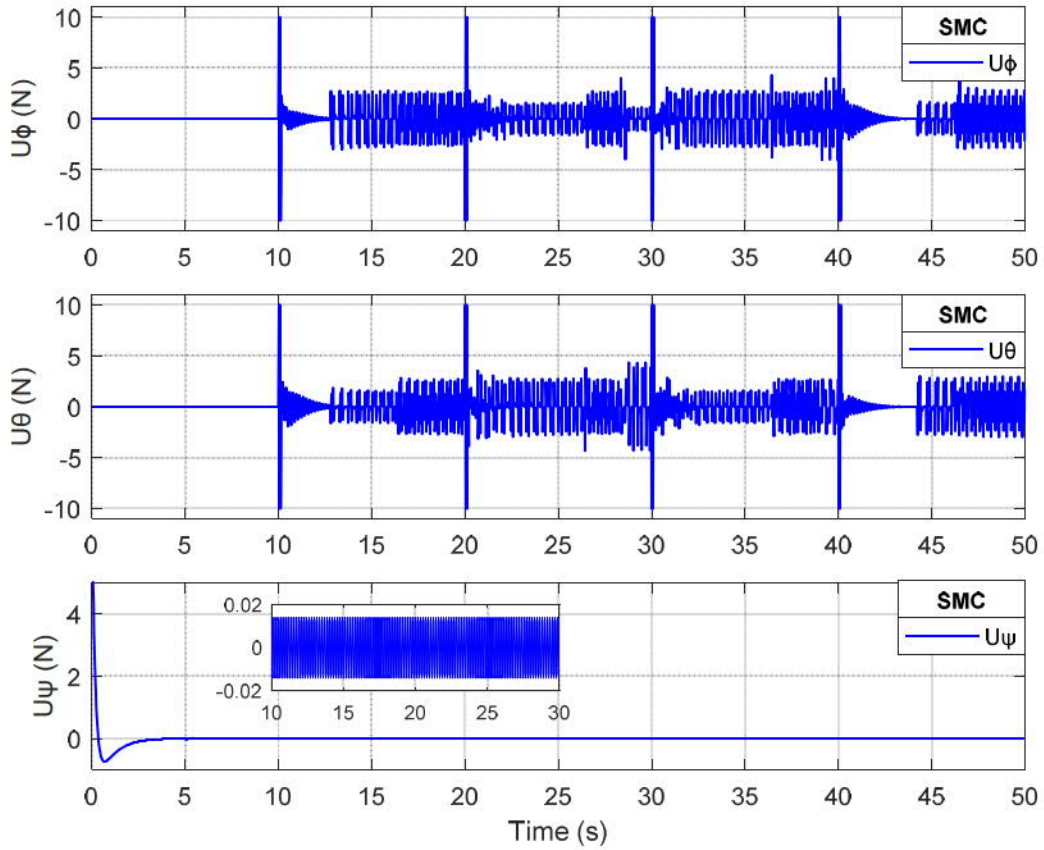

Figure.3. 17 : The outputs U_ϕ, U_θ, U_ψ of the SMC controller

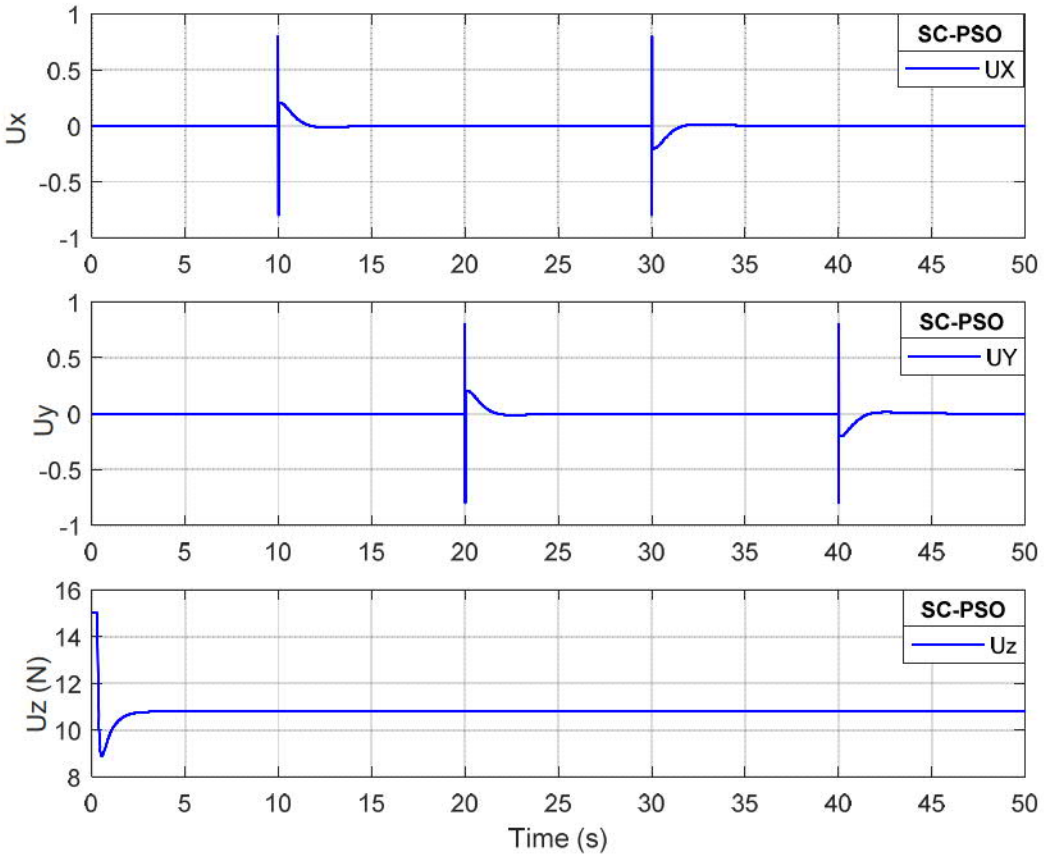

Figure.3. 18: The outputs U_x, U_y, U_z of the SC-PSO controller

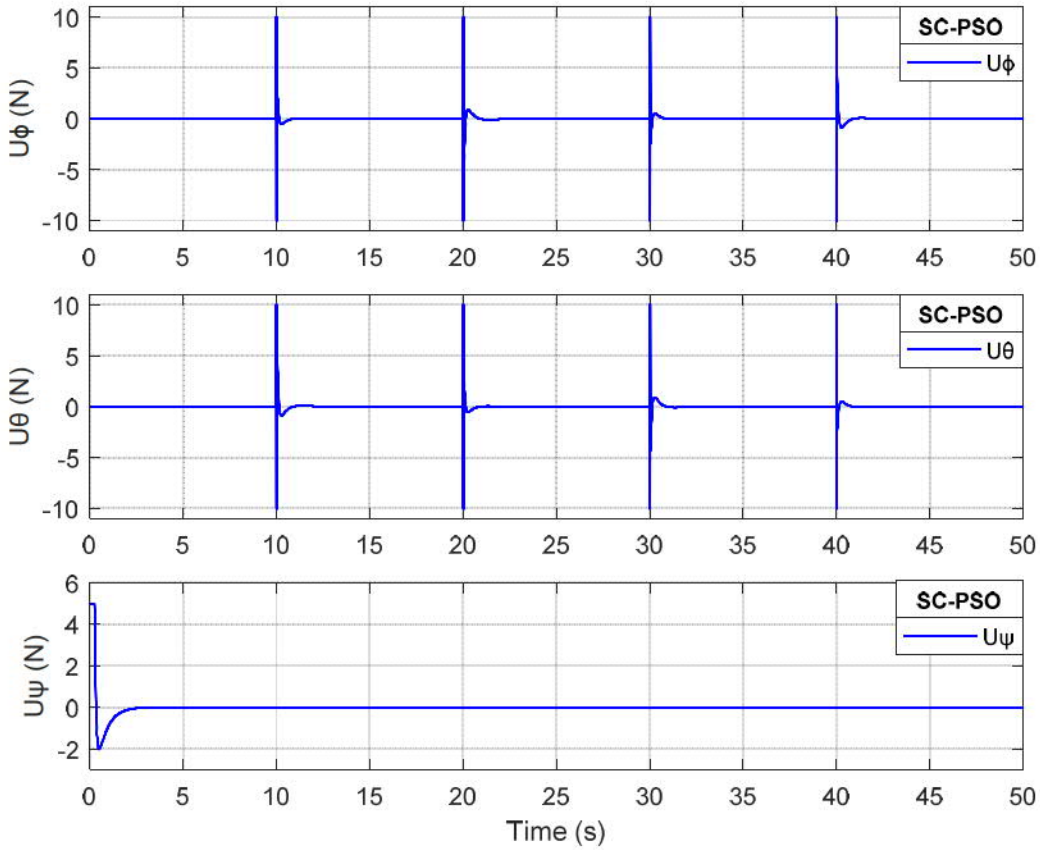

Figure.3. 19: The outputs U_{ϕ}, U_{θ}, U_{ψ} of the SC-PSO controller

3.2.5 Hardware-in-the-loop (HIL) test results

Thorough and reliable system testing is necessary to check and confirm the system design. But with modern systems becoming increasingly complex, especially software, this step is difficult to implement. Consider testing the new aircraft's electronics. To compete with its predecessor in today's market, modern vehicles must include autopilot systems, cameras, radar, etc. Testing these subsystems on the assembled product under the desired use cases guarantees that the test takes place in the ideal context, but also results in significant testing expenses and the challenge of testing each scenario. Additionally, delaying testing until final assembly carries significant risks, and test-driven changes can have disastrous effects on the schedule. Unimaginable testing costs and unexpected time to market are sure to follow. This problem becomes more complex when you consider that only one of many aircraft ECUs equates to a large number of signals representing different I/O types and functions, which makes full test coverage difficult. These factors seem to be the causes of an impossible problem that calls into question the reasonableness of a comprehensive test that would be time- and cost-effective.

3.2.6 The experimental validation Hardware-in-the-loop (HIL) test results

The experimental validation for the quadrotor system based on **SC-PSO** technique under **MATLAB/Simulink®** environment based on **H**ardware-**I**n-the-**L**oop (**HIL**)Real-Time testing method. The experiment contains the following devices as show in **Figures (3.20)**.

- Two **PC** (**MATLAB/Simulink®** environment).
- Two **dSPACE 1104 card**.
- **Oscilloscope** for obtained the results

The Experimental test is divided into four steps

- The first step is the implementation of the quadrotor system model in a dspace environment (dSPACE 1104 card 1)
- The second step is implementing the six controllers of SC-PSO in a dSPACE environment (**dSPACE 1104** card 2)
- The third step is connected all the output with the input and vice versa for each **dSPACE 1104** card
- The fourth step is to synchronize the input and output information

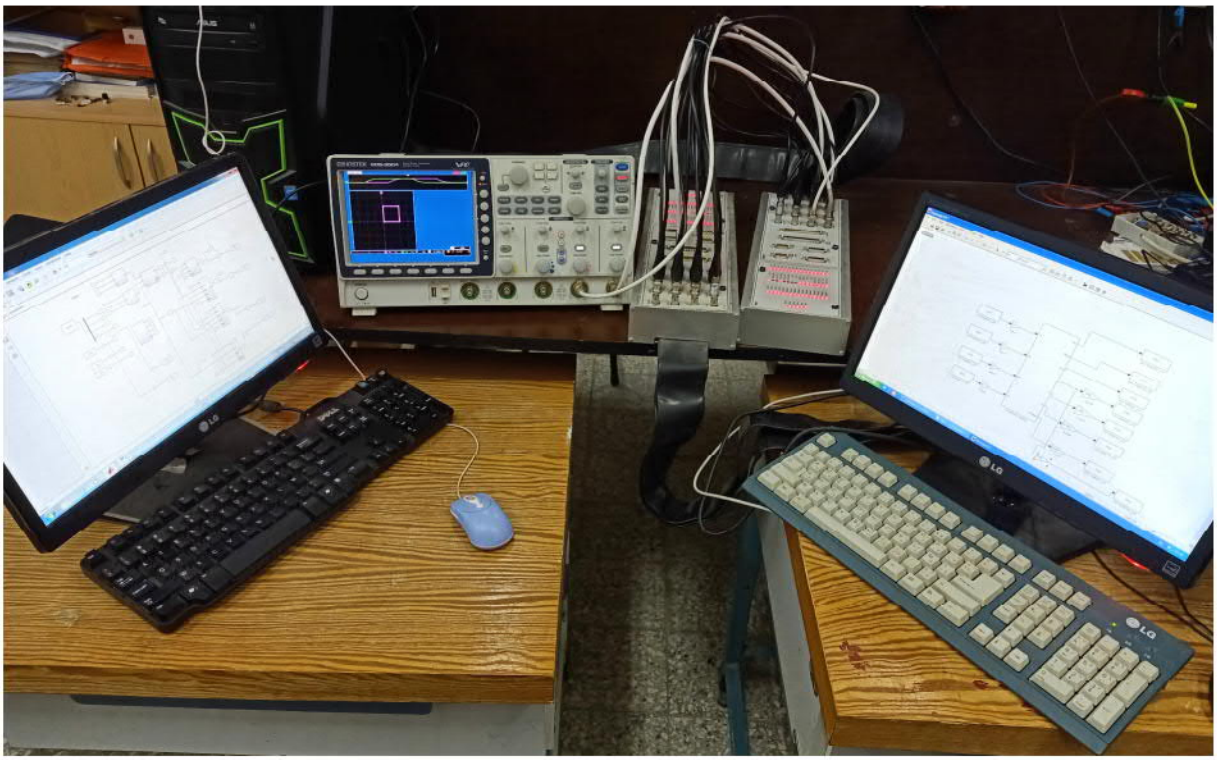

Figure.3. 20: Hardware-in-the-loop (HIL) Simulink Real-Time for quadrotor

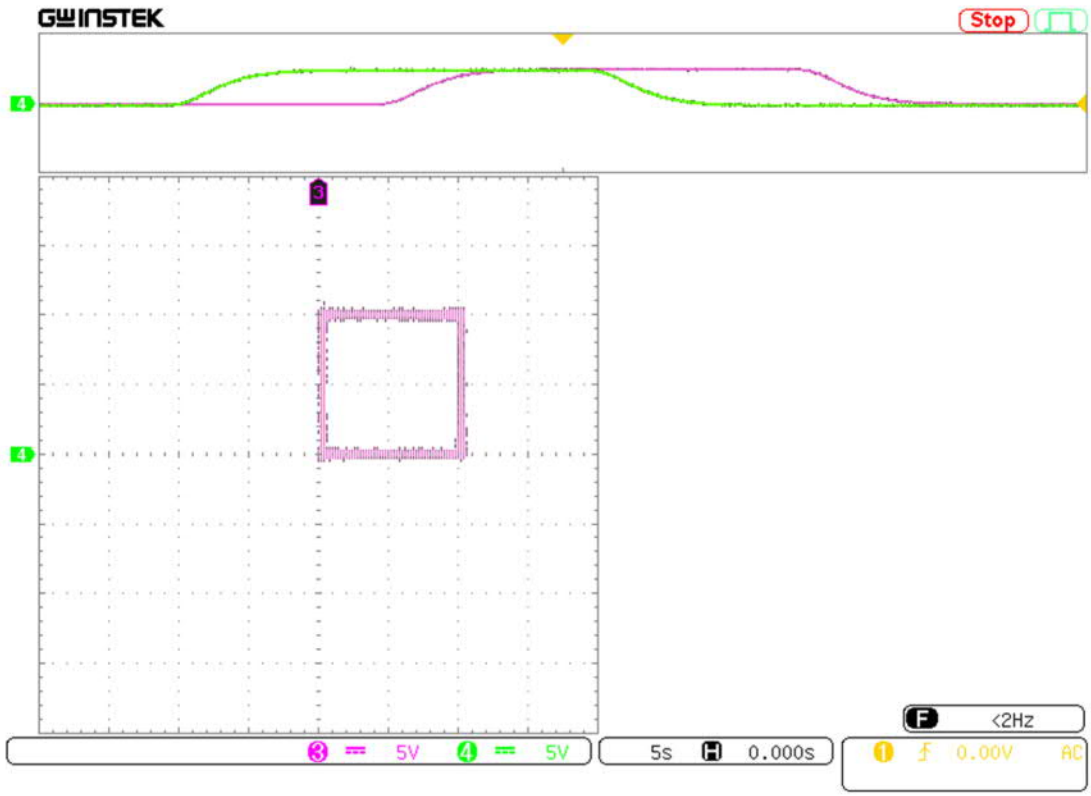

Figure.3. 21: 2D path of the quadrotor (HIL, SC-PSO)

Figure.3. 22: X Y Z position (HIL, SC-PSO)

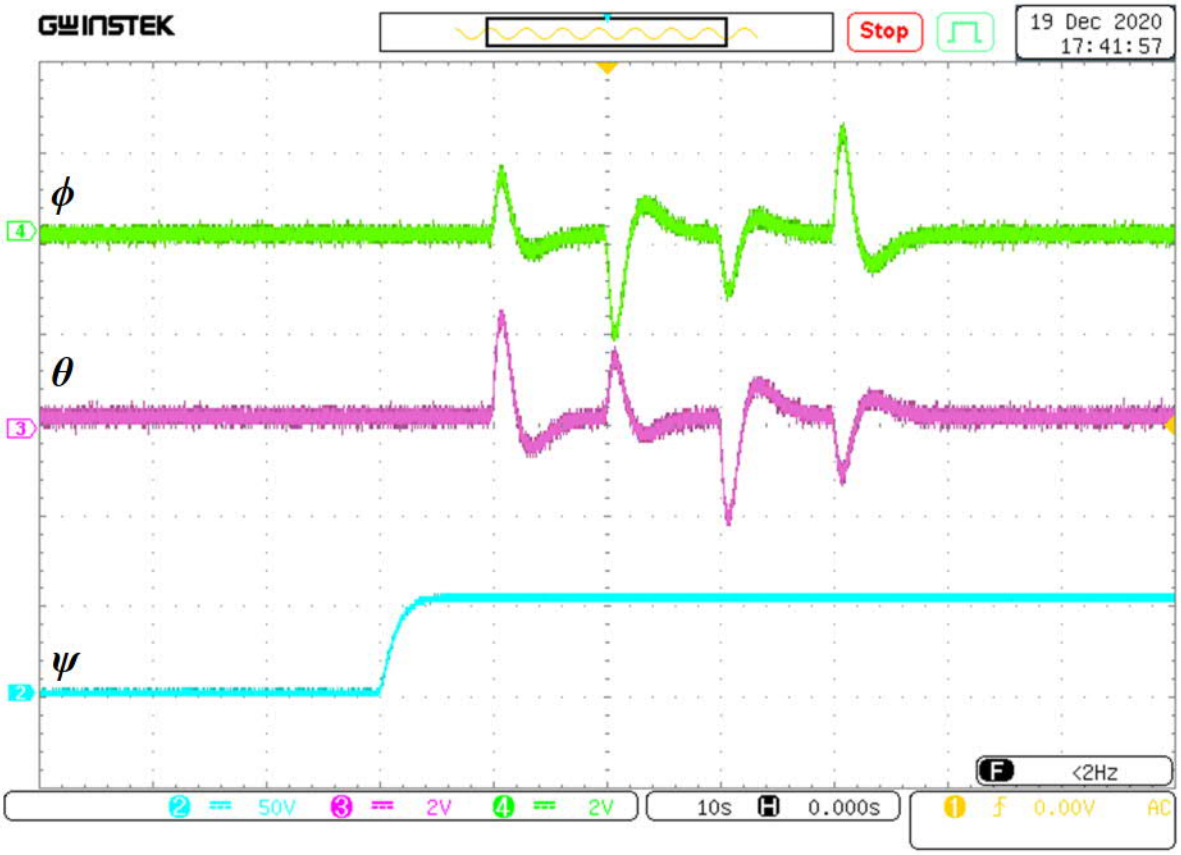

Figure.3. 23: Roll, pitch and yaw angles (HIL, SC-PSO)

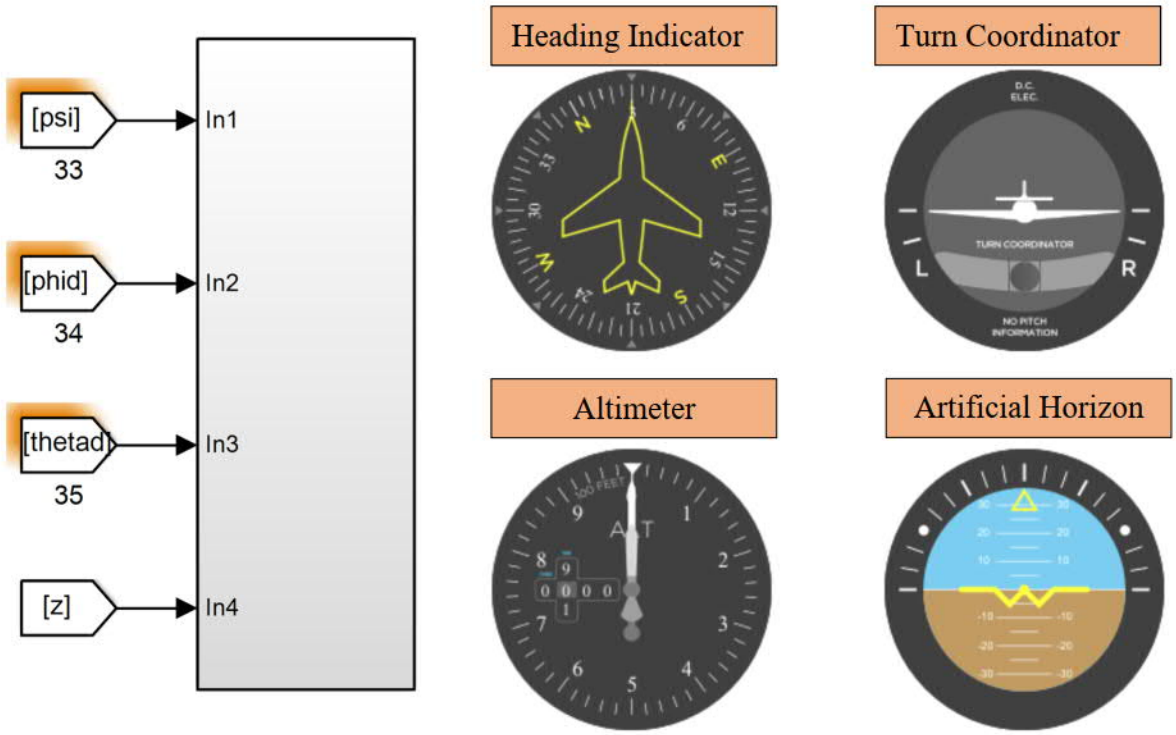

Figure.3. 24: Visualization sensor of the quadrotor

Figure (3.21) shows the 2D square trajectory of a quadrotor aircraft based on

the SC-PSO controller during flight. The HIL test results given by this **Figures (3.22) (3.23)** demonstrate a robustness and successful of the suggested **SC-PSO** control strategy for trajectory tracking even after a lane change. The Sensors screen to supervise the flight of the quadrotor aircraft, displays in **Figure (3.24).**

3.3 Conclusion

In this chapter, a control block based on the proposed method **SC-PSO** controller has been investigated for the steering of a quadrotor UAV to achieve the desired position and attitude. Six controllers have been developed for the corresponding six system states. The global system is divided into two subsystems, namely, the position control subsystem, the attitude and altitude control subsystem.

This strategy has been adopted in order to get efficient control even though the under-actuation property is still present. The **SC-PSO** technique is chosen due to its useful advantages, i.e., it guarantees robustness versus parameter fluctuations, model uncertainties, and random external disturbances. Moreover Simulations (**MATLAB/ Simulink®**) have been conducted to assess the proposed controller. The simulation results show the efficiency of the proposed controller in path tracking even under sudden changes. In addition, these results have demonstrated the superiority of the proposed controller in comparison with the **PID** and **SMC**. In order to support the simulations results of the proposed **SC-PSO**, an experimental test was conducted using a **H**ardware-**I**n-the-**L**oop (**HIL**) Simulink Real-Time testing method using **dSPACE 1104** card for path tracking.

Reference:

[59] ZHENG, En-Hui, XIONG, Jing-Jing, et LUO, Ji-Liang. Second order sliding mode control for a quadrotor UAV. *ISA transactions*, 2014, vol. 53, no 4, p. 1350-1356.

Chapter 4

Introduction to Power Quality

4.1 Introduction

All over the world, Power quality (PQ) has been given increased attention especially after the coronavirus. It is the set of electrical limitations that permit a device to operate in its expected configuration without significant loss in performance or slowly destroying the system [60]. In the 21st, the importance of power quality is very significant due to the

deregulation of the power industry and proliferation of sensitive loads that need clean and uninterrupted power such as microprocessor based controller, power electronic drives, etc. Non-linear loads are causing a number of power quality problems including [61] [62]

- low power factor.
- low efficiency.
- electromagnetic interference (EMI).
- distortions in the voltage and current signals.

More issues result from zero, negative, and positive components caused by single-phase load or unbalanced loads. Power quality issues have very negative impacts on the power system, and they should be resolved to have reliable and secure power systems [63,64].

4.2 Power Quality Problems

Any power supply is defined as any power problem manifested by current, voltage, or frequency and load variations deviations that lead to poor operation of customer equipment or complete failure is defined as a power quality problem. One of the most important problems faced by the power quality and that occurs permanently in the power system are:

- Voltage fluctuations.
- Voltage sag.
- Interruption.
- Unbalance.
- Harmonics.

Harmonic distortion is the main problem for the current.

4.2.1 Unbalanced system

A balanced three-phase electrical network supplying an unbalanced three-phase electrical load leads to voltage imbalances due to the circulation of unbalanced currents in the grid impedances. The unbalance of the three-phase system is therefore generated when the three voltages are not identical in amplitude and/or are not offset by an angle of 120°.

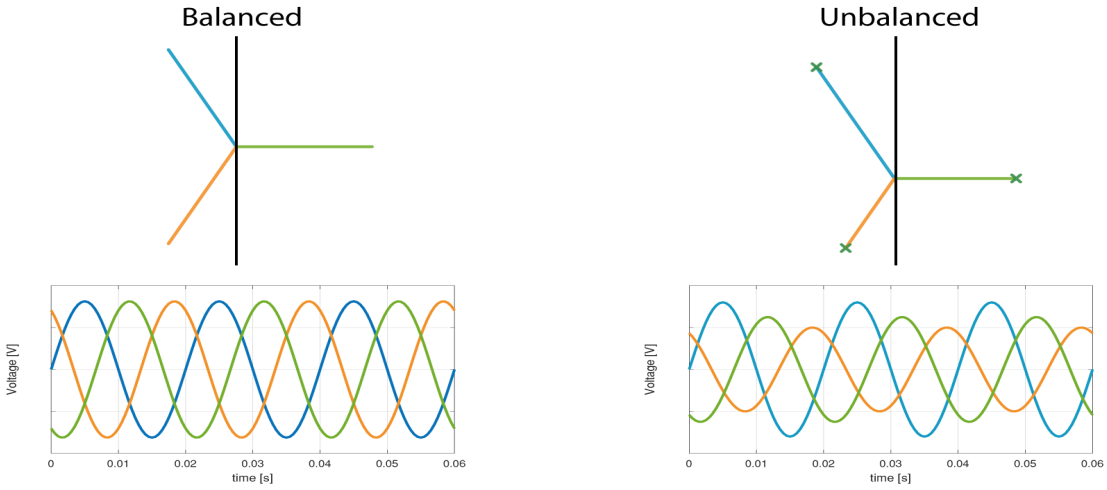

Figure.4. 1 : Voltage three-phase system unbalance

4.2.2 Frequency variation

Significant variation in grid frequency is very rare and only exists in exceptional circumstances, such as in grids fed by an independent heat source. The fundamental frequency average value should be within the range of 50 Hz ±1%, during normal conditions.

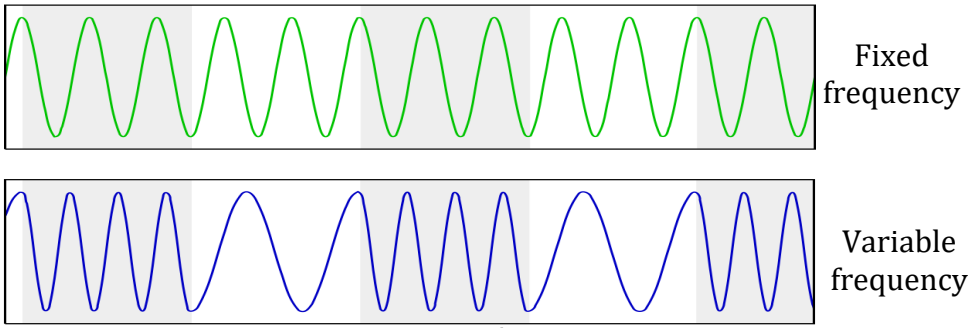

Figure.4. 2 : Frequency variation waveform.

4.2.3 Interruption

Voltage sag is a drop in nominal voltage to a value between 10% and 90%. This fall can last for a time ranging from 10 ms to a few seconds. The voltage dip can be caused by natural phenomena like lightning, as well as by the presence of faults on the installation in the public or private grid. These voltage dips also appear during switching operations causing high currents such as motors, transformers, etc.

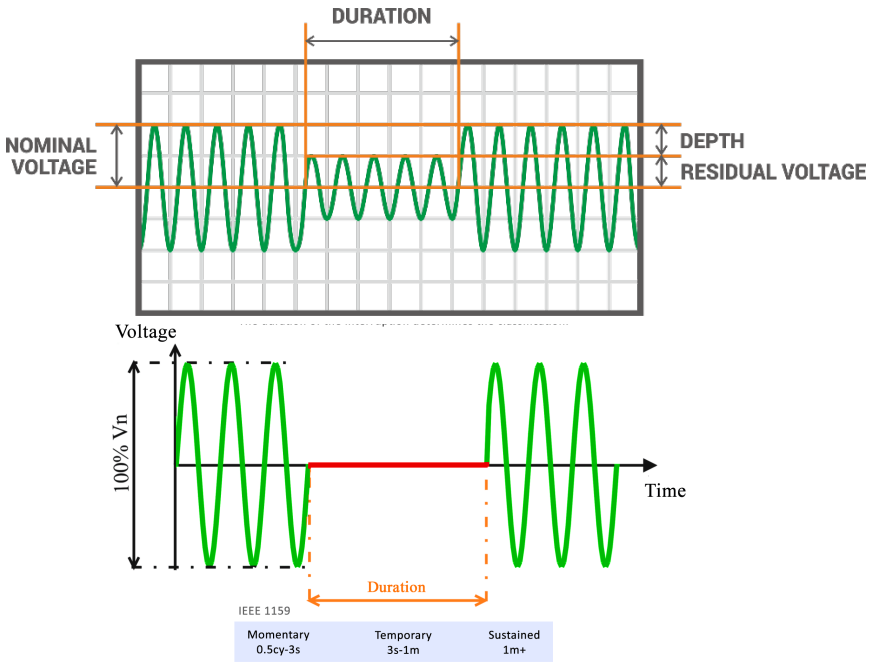

Figure.4. 3 : Voltage Dips and Interruptions

4.2.4 Harmonics

Advances in power generation technology and its renewable sources installed in the grid and highly advanced equipment for customers have increased [63]. In many applications, the use of power electronic devices has given more effectiveness and flexibility [66]. But the excessive use on the grid of these power electronic devices that consider you non-linear loads leads to many problems which have become a major concern [66,67]. There has been an increase in nonlinear loads in industrial and commercial spaces (appliances, and adjustable speed drives). The use of non-linear loads leads to distortion and imbalance in the power supply. Disturbances like harmonic distortion lead to an unstable and insecure power system.

The harmonic currents flow back in the direction of the source through the point of common coupling (PCC) [68].

Harmonics have two effects on the power system

- Short-term impacts are related to excessive voltage distortion.
- Long-term impacts are an increase in resistive losses and voltage stresses.

Among the losses that occur due to harmonic currents interacting with the equipment of the power system, resulting additional losses, overloading, overheating and errors in

metering devices. Another effect is to reduce the system's **P**ower **F**actor (**pf**), which is described as follows

$$pf = \frac{P}{\sqrt{P^2 + Q^2}} \tag{4.1}$$

$$S = \sqrt{P^2 + Q^2} \tag{4.2}$$

where

P : The active power.

Q : The reactive power

S : The apparent power.

As a result, regulatory guidelines and standards for managing the acceptable limits for voltage and current harmonics are provided by **IEEE** (**I**nstitute of **E**lectrical and **E**lectronics **E**ngineers) as shown in **Table 4.1** [69].

Two important definitions of current harmonics have been given [70]:

- **T**otal **D**emand **D**istortion (**TDD**).
- **T**otal **H**armonic **D**istortion (**THD**).

In many applications, THD is the most commonly used harmonic index and is calculated as follows:

$$THD_{current} = \frac{\sqrt{I_{RMS}^2 - I_1^2}}{I_1} = \frac{\text{RMS of all harmonic current}}{\text{RMS of the fundamental current}} \tag{4.3}$$

a: Even harmonics are limited to 25% of the odd harmonic limits above.

b: Current distortions that result in a dc offset, e.g., half-wave converters, are not allowed.

c: All power generation equipment is limited to these values of current distortion, regardless of actual Isc/IL.

where Isc = maximum short-circuit current at PCC

IL = maximum demand load current (fundamental frequency at the PCC under normal load operating conditions

Table 4.1: IEEE 519-2014 current harmonic distortion limits [69]

Maximum current harmonic distortion in percent of I_L						
Individual harmonic order (Odd harmonics)[a,b]						
ISC/IL	<11	11≤h<17	17≤h<23	23≤h<35	35≤h	TDD
< 20 [c]	4.0	4.0	4.0	4.0	4.0	4.0
20<50	7.0	7.0	7.0	7.0	7.0	7.0
50<100	10.0	10.0	10.0	10.0	10.0	10.0
100<100	12.0	12.0	12.0	12.0	12.0	12.0
0>1000	15.0	15.0	15.0	15.0	15.0	15.0

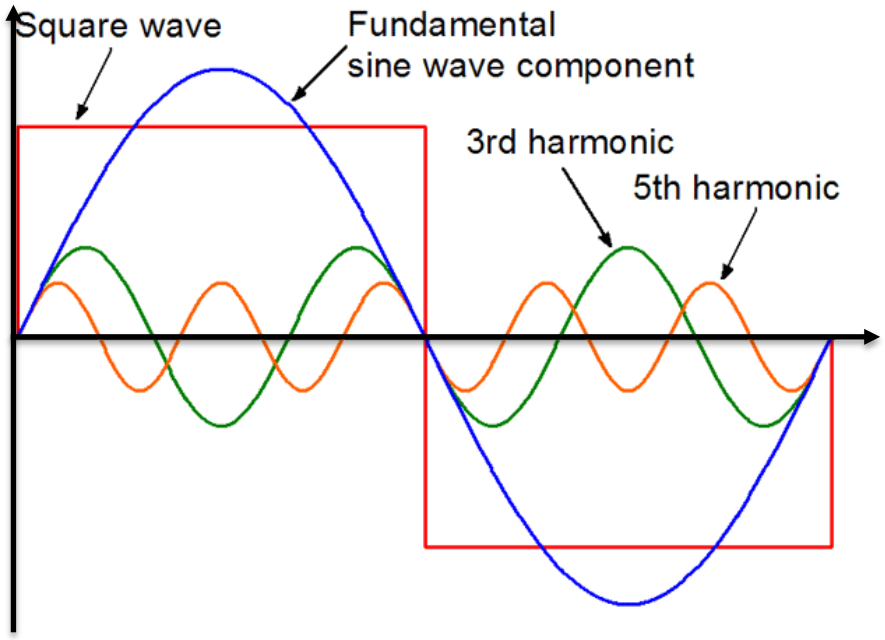

Figure.4. 4 : Harmonics.

4.3 Electrical loads connected to the electrical grid

4.2.5 Linear load

A load is considered as linear, when it is supplied by a sinusoidal voltage source, it absorbs a sinusoidal current, as an example of linear loads resistors, inductors ... etc. The **Figure (4. 5)** illustrates this type of electric loads.

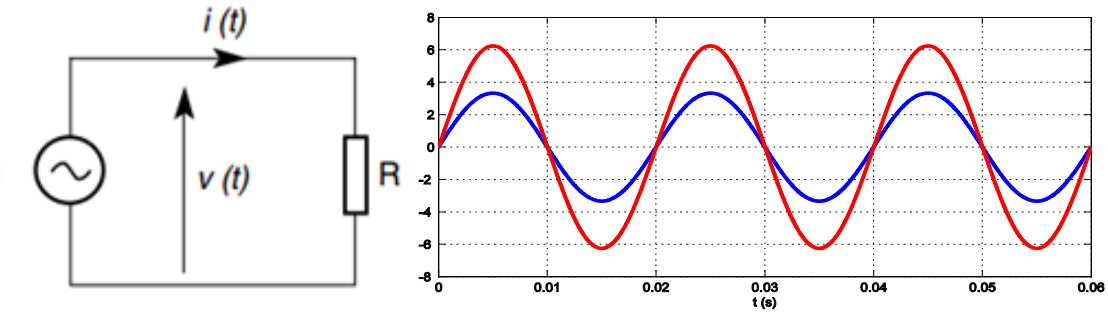

Figure.4. 5 : Waveforms of voltage and current absorbed by a resistive load

4.2.6 Non linear loads

A load is said to be nonlinear when the current it absorbs does not have the same shape as the voltage that supplies it [70]. This class of loads includes static converters (dimmers, rectifiers, etc.), saturated magnetic circuits, lamps, etc.

With the contribution of semiconductor technology to electronics, and the development known by power devices, the loads supplied by a sinusoidal voltage absorb a current which is distorted, the current and the voltage are therefore no longer proportional. The **Figure (4. 6)** presents the structure of a nonlinear load represented by a diode bridge output on an load, and powered by a grid.

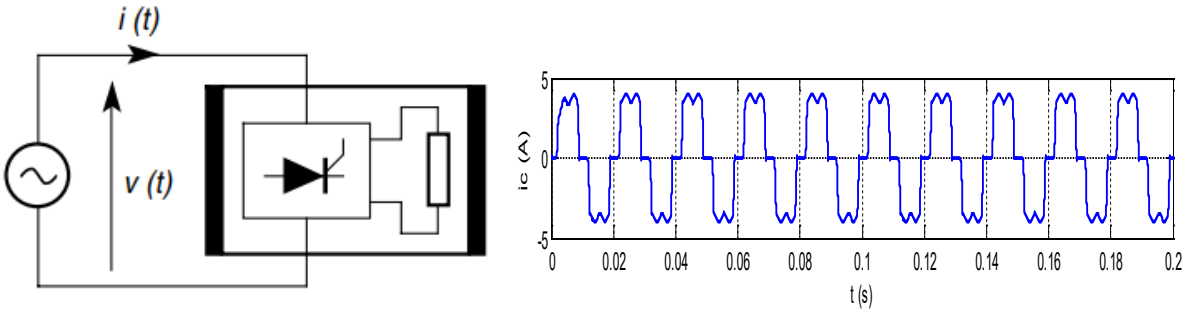

Figure.4. 6 : Mains current waveform by the effect of the pollutant load.

4.4 Mitigation of Power Quality Problems

In order to improve the quality of electrical energy and energy efficiency, the implementation of effective solutions to deal with the current problem of harmonics and their technical and economic consequences is essential [60]. The suppression of the current harmonics is important in improving the power quality [63,64]. in this section, we reveal the different depolluting remedies. we present the following solutions:

1- Oversizing of network components,

2- Use of special transformers,

3- Use of special devices (PWM rectifier, etc.),

4- Use of filtering devices (passive filtering, active filtering and hybrid filtering).

A common technique for eliminating harmonics is to use filters. the types of the most used filters to eliminate current harmonics are: passive and active filters.

Passive filtering was a solution for pollution control and power factor improvement on electrical grids. However, the increase of power electronic devices in electrical grid has limited the use of these filters which are no longer suitable for current grids. therefore, the active power filter (APF) was introduced to overcome the limitation that presents the passive filters.

4.2.1 Passive filters

Using passive components such as inductors, capacitors and transformers, these techniques offer a rapid and easy solution [77]. It can be noted that passive filters are characterized by their large size. This equipment can also cause resonance problems with the grid impedance [78]. Table 1.2 presents the advantages and disadvantages of passive filters [77].

Table 4.2: Advantages and disadvantages of passive filters.

Advantages	Disadvantages
Simple implementation of a given transfer function in terms of the number of required components	Provide no signal gain because of no active elements.
Require no power supplies because they do not have active components	May need to use buffer amplifier to have the desired values of input and output impedances
Work fine at very high frequencies since there are no bandwidth limitations of op amps	May cost a lot because of inductor characteristics such as high accuracy, small physical size and large value.
Work in applications having large current or voltage levels that the active devices cannot handle	Tuning the adjustable inductors to the required values is time-consuming and expensive when producing large quantities of filters.
Generate little noise (compared with active elements).	Can be difficult and time consuming to design complex passive filters (higher than 2nd-order)

4.2.2 Active power filters

For the purpose of minimizing the power quality problem, active power filters are introduced [61]. For some specific conditions of a system, new resonances appear with the application of passive filters [79]. In addition, the number of passive filters to implement increases with the increase in the number of harmonics to eliminate.

In the last decade, several publications have appeared on active power filters (APF) to reduce harmonics in the source currents. Active filters are adjustable with the system conditions in terms of harmonic reduction and reactive power compensation [61]. Unlike passive filters, active filters use amplifying components to synthesize the desired filter characteristics [77]. The concept of an active filter is to compensate disturbances in real time by injecting, in series or in parallel, harmonic currents or voltages in opposition to

the existing harmonics in the electrical grid. **Table 4.3** shows the advantages and disadvantages of active filters [77].

Table 4.3: Advantages and disadvantages of active filters.

Advantages	Disadvantages
Can have high input impedance, low output impedance, and virtually any arbitrary gain.	Effect on capacitors due to the problem of accuracy and value spacing. Effects here are lesser than for passive filters.
Achieve very good accuracy within the operating frequency.	Limit the performance at high frequencies because of the gain-bandwidth product of the active filter elements (such as amplifiers).
Reduce the number of the inductors.	Generate noise because of the amplifying circuitry which can be minimized by using low-noise amplifiers.

4.2.3 Active power filter topologies

APFs have different topologies depending on the type of harmonics to be eliminated, the active filters are connected either in series, in parallel or in combination of both (series and parallel). So, we distinguish three types of APFs are: series APF, shunt APF and hybrid APF [79]. The usual type of APFs is the shunt APF [65], which is used to correct the grid/source currents.

4.2.3.1 Series active power filters

This filter is considered as a voltage source since it generates harmonic voltages which oppose the disturbing voltages in order to eliminate them and preserve a perfectly sinusoidal voltage form. However, harmonic currents are not compensated by this type of filter. This type of filters utilizes a current-source inverter as shown in Figure 4.1.

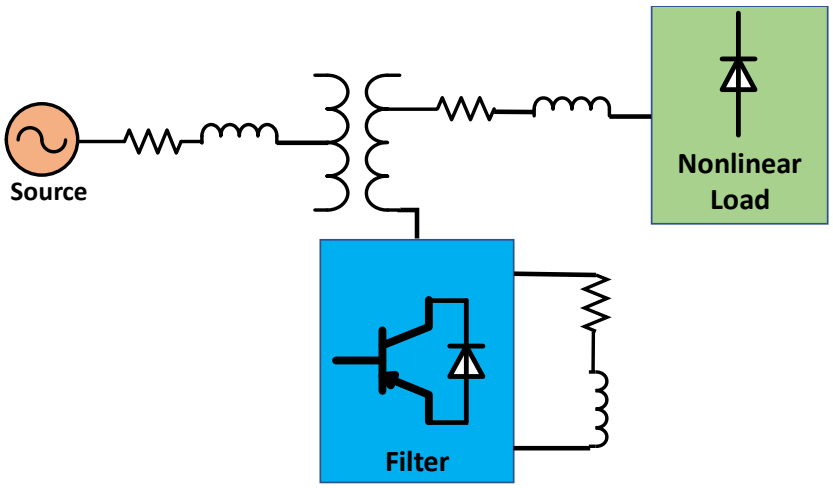

Figure.4. 7 : Series APF

4.2.3.2 Shunt active power filters

The concept of the parallel active filter is to inject harmonic currents in order to compensate the harmonic currents generated by the load. As shown in Figure, this filter employs a voltage-source inverter.

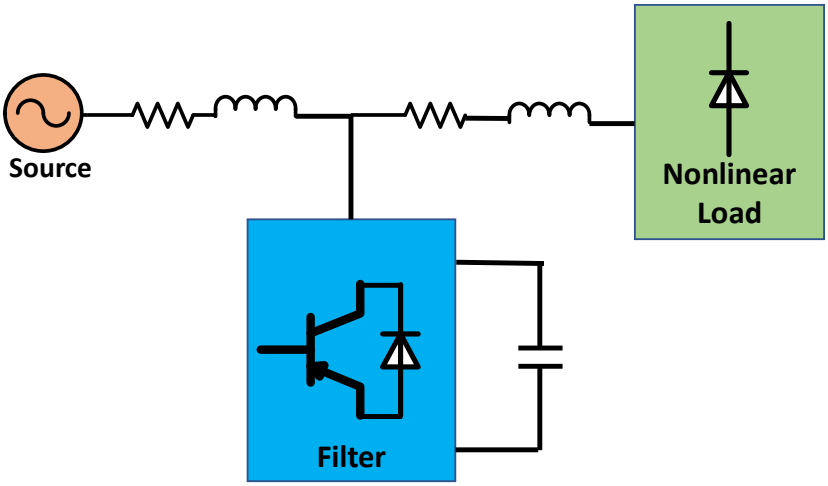

Figure.4. 8 : shunt APF

4.2.3.3 Hybrid APF

The idea of this filter is to combine the other two types [65], serial and parallel, and connect them to the network in order to benefit from their advantages (**Figure.4.1**). Therefore, this topology ensures a sinusoidal current and voltage of the electrical grid from the disturbed current and voltage. This device is obviously more powerful, however, its high price and the complexity of the control of the many switches limit its use.

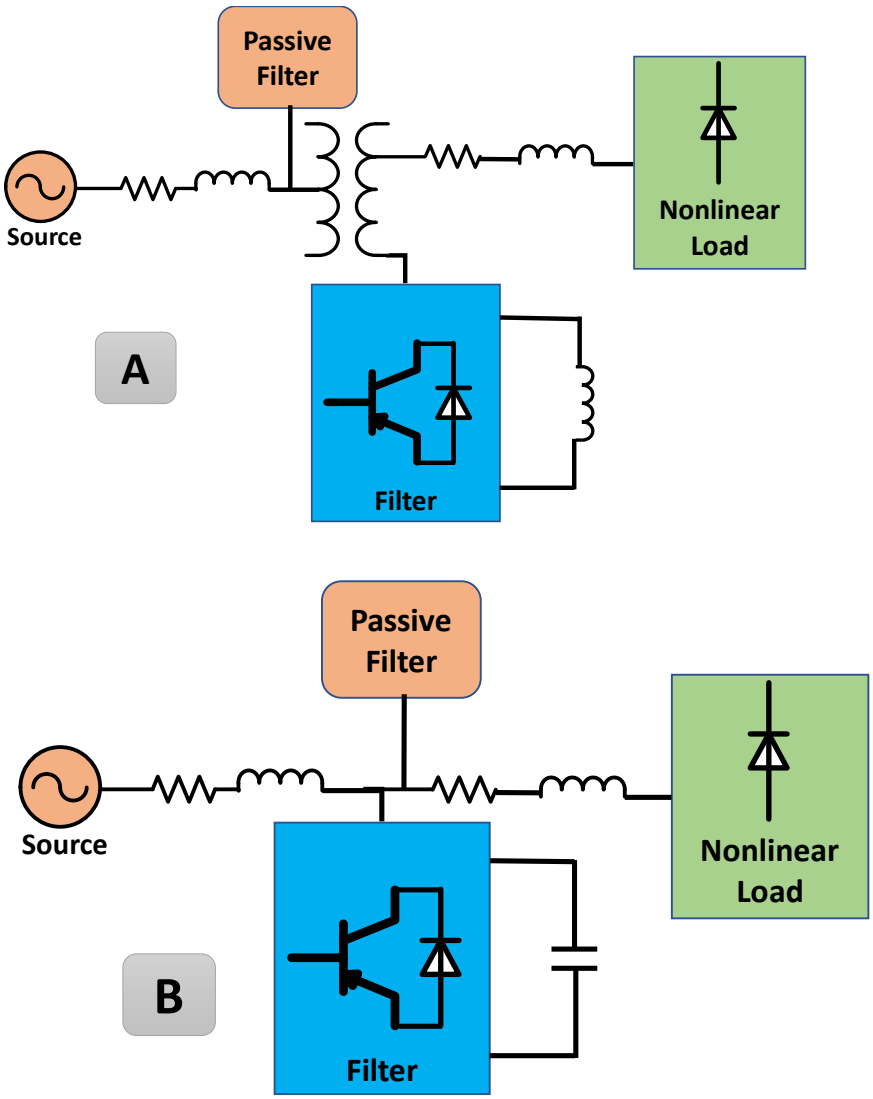

Figure.4. 9 : (A) Hybrid series APF. (B) Hybrid shunt APF

4.2.4 Proposed study system Shunt active power filters

The objective of the shunt active filters eliminate distorted components of network load currents; therefore, the source currents have low harmonic distortion and are in phase with the source voltages. Its basic principle is to compensate the load current harmonics and supply the load reactive power. Therefore, the source provides only the active power. This filter is able to compensate for any type of load and adjust itself when the load changes. Since the APF is connected in parallel to the AC mains, it does not require a transformer in the system. Shunt APFs have shown excellent performance in eliminating power quality problems associated with source currents [62, 80].

Non-linear and unbalanced loads are responsible for current harmonics and unbalanced currents. Consequently, the source currents are distorted and/or unbalanced.

The shunt active filter is mainly located on the load side and responsible for injecting harmonic currents to compensate for harmonics, unbalance and reactive power. The injected currents have equal magnitudes of and opposite phase of the source currents. This allows the source currents to provide only the fundamental components [81].

4.5 Conclusion

One of the most important problem of harmonics in the distribution grid, its characteristics, sources, and consequences have been clarified in this chapter, and because of these problems, immunity and emissions standards have been imposed to protect consumers as well as energy producers and distributors, and these standards are set by experts in the field of electrical engineering. Therefore, scientists in the field of research and technological development competed to find solutions to reduce this harmonic pollution. So that many solutions for decontamination were found. From one of these solutions, we chose the Active power filters because they are superior to the passive power filters in terms of size and resonance.

In the next section, we will discuss finding a new and robust way to control this filter.

Reference:

[60] Ali A., Aydin S., "Designing, Modeling, and Simulating a Single-phase Active Power Filter for Harmonic Compensation and Reactive Power" Bulletin of Environment, Pharmacology and Life Sciences, 2014 Academy for Environment and Life Sciences, India, Vol. 4, pp 80-89.

[61] P. Neves, D. Gonçalves, J. G. Pinto, R. Alves and J. L. Afonso, "Single-phase Shunt Active Filter interfacing renewable energy sources with the power grid," Industrial Electronics, 2009. IECON '09. 35th Annual Conference of IEEE, Porto, Portugal, 2009, pp. 3264-3269.

[62] F. Pottker de Souza and I. Barbi, "Single-phase active power filters for distributed power factor correction," 2000 IEEE 31st Annual Power Electronics Specialists Conference. Conference Proceedings (Cat. No.00CH37018), Galway, Ireland, 2000, pp. 500-505 vol.1.

[63] S. Biricik, S. Redif, O. C. Ozerdem and M. Basu, "Control of the shunt Active Power Filter under non-ideal grid voltage and unbalanced load conditions," Power Engineering Conference (UPEC), 2013 48th International Universities, Dublin, Ireland, 2013, pp. 1-5.

[64] S. Biricik, S. Redif, Ö C. Ozerdem, S. K. Khadem and M. Basu, "Real-time control of shunt active power filter under distorted grid voltage and unbalanced load condition using self-tuning filter," IET Power Electronics, vol. 7, no. 7, pp. 1895-1905, July 2014.

[65] T. Demirdelen, M. İnci, K. Ç. Bayindir and M. Tümay, "Review of hybrid active power filter topologies and controllers," 4th International Conference on Power Engineering, Energy and Electrical Drives, Istanbul, Turkey, 2013, pp. 587-592.

[66] A. Mortezaei, C. Lute, M. G. Simões, F. P. Marafão and A. Boglia, "PQ, DQ and CPT control methods for shunt active compensators — A comparative study," 2014 IEEE Energy Conversion Congress and Exposition (ECCE), Pittsburgh, PA, 2014, pp. 2994-3001.

[67] S. Khalid, B. Dwivedi and V. M. Mishra, "Constant instantaneous power based controller for a shunt active power filter under balanced, unbalanced, and distorted supply conditions," Computing, Communication & Automation (ICCCA), 2015 International Conference, Noida, India, 2015, pp. 963-967.

[68] N. Gupta, S. P. Singh and S. P. Dubey, "Neural network based shunt active filter for harmonic and reactive power compensation under non-ideal mains voltage," 2010 5th IEEE Conference on Industrial Electronics and Applications, Taichung, Taiwan, 2010, pp. 370-375.

[69] "IEEE Recommended Practice and Requirements for Harmonic Control in Electric Power Systems," IEEE Std 519-2014 (Revision of IEEE Std 519-1992), vol., no., pp.1-29, 11 June 2014.

[70] A. Teke, "Unified power quality conditioner: design, simulation and experimental analysis," PhD dissertation, University Of Cukurova, Institute of natural and applied science, Adana, Turkey, 2011.

[71] "Definitions of Voltage Unbalance," IEEE Power Engineering Review, vol. 22, no. 11, pp.49- 50, Nov. 2002.

[72] "IEEE Recommended Practice for Electric Power Distribution for Industrial Plants," IEEE Std 141-1993, pp.1-768, April 29 1994.

[73] P. Pillay and M. Manyage, "California Electricity Situation," IEEE Power Engineering Review, vol. 21, no. 5, pp. 10-12, May 2001.

[74] R. K. Varma, R. M. Mathur, G. J. Rogers and P. Kundur, "Modeling effects of system frequency variation in long-term stability studies," IEEE Transactions on Power Systems, vol. 11, no. 2, pp. 827-832, May 1996.

[75] R. Verma, P. Sahu, "Frequency fluctuation in power system: sources, control and minimizing techniques," International Journal of Advanced Research in Electrical, Electronics and Instrumentation Engineering (IJAREEIE), Vol. 3, No. 8, Aug 2014.

[76] M. Kmail, "Investigation of shunt active power filter for power quality improvement," MS Thesis, Near East university, Nicosia, Cyprus, 2012.

[77] Kerry L., "Application Note 779 A Basic Introduction to Filters - Active, Passive, and Switched Capacitor" National Semiconductor, Texas Instruments, 2010.

[78] S. Ahmed, G. Madjid, M. Youcef, T. Hamza, "Real Time Control of an Active Power Filter under Distorted Voltage Condition," IJPEDS, Vol.2, No.4, Dec 2012, pp. 424~433

[79] D. C. Bhonsle and R. B. Kelkar, "Design and simulation of single-phase shunt active power filter using MATLAB," Recent Advancements in Electrical, Electronics and Control Engineering, 2011 International Conference, Sivakasi, India, 2011, pp. 237-241.

[80] G. S. Raj and K. Rathi, "P-Q theory based Shunt Active Power Filter for power quality under ideal and non-ideal grid voltage conditions," 2015 International Conference on Power, Instrumentation, Control and Computing (PICC), Thrissur, India, 2015, pp. 1-5.

[81] Jeevananthan K. S., "Designing of Single-Phase Shunt Active Filter Using Instantaneous Power Theory" International Journal of Electrical and Electronics Research, 2014, Vol. 2, pp: 1-10. ISSN 2348-6988 (online).

CHAPTER 5

Single Phase Shunt Active Power Filter Based On Artificial Intelligence Algorithm

5.1 Introduction

This chapter presents a robust control strategy **SC-PSO** for **SP-SAPF** systems compared with others controllers (**HY**, **SMC** and **SC**). However, in published works, hysteresis controllers have been introduced and have attracted much interest in **SP-SAPF** applications. This type of controllers provides over-current protection capability for versatility and simplicity of practical implementation. To practically validate the hysteresis controller, the digital signal processor ensures a high and fast dynamic response over other types of digital controllers [82]. Despite the good performance of the hysteresis controller, it still faces the problem of a variable and high switching frequency. This causes increased power losses and produces "severe electromagnetic compatibility»

EMC noise in **SP-APF** and also complicates the selection of the coupling inductor in hysteresis current regulators. [83]. Also, the method **SMC** has good robust characteristic, but introduces the chattering effect which can cause wear, tear in actuating system and increases the energy [84] consumption of the controller (from a control effort point of view). Although one of the ways to mitigate the chatter phenomenon is used to replace the signal function in the control device with the saturation function, it does not eliminate the chatter phenomenon completely. This gives the proposed synergetic control method a major advantage over the **SMC**.

The objective in this chapter is to design a robust controller that gives good results. This is made possible by optimizing the parameter of **SC** using the **PSO** algorithm for efficient tracking of the control objectives. The **SC-PSO** is designed for **SP-SAPF** and is known for its robustness to matched "uncertainties/perturbations" and which is known for being a smooth controlled with low energy consumption.

In the sequel, simulations show the effectiveness of the **SC-PSO** controller and its performance is mainly compared to that of the **Hy** and **SC** controller. After we get the results, we will do an experimental test to prove the results in reality.

5.2 Control design of single-phase shunt active power filter

5.2.1 DC link voltage regulator

The DC input voltage of the inverter in an APF is provided by a capacitor [87]. This DC link voltage can stay constant if there is no active power exchange between the shunt APF and the grid, and if there are no losses in the inverter. Practically, both conditions can be not realized.

The power losses of the inverter can be compensated for by drawing balanced power from the grid to the DC bus. A DC-bus voltage regulator can balance the losses. As a result, the DC-link voltage control is very important in order to stabilize the power exchange, to compensate for the inverter real power losses (pdc), to generate accurate reference currents, and to regulate the DC-link voltage [82:83]. Several methods for controlling the DC-link voltage are employed in controlling a shunt APF such as a PI controller and a sliding mode controller.

PI controller is offered to decrease the instability and variations of the DC link voltage, such as indicated in "**Figure 5.1"** The DC link voltage regulator consists of the proportional gain (K_p) for enhancing the rise time and the integral gain (K_i) for smooth operation, eliminating the error between the sensed DC link voltage (V_C) and its reference (V_C^*) in steady state [33].

As shown in **Figure. 5.1**, a PI controller is cascaded with a current controller for obtaining unity power factor in a single-phase SAPF. These controllers purely filter out the load current harmonics. In fact, harmonic components are taken from the main and transferred to the SAPF.

In this condition, grid current i_s would be completely sinusoidal and in phase with the utility voltage V_s.

$$i_s^* = i_s = k \sin\theta \tag{5.1}$$

k: is a constant coefficient, which depends on local load active power consumption. Also i_s^* is reference value of the grid current. As it is explained in the next section, sin θ is generated using a single-phase PLL. The value of the k can be determined in an outer loop according to DC-link voltage error.

To calculate the PI controller's gains, firstly we must determine the transfer function of the studied system with PI controller through the Eq. (5.1) [85]:

$$\frac{V_C}{V_C^*} = \frac{(K_P/C)(s + K_i/K_P)}{s^2 + (K_P/C)\cdot s + K_i/C} \tag{5.2}$$

We notice from the Eq. (1) that the closed loop system is presented by a canonical second order transfer function.

$$\frac{V_C}{V_C^*} = \frac{\omega^2}{s^2 + 2\xi\omega_n \cdot s + \omega_n^2} \tag{5.3}$$

Through the equalization of the two denominators of equations 1 and 2, the controller's gains (K_p and K_i) are quantified as follows:

$$\begin{cases} K_P = 2\xi\omega_n C \\ K_i = C\omega_n{}^2 \end{cases} \tag{5.4}$$

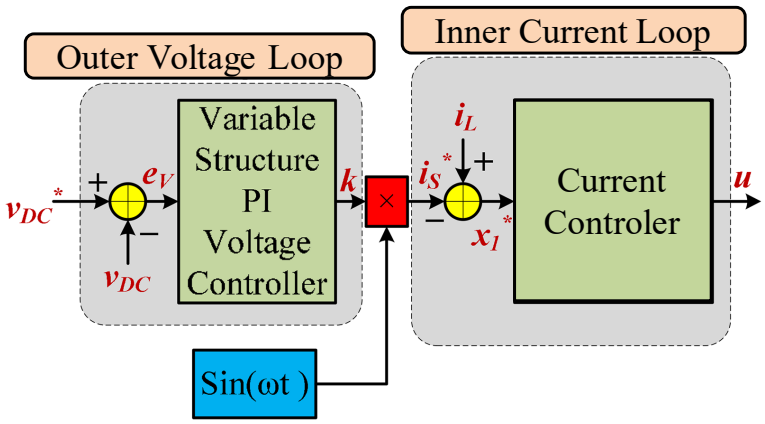

Figure.5.1: Proposed two loop controllers

5.2.2 Current control design using single-band hysteresis controller

The single-band hysteresis current controller is known for its quick response, easy implementation, maximum current limit and independency to load parameter variations. It is used to control the current in a single-phase APF so that it can produce an output current which follows a reference current signal. This technique controls the switches in a VSI such that it can force the current to go up and down to track a reference current signal. The error signal e(t), that is the difference between the reference current, $i_f^*(t)$ and the current generated by the VSI, $i_f(t)$, is used to control the switches of a V_{SI}. If the error attains the upper limit then it will cause the switches of an inverter to make the current go down, whereas, the current is forced to go up if the error reaches the lower limit. "**Figure. 5.2"(a)** illustrates the single-band hysteresis current controller, but the limitation of this controller is that its average switching frequency is not constant, which leads to losses. The maximum switching frequency for single-band hysteresis controller is given by the following equation [86]:

$$f_{sw(\max)} = \frac{V_c}{9hL} \tag{5.5}$$

where, h is the hysteresis limit, V_c is the DC-link voltage on the single-phase APF, and L_F is the value of the inductance through which the current flows.

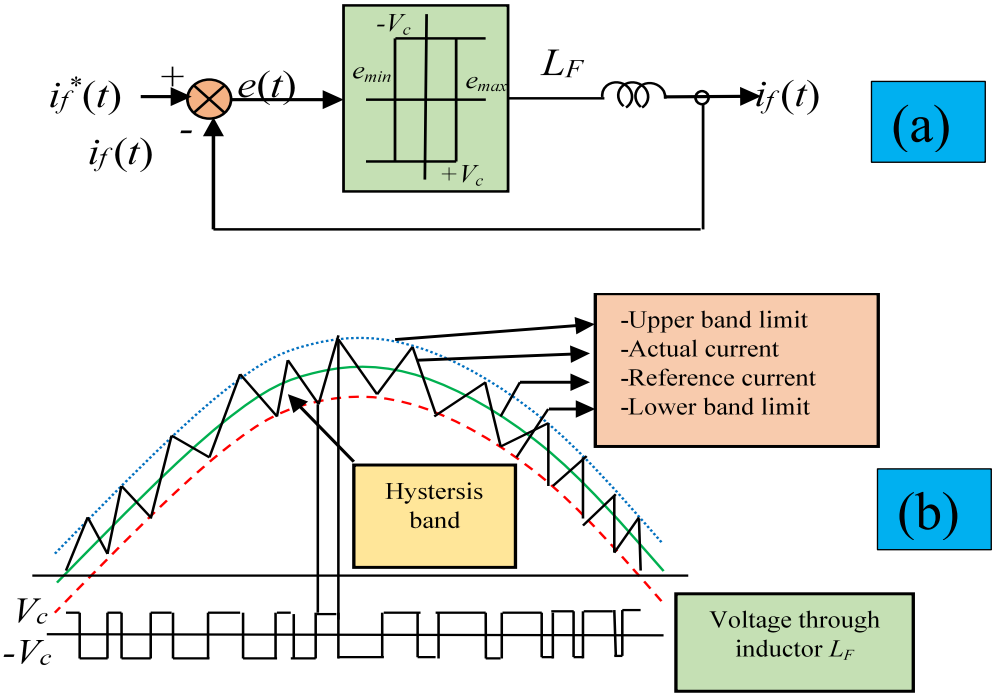

Figure.5.2: Single-band hysteresis current controller for single-phase APF.
(a) Block diagram. (b) Switching function.

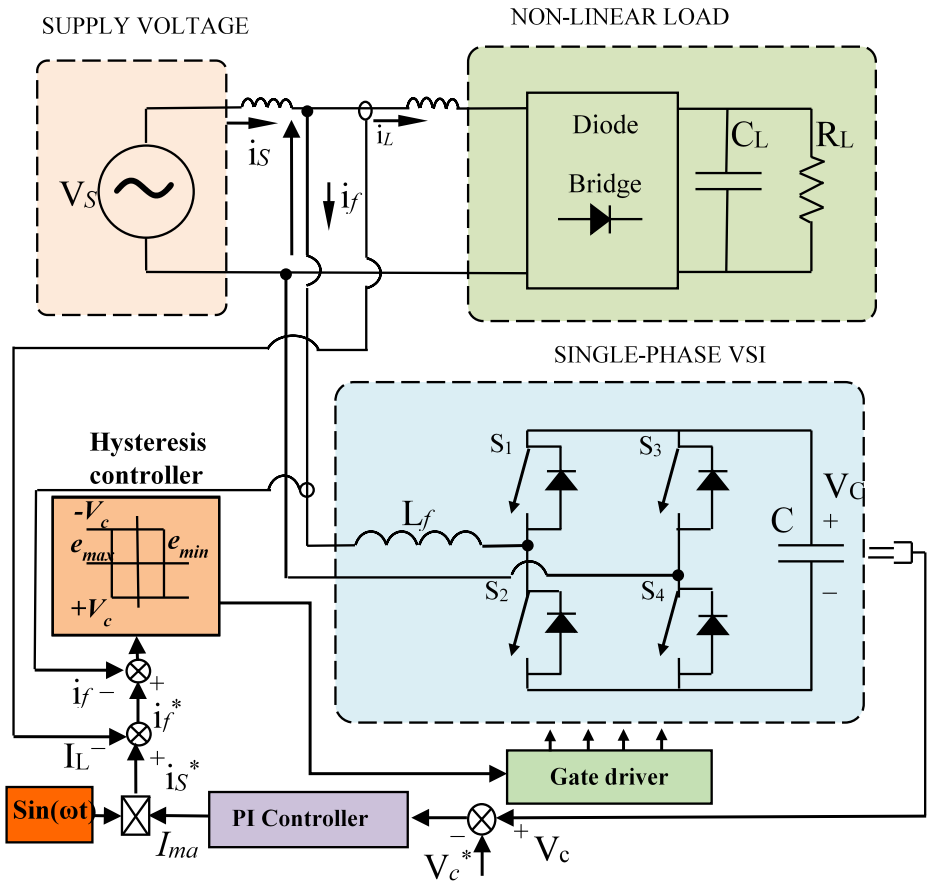

Figure.5.3: Control block diagram of **SP-SAPF** using hysteresis current controller.

5.2.3 Control design using sliding mode control

The shunt APF with the **SMC** method is operated in bipolar mode illustrated in **Figure. 5.4**. At positive half cycle of the grid voltage, Q1, Q3 are on and Q2, Q4 are off during $0<t<dT_s$, and Q2, Q4 are on and Q1, Q3 are off during $dT_s<t<T_s$, vice versa at negative half cycle, where T_s is the switching period, and d is the duty ratio of the converter.

Figure. 5.5. (a) and (b) show the equivalent circuit of the SAPF during one switching cycle in which the non-linear load is expressed as a constant current source i_L.

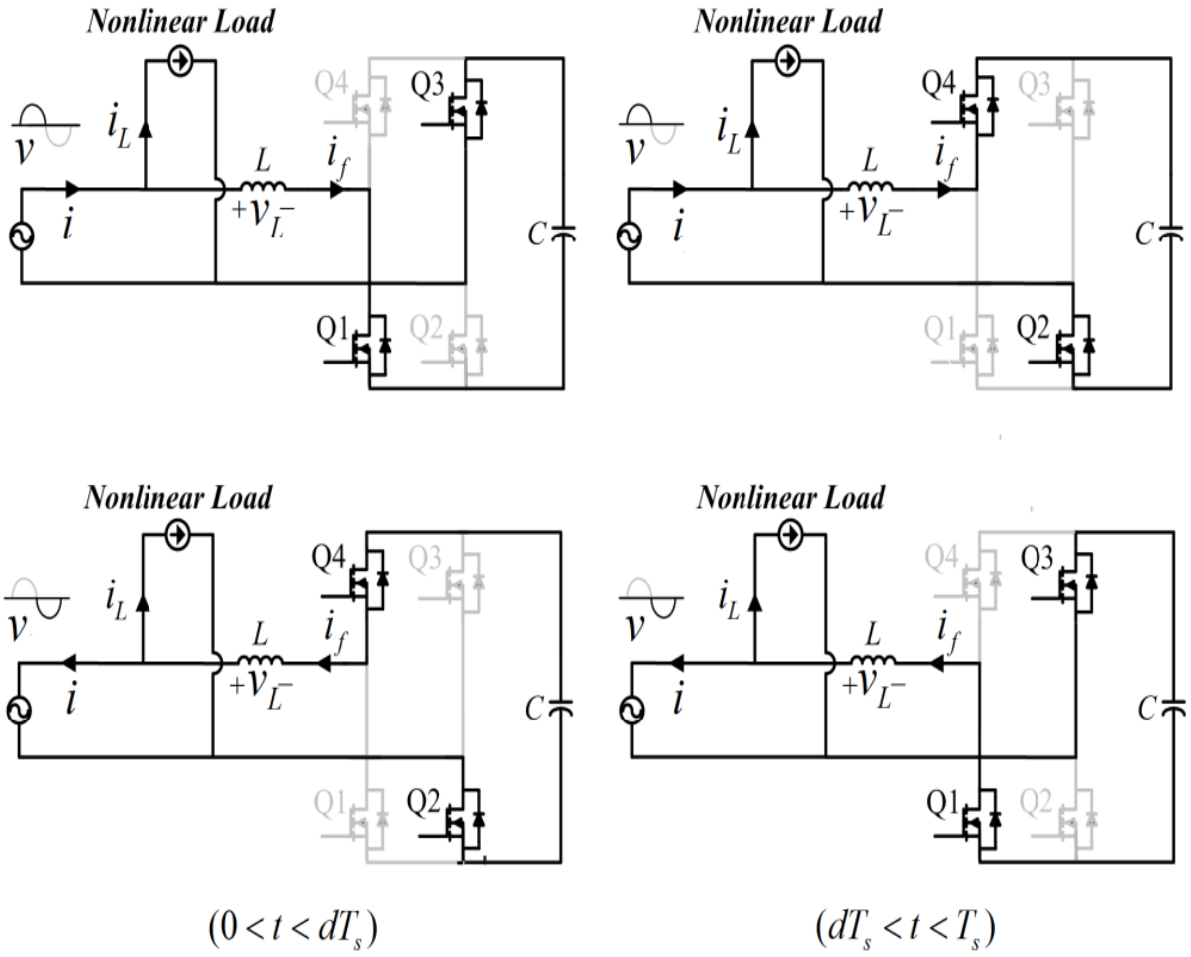

Figure.5.4: Operation modes of the shunt APF power stage

On the assumption that at first the switching frequency fs of the SAPF is much higher than those of the line and the non-linear load currents, second the capacitance of the dc-link capacitor C is large enough so that Vc is regulated to be a constant value in each switching cycle, the current if is approximately constant during the switching period. Then, by using volt-second balance of the APF inductor L in the equivalent circuit of the SAPF shown in Figure. 5.5.

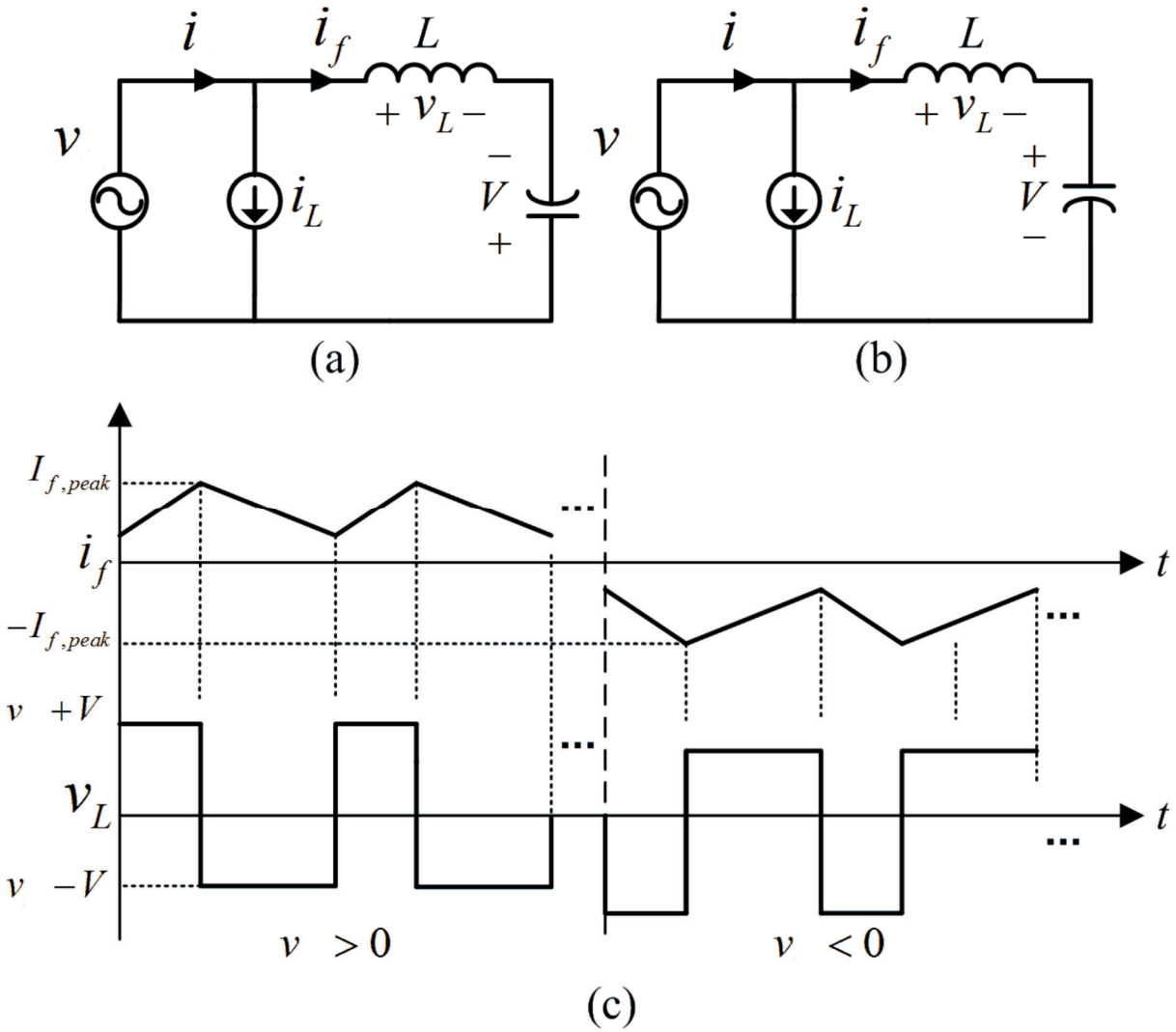

Figure.5.5: Equivalent circuit of the SAPF and operation waveforms.
(a) 0<t<dTs when vs>0, (b) dTs<t<Ts when vs>0,
(c) APF inductor current and voltage.

By using the State space averaging technique The differential equations form of nonlinear dynamic for **SP-SAPF** system is given by the Eq. (5.6).

$$\begin{cases} \dot{x}_1 = \dfrac{-1}{L_f} x_2 (1-2U_d) + \dfrac{V_{SS}}{L_f} \\ \dot{x}_2 = \dfrac{1}{C} x_1 (1-2U_d) \end{cases} \qquad (5.6)$$

$$\begin{cases} f(x) = \dfrac{-1}{L_f} x_2 + \dfrac{V_{SS}}{L_f}, \quad g(x) = \dfrac{2}{L_f} x_2, U = U_d \end{cases}$$

As reminder: *x(t)* represents the state coordinate; x_1 represents the current filter (i_f); x_2 represents the DC link voltage (V_C); U_d is the control input (the duty ratio); L_f is the inductor of **SP-SAPF** and *C* is the capacitor of the DC link voltage.

The basic idea of the **SMC** is first to attract the tracking errors of the system's state variables into a suitably selected region $\sigma(X,\ t)=0$, then design a control law $\mathbf{U_{sw}}$ that always maintains the system in that region. In summary, an **SMC** consists of two parts like in Eq(1.1). The equivalent control $\mathbf{U_{eq}}$ is determined by the model of the system. It is designed with the equivalent control method, whose principle is based on the determination of the system behavior when it is on the sliding surface S.

The control objective is to force the output $\mathbf{i}_f$ towards a reference trajectory $\mathbf{i}_f^*$. The relative degree with respect to the error $e_{\mathbf{i}_f}=\mathbf{i}_f-\mathbf{i}_f{}^*$ is equal to 2, satisfying **Assumption 1.1**. Then, following Eq(1.5), define the sliding variable as:

$$\sigma_{\mathbf{i}_f}=e_{\mathbf{i}_f}+c_{\mathbf{i}_f}\int e_{\mathbf{i}_f}\qquad e_{\mathbf{i}_f}=x_1-x_1{}^*=\mathbf{i}_f-\mathbf{i}_f{}^* \tag{5.7}$$

with $c_z>0$. Then, the sliding surface is given by:

$$S=\left\{x\in \mathrm{X}\ \middle|\ \sigma_{\mathbf{i}_f}=\dot{e}_{\mathbf{i}_f}+c_{\mathbf{i}_f}e_{\mathbf{i}_f}=0\right\} \tag{5.8}$$

We start by determining the equivalent order U_{zeq}, it is calculated when:

$$\sigma_{\mathbf{i}_f}=0 \text{ and } \dot{\sigma}_{\mathbf{i}_f}=0 \tag{5.9}$$

The relative degree of the altitude equation Eq(5.6) with respect to σ is equal to 1 and has the following Equation

$$\dot{\sigma}_{\mathbf{i}_f}=\dot{e}_{\mathbf{i}_f}+c_{\mathbf{i}_f}e_{\mathbf{i}_f}=\dot{x}_1-\dot{x}_1{}^*+c_{\mathbf{i}_f}e_{\mathbf{i}_f} \tag{5.10}$$

By replacing Eq(5.6) in Eq(5.10) we find

$$\begin{aligned}\dot{\sigma}_{\mathbf{i}_f}&=f\ (x,t)-\dot{x}_1{}^*+c_{\mathbf{i}_f}e_{\mathbf{i}_f}+g\ (x,t)U_{\mathbf{i}_f}\\ \dot{\sigma}_{\mathbf{i}_f}&=\bar{a}(x,t)+\bar{b}(x,t)u\end{aligned} \tag{5.11}$$

which is of the form of Eq(1.7) satisfying **Assumption 1.2**.
From Eq(5.8) and Eq(5.9) we find

$$\dot{x}_{\mathbf{i}_f} - \dot{x}^*_{\mathbf{i}_f} + c_{\mathbf{i}_f}\left(x_{\mathbf{i}_f} - x^*_{\mathbf{i}_f}\right) = 0 \tag{5.12}$$

$U_{\mathbf{i}_f eq}$ it is calculated when $\dot{\sigma}_z = 0$, From Eq(3.11) we obtain

$$U_{\mathbf{i}_f eq} = \frac{1}{g(x,t)}\left[\dot{x}_1^* - f(x,t) - c_{\mathbf{i}_f}\left(x_{\mathbf{i}_f} - x^*_{\mathbf{i}_f}\right)\right] \tag{5.13}$$

$$U_{veq} = \frac{1}{\frac{2}{L_f}x_2}\left[\dot{x}_1^* + \frac{1}{L_f}x_2 - \frac{V_{SS}}{L_f} - c_{\mathbf{i}_f}\left(x_{\mathbf{i}_f} - x^*_{\mathbf{i}_f}\right)\right] \tag{5.14}$$

As previously indicated Eq(1.1), the control law is formed by two terms, the equivalent control law and the switching control law:

$$U = U_{zsw} + U_{zeq} \tag{5.15}$$

The equivalent part is a continuous control law deduced from $\frac{\partial \sigma_z(e,t)}{\partial t} = \dot{\sigma}_z(e,t) = 0$ and the second control part us has a discontinuous $U_{i_f sw}$ feature defined as in chapter 1:

$$U_{\mathbf{i}_f sw} = -k_{\mathbf{i}_f} sign(\sigma_{\mathbf{i}_f}) \tag{5.16}$$

where ***Kif*** is a positive constant and sign is the sign function.

Consequently

$$\begin{aligned} U_{\mathbf{i}_f} &= -k_{\mathbf{i}_f} sign(\sigma_{\mathbf{i}_f}) + \frac{1}{g(x,t)}\left[\dot{x}_1^* - f(x,t) - c_{\mathbf{i}_f}\left(x_1 - x_1^*\right)\right] \\ U_{\mathbf{i}_f} &= -k_{\mathbf{i}_f} sign(\sigma_{\mathbf{i}_f}) + \frac{L_f}{2x_2}\left[\dot{x}_1^* + \frac{1}{L_f}x_2 - \frac{V_{SS}}{L_f} - c_{\mathbf{i}_f}\left(x_{\mathbf{i}_f} - x^*_{\mathbf{i}_f}\right)\right] \end{aligned} \tag{5.17}$$

Considering the sliding variable σ_z Eq(5.7), a Lyapunov function candidate satisfying **Definition 1.2** takes the following form

$$V(x,t) = \frac{1}{2}\sigma_z^2(x,t) \tag{5.18}$$

In order to ensure the asymptotic convergence of the sliding variable σ_z, the time derivative of **V** has to be negative definite i.e. Therefore, the derivative of the function Eq(5.18) is:

$$\dot{V}(x,t) = \sigma_z(x,t)\ \dot{\sigma}_z(x,t) \tag{5.19}$$

In order for the function $\dot{V}(x,t)$ to decrease, it is sufficient to ensure that its derivative is negative. This is only true if condition Eq(3.19) is satisfied.

$$\sigma_z(x,t)\ \dot{\sigma}_z(x,t) < 0 \tag{5.20}$$

By emplacing Eq(5.11) in Eq(5.19) we obtain

$$\dot{V}(x,t) = \sigma_{\mathbf{i}_f}(x,t)\ \left[-\dot{x}_1^{\,*} + f(x,t) + c_{\mathbf{i}_f} e_{\mathbf{i}_f} + g_6(x,t)U_z\right] \tag{5.21}$$

By emplacing Eq(3.17) in Eq(3.21) we obtain

$$\dot{V}(x,t) = \sigma_{\mathbf{i}_f}(x,t) \begin{bmatrix} -\dot{x}_1^{\,*} + f(x,t) + c_{\mathbf{i}_f} e_{\mathbf{i}_f} + g(x,t) - k_{\mathbf{i}_f} sign(\sigma_{\mathbf{i}_f}) \\ +\dfrac{L_f}{2x_2}\left[\dot{x}_1^{\,*} + \dfrac{1}{L_f}x_2 - \dfrac{V_{SS}}{L_f} - c_{\mathbf{i}_f}\left(x_{\mathbf{i}_f} - x_{\mathbf{i}_f}^{*}\right)\right] \end{bmatrix}$$

$$\dot{V}(x,t) = \sigma_{\mathbf{i}_f}(x,t) \begin{bmatrix} -\dot{x}_1^{\,*} + f(x,t) + c_{\mathbf{i}_f} e_{\mathbf{i}_f} + \dot{x}_1^{\,*} - f(x,t) - c_{\mathbf{i}_f} e_{\mathbf{i}_f} \\ -g(x,t)k_{\mathbf{i}_f} sign(\sigma_{\mathbf{i}_f}) \end{bmatrix}$$

$$\dot{V}(x,t) = \sigma_{\mathbf{i}_f}(x,t)\ \left[-g(x,t)k_{\mathbf{i}_f} sign(\sigma_{\mathbf{i}_f})\right] \tag{5.22}$$

$$-g(x,t)k_{\mathbf{i}_f} sign(\sigma_{\mathbf{i}_f}) < 0 \quad \Rightarrow \dot{V}(x,t) < 0$$

Note that

$$g(x,t) = \frac{2}{L_f}x_2 > 0 \Leftrightarrow x_2 > 0, \quad and \quad k_{\mathbf{i}_f} > 0$$

$$-sign(\sigma_{\mathbf{i}_f}) < 0 \Rightarrow -\left|\sigma_{\mathbf{i}_f}\right| < 0$$

Therefore, under the **SMC** controller, the system state can reach, and, thereafter, stay on the manifold S=0 in finite-time.

The equations Eq(5.18), explains that the square of the distance between a given point of the phase plane and the sliding surface expressed by $\sigma_{\mathbf{i}_f}^2(x,t)$ decreases all the

time, i.e. the state system will be attracted to the sliding surface, hence the name of attractivity.

Form Eq(5.22) it can be found that $\dot{V}(x,t) < 0$. On the basis of Lyapunov theory, the stability of the **SP-SAPF** system is assured via the SMC control law.

5.2.4 Control design using Synergetic control synthesis for SP-SAPF

The synergetic control synthesis in Eq(5.23)of the system that we have presented in Eq. (5.6) started by demonstrating a designer that is been chosen as macro-variable and given in Eq(5.24).

$$T\frac{d\xi}{dt} + \xi = 0, \quad T > 0 \tag{5.23}$$

T is a positive constant to be imposed by the designer. In our paper, its value is optimized by PSO algorithm.

$$\xi = e_{if} + \lambda\int e_{if} = (x_1 - x_1^*) + \lambda\int (x_1 - x_1^*)dx(t) \tag{5.24}$$

$$\dot{\xi} = \dot{e}_{if} + \lambda e_{if}$$
$$\dot{\xi} = \left[\frac{1}{L_f}x_2(2U_d - 1) + \frac{V_{ss}}{L_f} - \dot{x}_1^*\right] + \lambda(x_1 - x_1^*) \tag{5.25}$$

Moreover, having Eq(1.23) and Eq(5.25), the resulting control law U_d is given by Eq(5.27):

$$T\left[\frac{1}{L_f}x_2(2U_d - 1) + \frac{V_{ss}}{L_f} - \dot{x}_1^*\right] + T.\lambda(x_1 - x_1^*) + \psi = 0 \tag{5.26}$$

$$U_{SC} = U_d = \frac{\frac{\xi}{\mathrm{T}} + \lambda(x_{if} - x_{if}^*) - x_{if}^* + \frac{1}{L_f}V_{ss}}{\frac{2}{L_f}x_2} + \frac{1}{2} \tag{5.27}$$

To confirm stability, we use the following Lyapunov function candidate:

$$V = \frac{1}{2}\xi^T\xi \tag{5.28}$$

Therefore:

$$\dot{V} = \xi^T \dot{\xi} \tag{5.29}$$

The use of Eq(5.25) in Eq(5.29) leads to Eq(30):

$$\dot{V} = \xi\left(\frac{-\xi}{T}\right) = -\frac{1}{\mathrm{T}}\xi^2 \tag{5.30}$$

Form Eq. (5.30) it can be found that $\dot{V} < 0$.

On the basis of Lyapunov theory, the stability of the **SP-SAPF** system is assured via the synergetic control law.

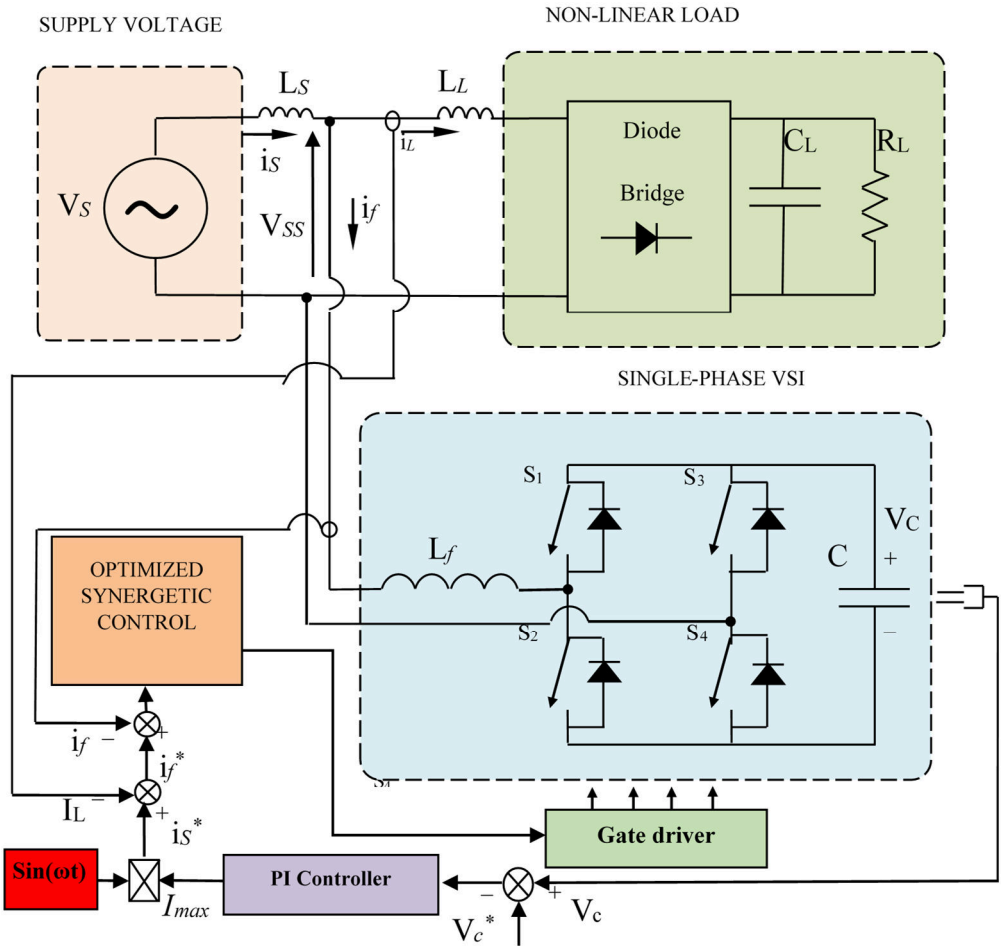

Figure.5.6: Description of proposed **SP-SAPF** system

5.2.4.1 Implementation of PSO for Synergetic controller (SC-PSO)

5.2.4.1.1 Formulation of the problem to be optimized

The formulation of the problem to be optimized is mainly concerned with minimizing the error *ERR = i_f – i_f** where the objective function *F(X)* can be written as fellow:

$$Min\,F(x) = Min(ERR) \tag{5.31}$$

With: X the control parameter set which can be written in the following form:

$$X = [T, \lambda] \tag{5.32}$$

The objective function is subjected to inequality constraints as shown below:

$$\begin{aligned} T^{\min} < \mathrm{T} < T^{\max} \\ \lambda^{\min} < \lambda < \lambda^{\max} \end{aligned} \tag{5.33}$$

5.3 Simulation results

The performance of the proposed **SP-SAPF** system based on SC strategy optimized by **PSO** has been evaluated by using MATLAB/Simulink software. The nominal values for **SP-SAPF** system parameters and components are listed in **Table 5.1**.

Table 5.1: Parameters of the studied system

Parameters	Symbol	Values
System frequency	f_s	50 Hz
Source voltage	V_S	50V
Input inductance	L_S	4mH
Load inductance	L_L	2mH
Load resistance	R_L	11.5Ω
Load capacitor	C_L	550µF
Filter inductance	L_f	8mH
Filter capacitor	C	1100µF
Voltage reference	V_C^*	110V

The obtained simulation results are ranging from 5 to 9. **Figure. 5.7** shows both source voltage (V_S), source current (i_S), load current (i_L) and the filter current (i_f). The source current is presented by a sinusoidal shape and in phase with the input voltage of the single-phase network. In their turn, both line and filter currents have been presented by their appropriate waveforms.

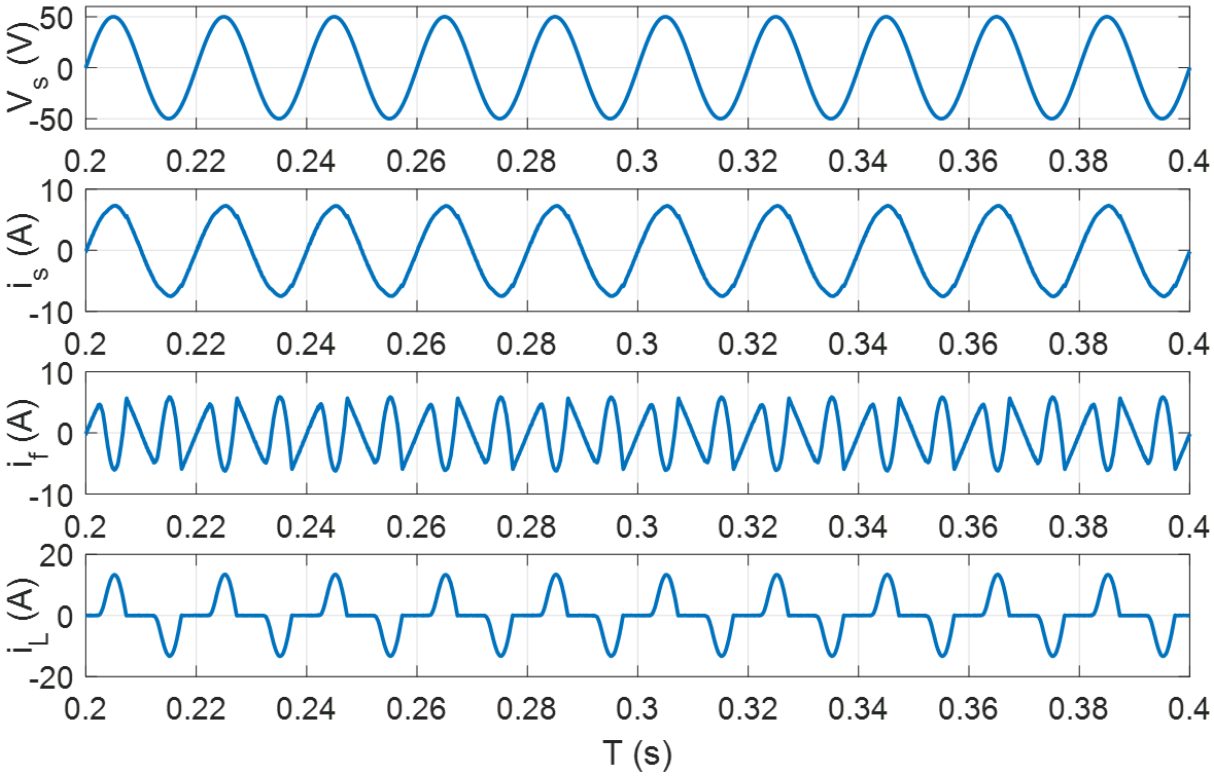

Figure.5.7: SP-SAPF performance waveforms under nonlinear load

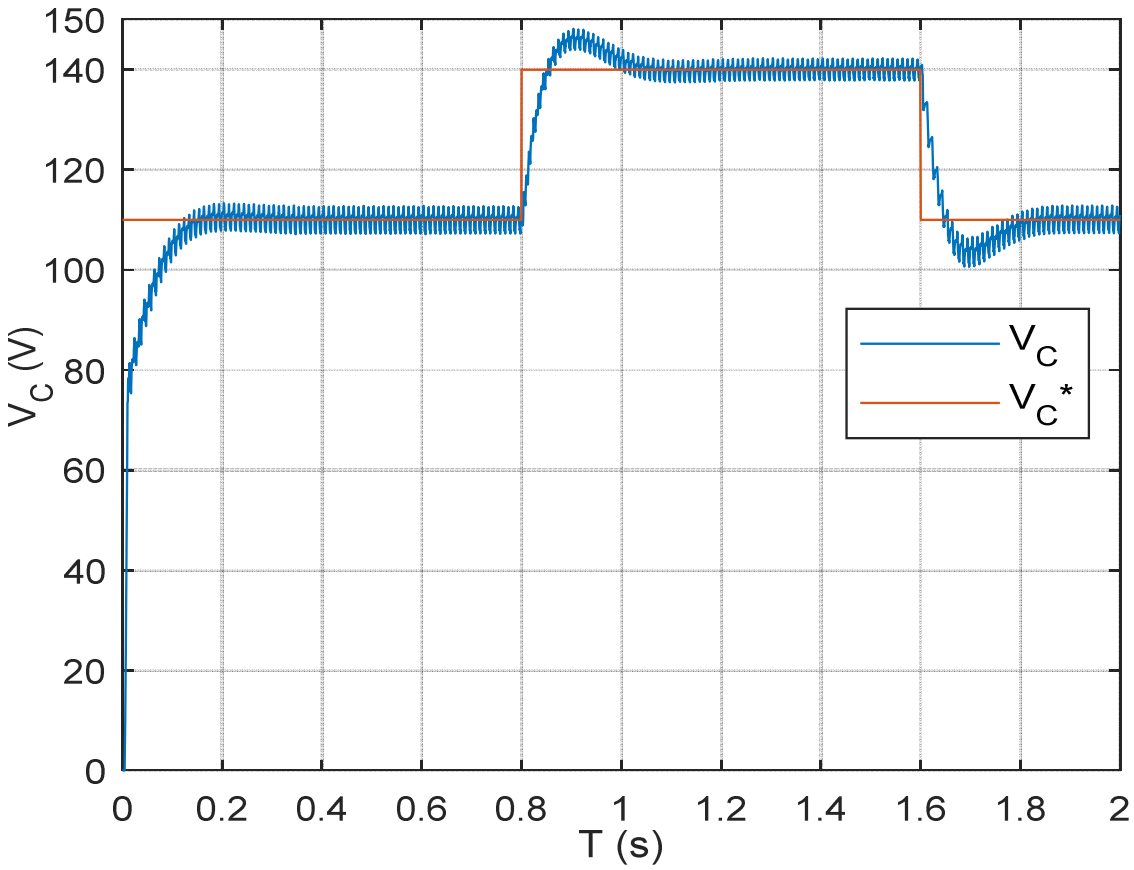

Figure.5.8: Simulation results of the output voltage (V_C) under change of voltage references (V_C*)

Figure. 5.8 shows the performance of the DC link voltage under the conventional PI controller used during start-up as well as its progression towards the imposed reference voltage. The sensed output voltage (V_C) correctly reaches its reference values (V_C^*) of: 110V, 140V and 110V in a very satisfactory manner.

To show the robustness of the suggested **SC-PSO** approach, the DC link voltage is fixed to 110V and the nonlinear load underwent a modification in t_1 = 1s by the addition of the resistance R = 23Ω in parallel with the old load then its elimination in t_2 = 1.5s.**THE** DC link voltage (V_C) and the source current (i_S) react correctly to these imposed operating conditions as shown in **Figure. 5.9**.

A comparative simulation study between the classical hysteresis control, the synergistic and optimized synergistic approach applied to the single-phase filter have been established in order to evaluate the quality of the source current (i_s) as shown in **Figure. 5.10**. The spectral analysis of these source currents has been presented in **Figure. 5.11**.

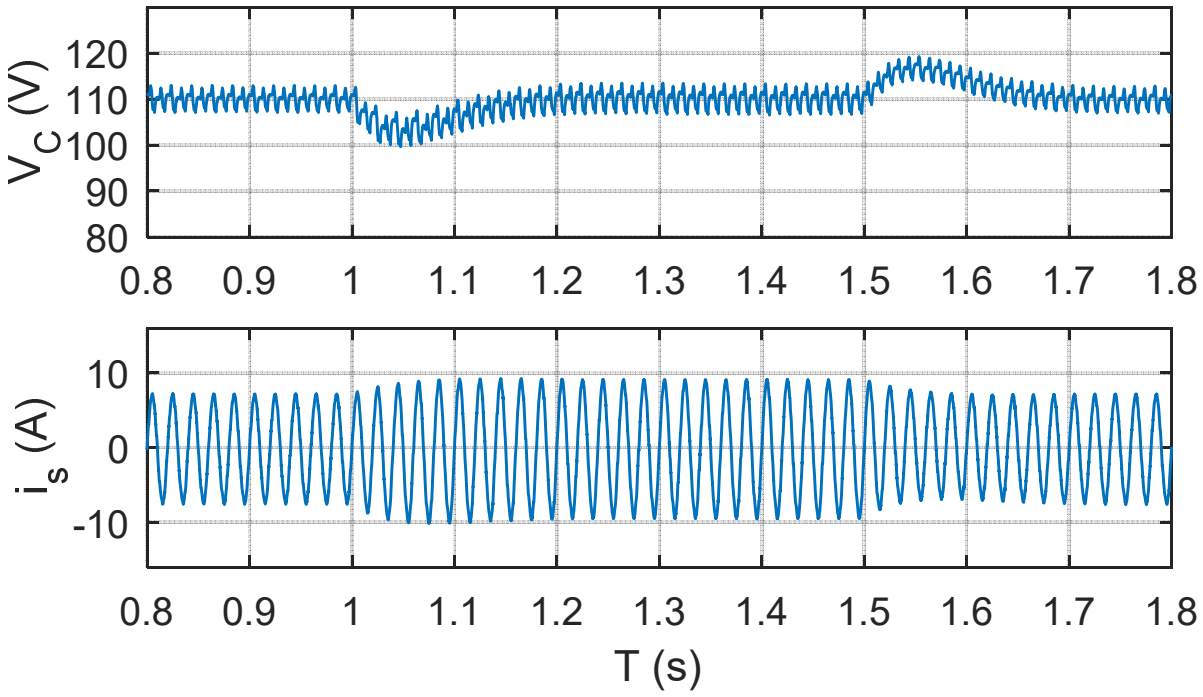

Figure.5.9: Simulation results of DC link voltage (V_C)and source current (i_s) during the change of the load

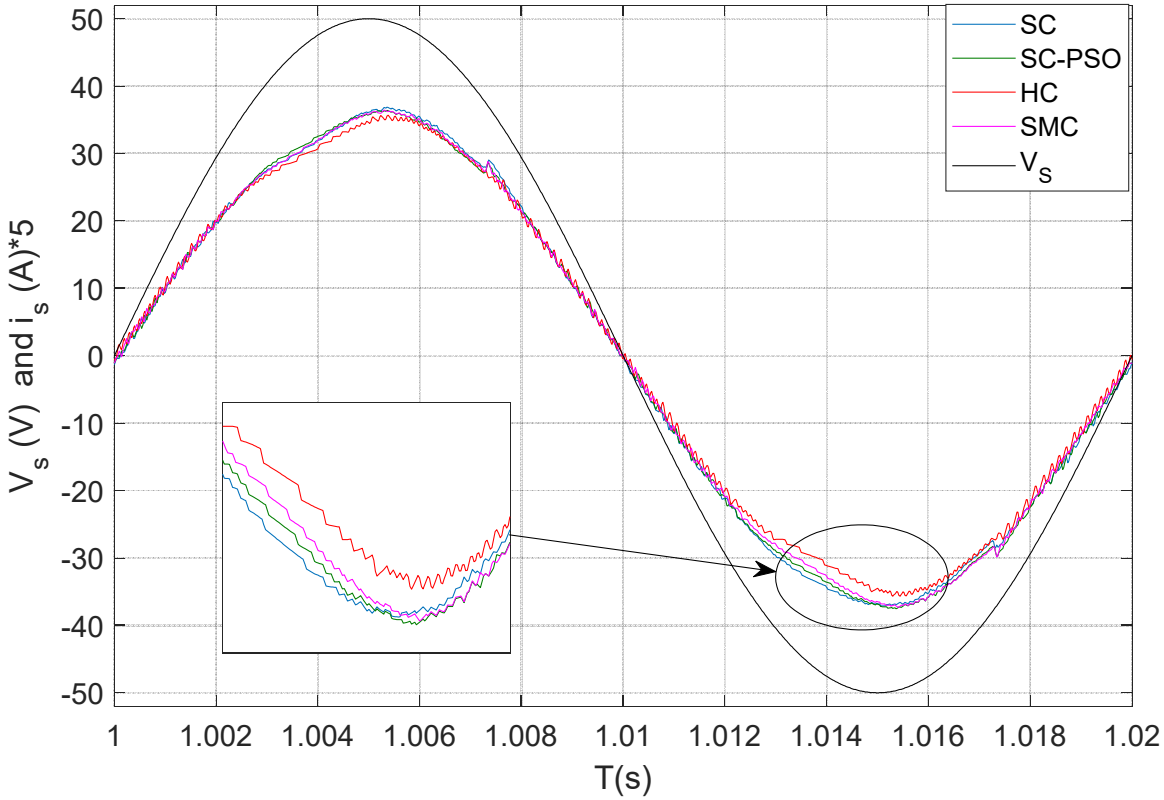

Figure.5.10: Compared waveforms of the source current (i_s)

It is clearly visible that in the absence of the parallel active filter, a THD of 49.07% was recorded. After activation of the parallel active filter controlled by the three techniques mentioned previously, new THD values were recorded which are respectively equal to: 3.63%, 2.82% and 2.35%. Through these results, the optimized synergistic control strategy of the **SP-SAPF** system clearly marked its superiority compared to other conventional hysteresis and non-optimized synergistic techniques.

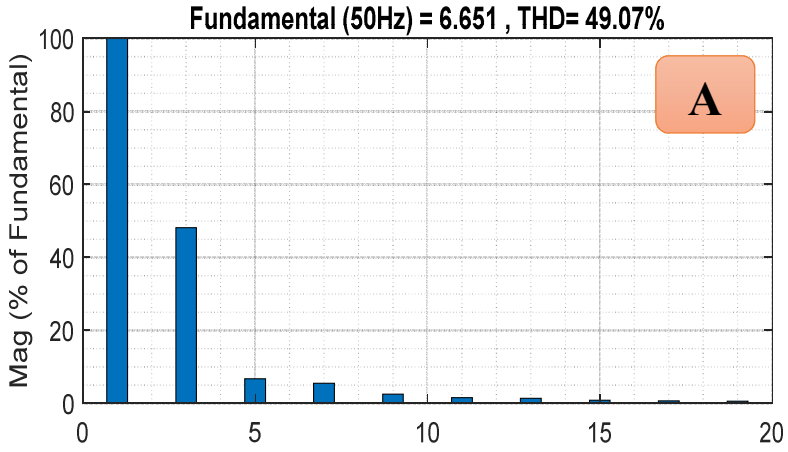

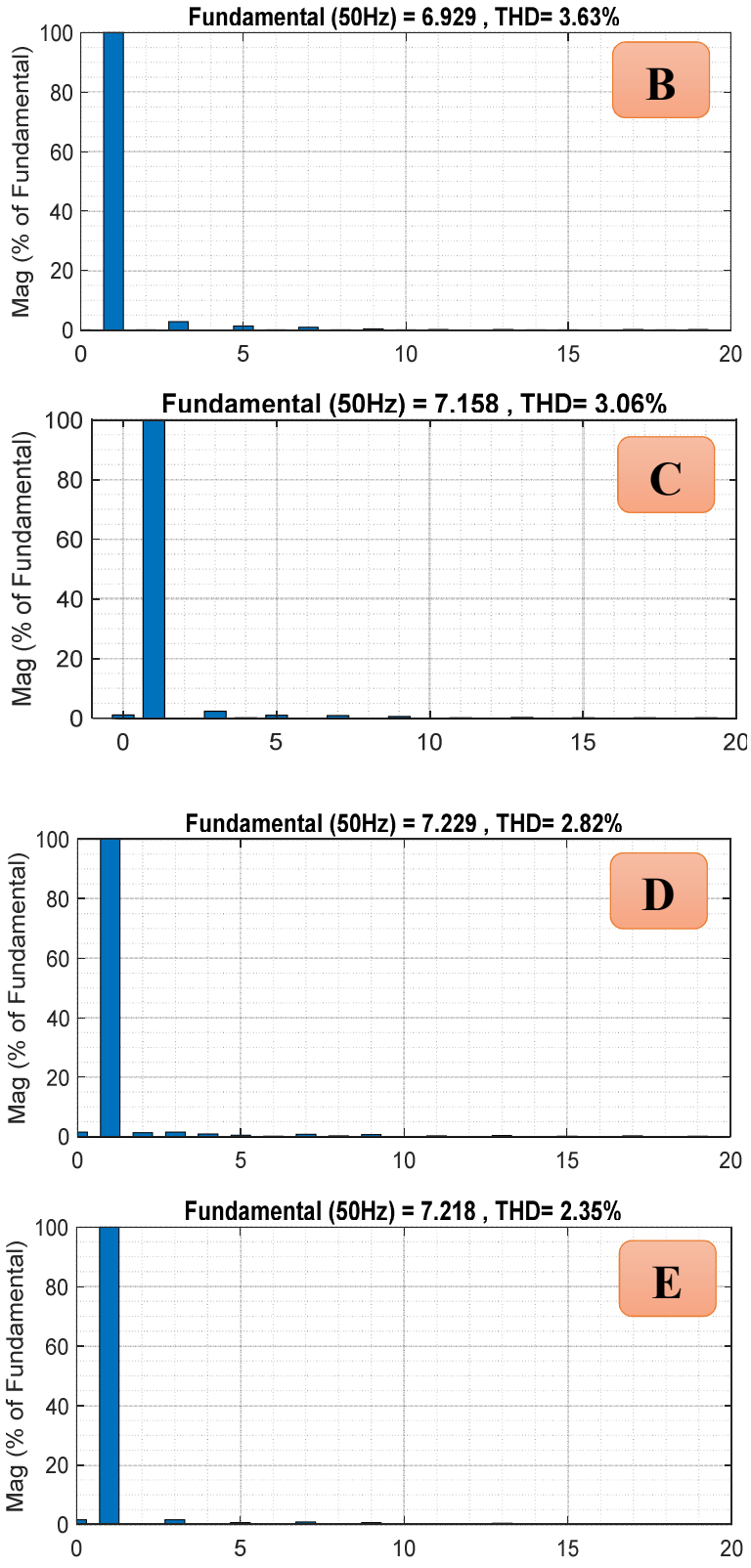

Figure.5.11: Source current spectral analysis: (A) without **SAPF**, (B) with **Hy** control, (C) with **SMC** method, (D) with **SC** method and (E) with the proposed **SC-PSO** method

5.4 Experimental results of SC-PSO for SP-SAPF

To give more confidence to our study, an experimental test bench is carried out using a dSPACE 1104 board as presented in **Figure. 5.12**. The performance of considered synergetic approach based on **PSO** algorithm and **PI** controller for the **SP-SAPF** has been tested for several conditions. For assess the studied control strategy, our **SP-SAPF** system is experienced in transient and steady states.

Furthermore, coverage of changes affecting the nonlinear load, the DC link voltage (V_C) and the power source (V_S) has been taken into consideration in this section. Using the power quality analyzer (Chauvin ArnouxC.A.8335) and the digital oscilloscope (GwinstekGDS-3504), the obtained practical results are recorded and presented in the following sections.

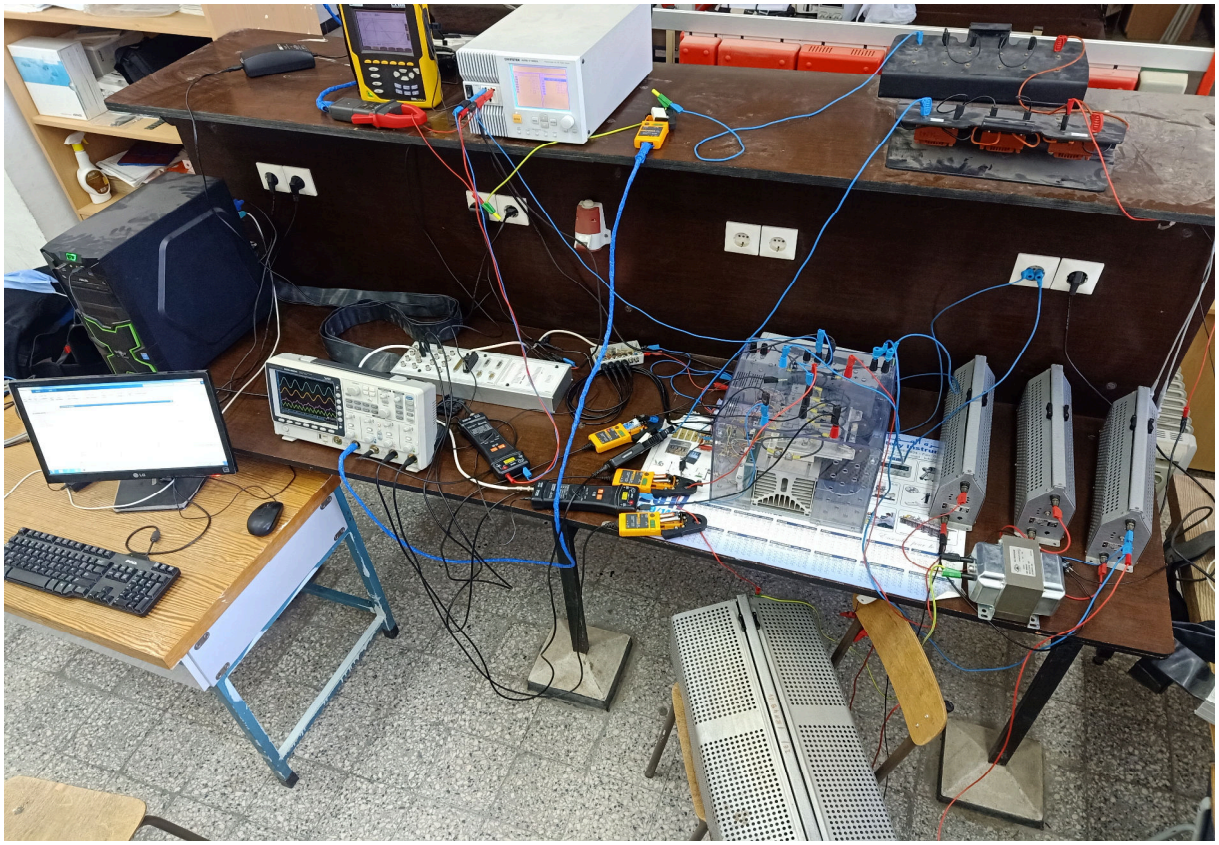

Figure.5.12: Photograph of platform of the experiment test.

5.4.1 SP-SAPF performance in transient and steady states

The start transient of the **SP-SAPF** at the reference point of DC link voltage V_C^* of 110V accompanied by the currents i_s, i_L and if responds smoothly without overshooting as shown in **Figure. 5.13**.

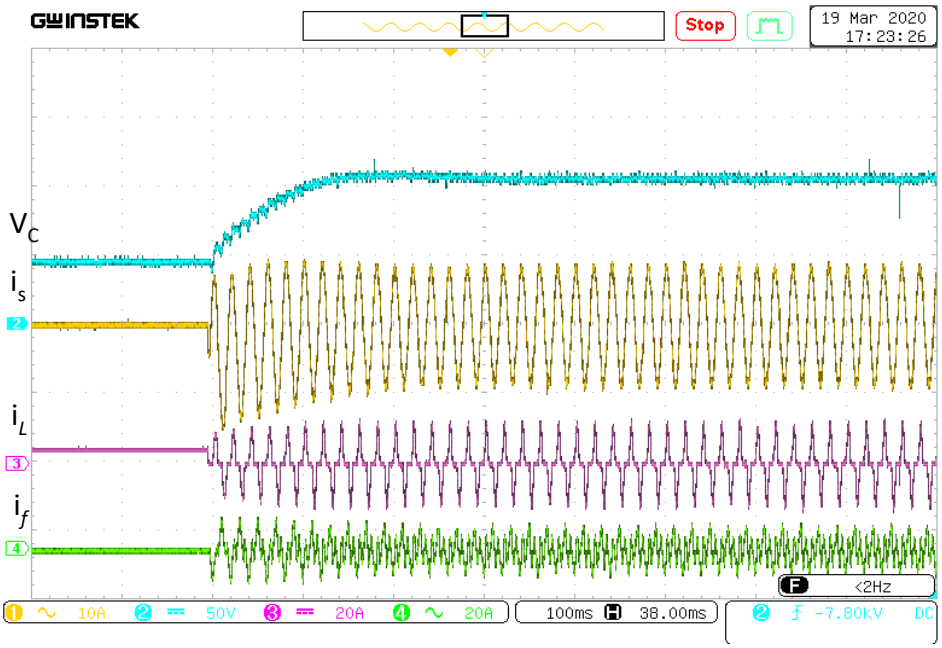

Figure.5.13: Transient response of **SP-SAPF** during increment of DC link voltage from V_C=0V to V_C=110V

Figure. 5.14 shows the steady-state responses of the suggested control law under non-linear RC load. The source current has a nearly perfect waveform sine and in phase with the supply voltage thanks to the filter current. For its part, the load current is presented in steady state by its usual form.

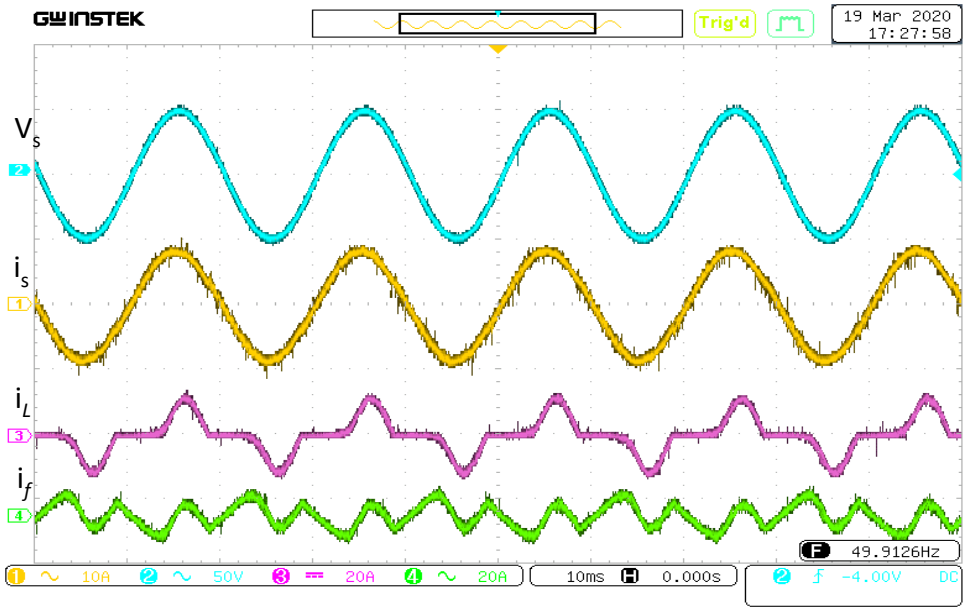

Figure.5.14: Steady-state performance of the proposed control of the **SP-SAPF** under a nonlinear RC load condition

Before connecting and commissioning the **SP-SAPF**, the source current is distorted and its THD is rated at 38% as shown in **Figure 5.15**.

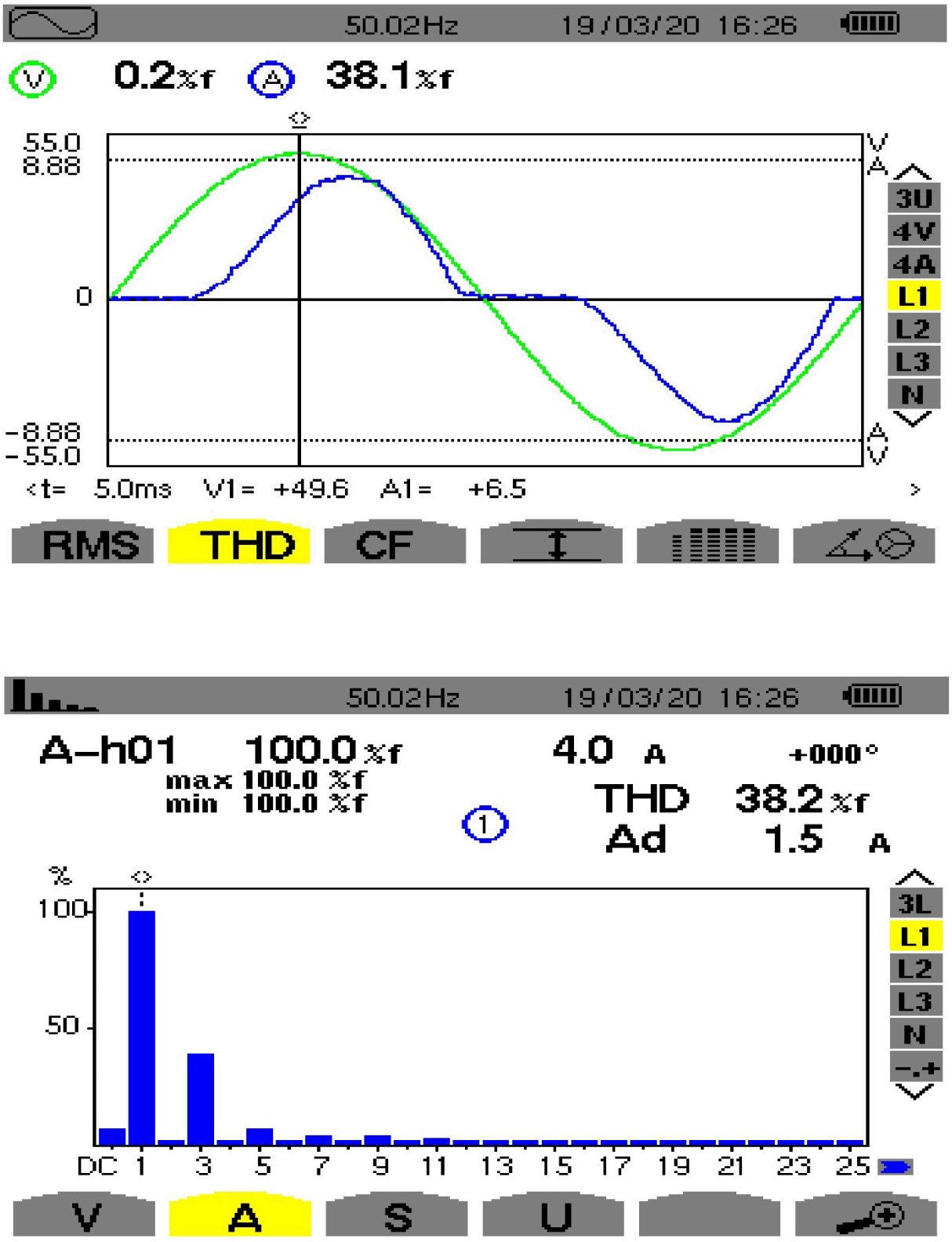

Figure.5.15: Power quality analysis of i_s without **SP-SAPF**

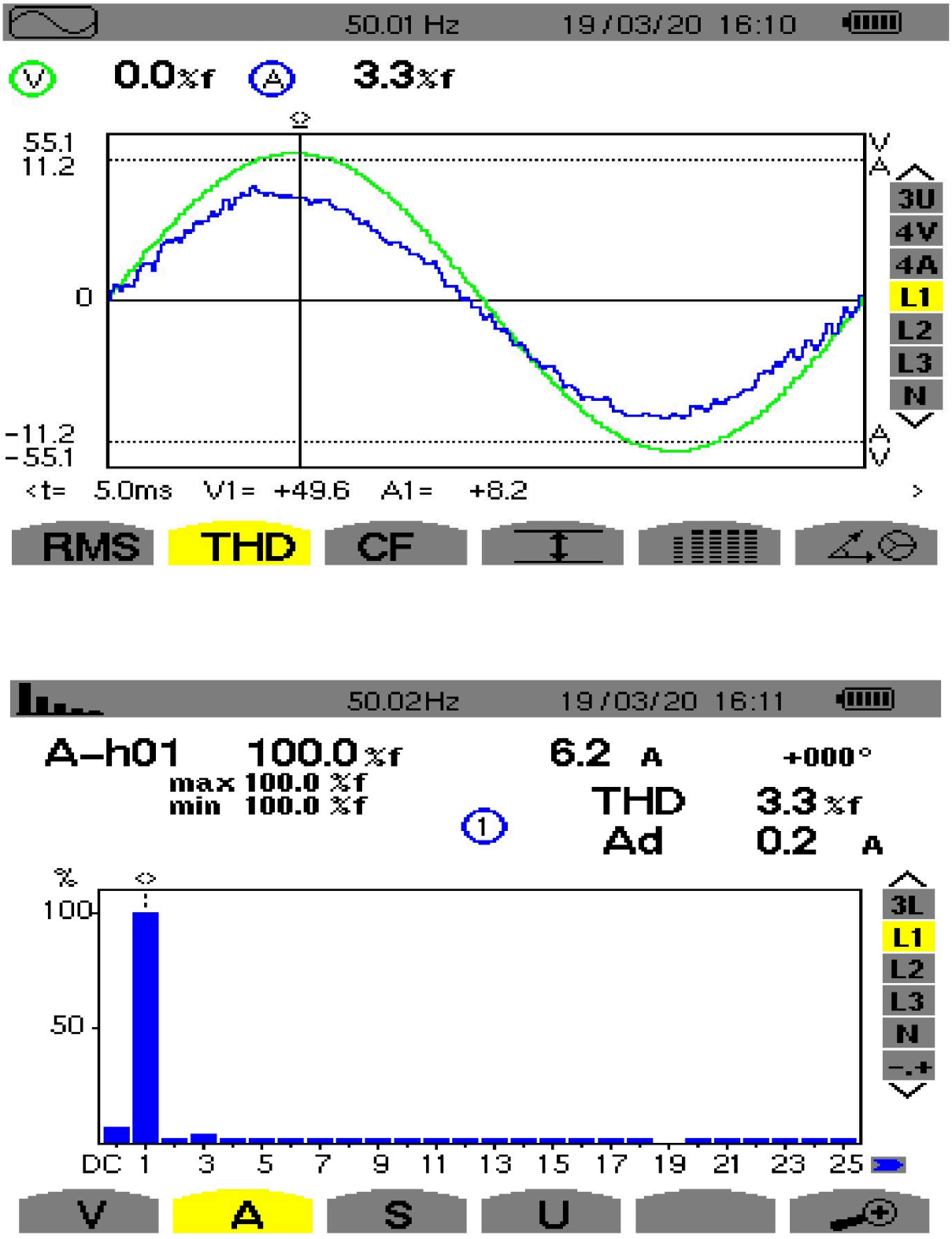

Figure.5.16: Power quality analysis of i_s with **SP-SAPF** controlled by **SC-PSO** strategy

After activation of **SP-SAPF** controlled by the synergistic strategy optimized by **PSO**, the source current has become sinusoidal in phase with the source voltage and its THD is 3.3% as shown in **Figure. 5.16**.

5.4.2 Performance of the SP-SAPF during change in the DC link voltage reference

The variation of the DC link reference voltage for the following values 110V, 140V and 110V was used to verify the performance of the **SP-SAPF** as shown in **Figure. 5.17**. The DC voltage of the filter quickly reaches and easily follows the various imposed references with recording of acceptable overshoots. In addition, the source, load and filter currents maintained their appropriate values during the changes made in the DC link voltage.

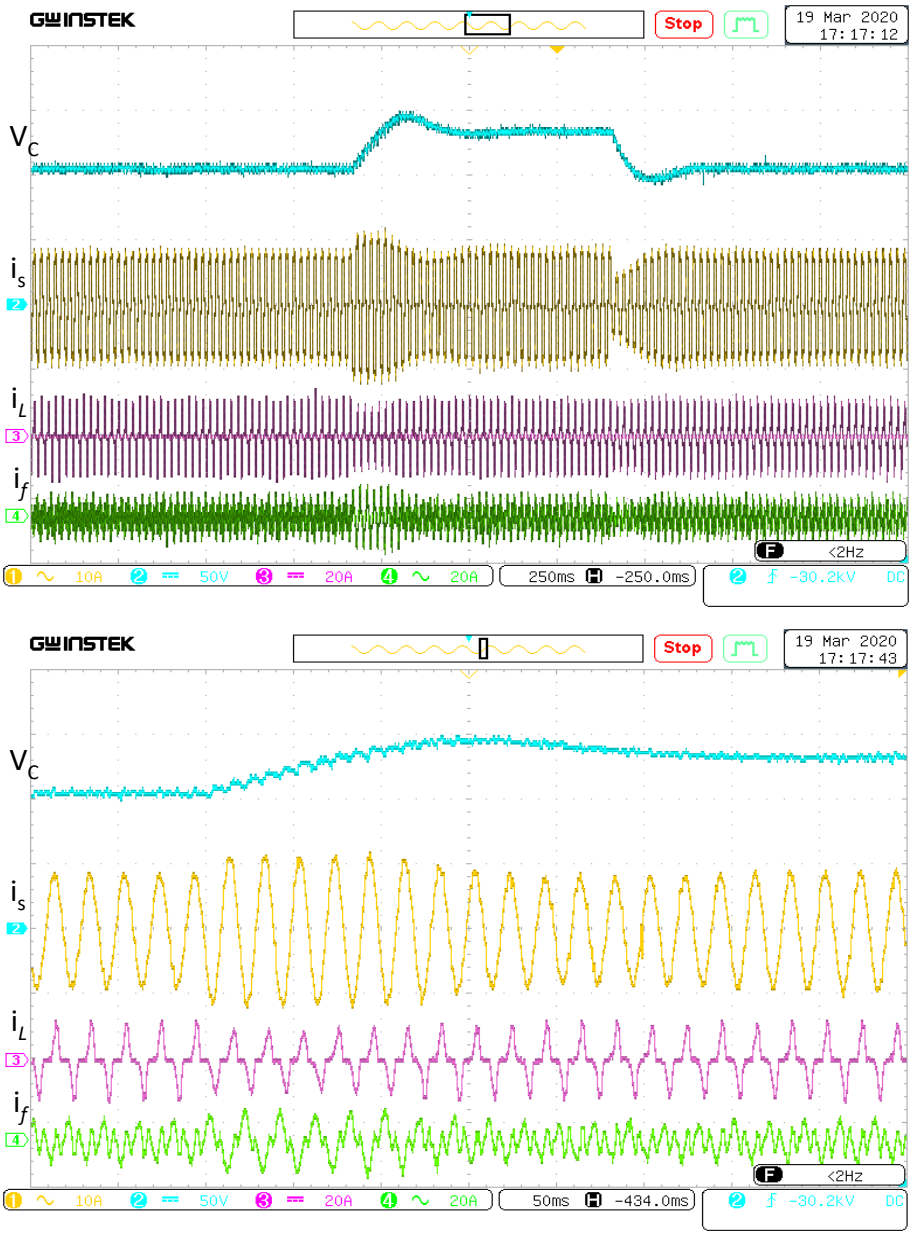

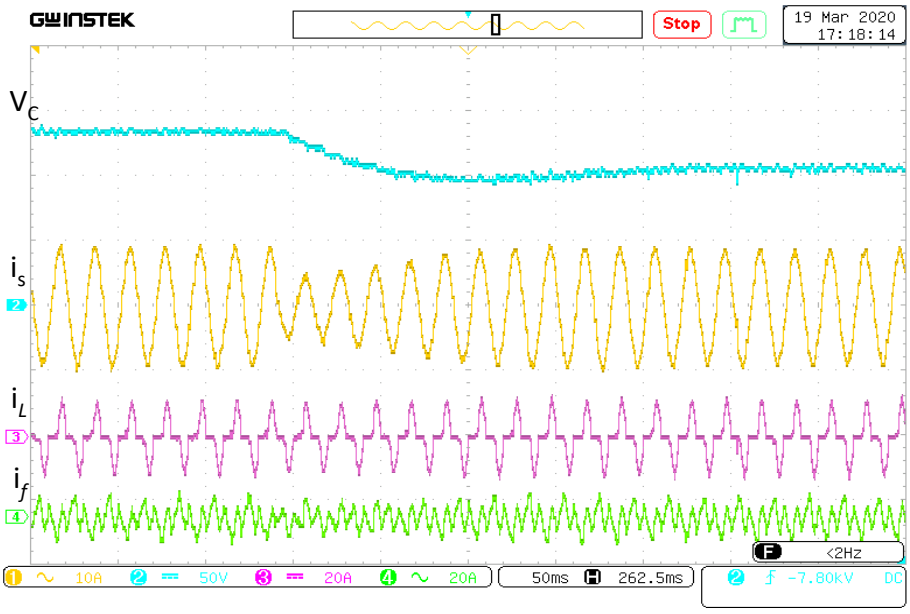

Figure.5.17: Dynamic response of the proposed control of the **SP-SAPF** under the DC voltage reference sudden change from [110V,140V] and inversely.

5.4.3 Performance of the SP-SAPF during change in the nonlinear load

A nonlinear load change is implemented by connecting/disconnecting an additional load in parallel of the old load. The real-time test results are shown in **Figure. 5.18**. Because of step change in nonlinear load, source current increases/decreases smoothly. DC link voltage remains fairly constant and does not experience the variations in nonlinear load. With the exception of certain distortions due to the change in the source current, the DC link voltage is maintained at a constant value of 110 V during the change in the nonlinear load. The load and filter currents react correctly to this established test.

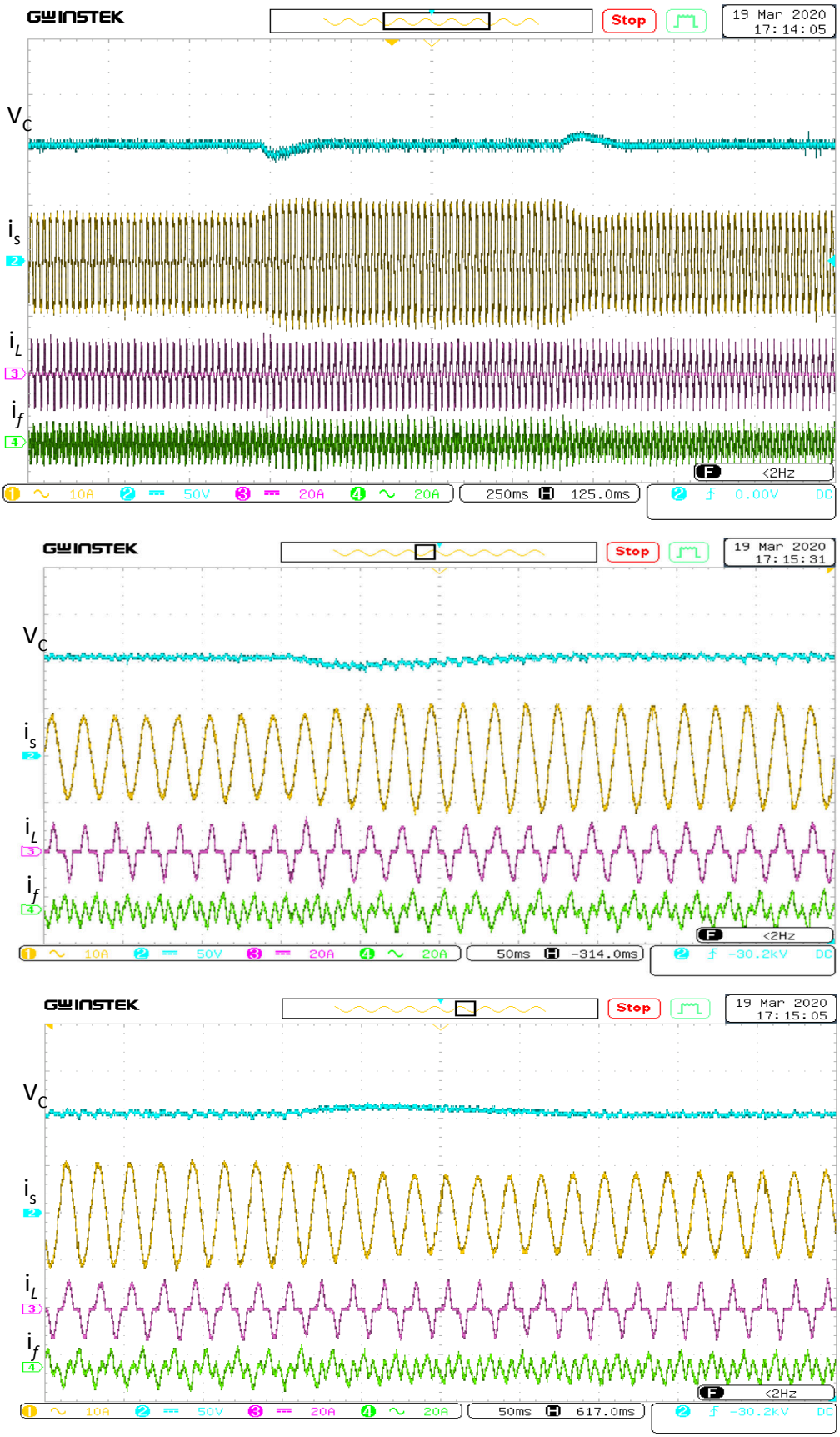

Figure.5.18: Dynamic response of the **SP-SAPF** under a nonlinear load variation

5.4.4 Performance of the SP-SAPF under a polluted power source

In this section, the aim is to prove the robustness of the proposed optimized synergetic control in case of a polluted power source with a THD of 20%. The obtained practical results in steady state of the source, load and filter currents are given in **Figure. 5.19.** Without **SP-SAPF** of the deformed power source, the THD of the measured source current is equal to 47.6% as indicated in **Figure. 5.20**.

In the event that the **SP-SAPF** is activated and the power source is deformed, the saved THD in **Figure. 5.21** of the source current is 5.3%. This experience has proved the ability of **SC-PSO** control law to enhance the shape form current in case of the degraded quality of the power source.

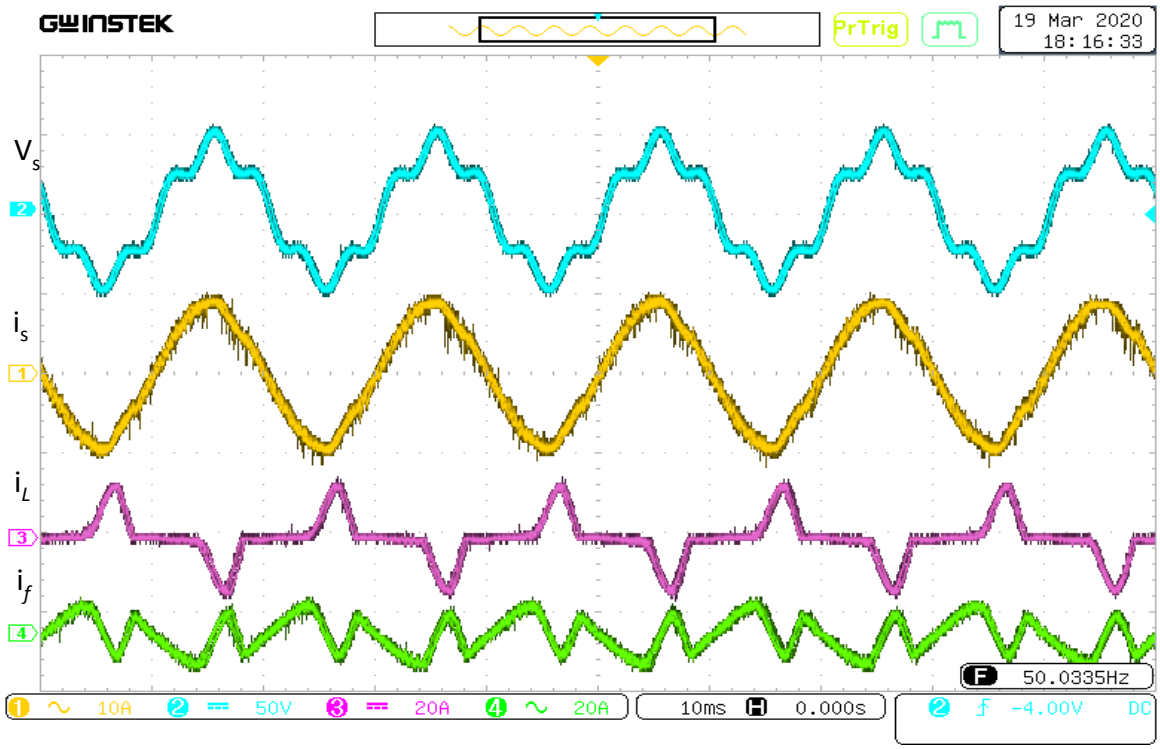

Figure.5.19: Steady-state performance of the proposed control of the **SP-SAPF** under distorted source voltage condition

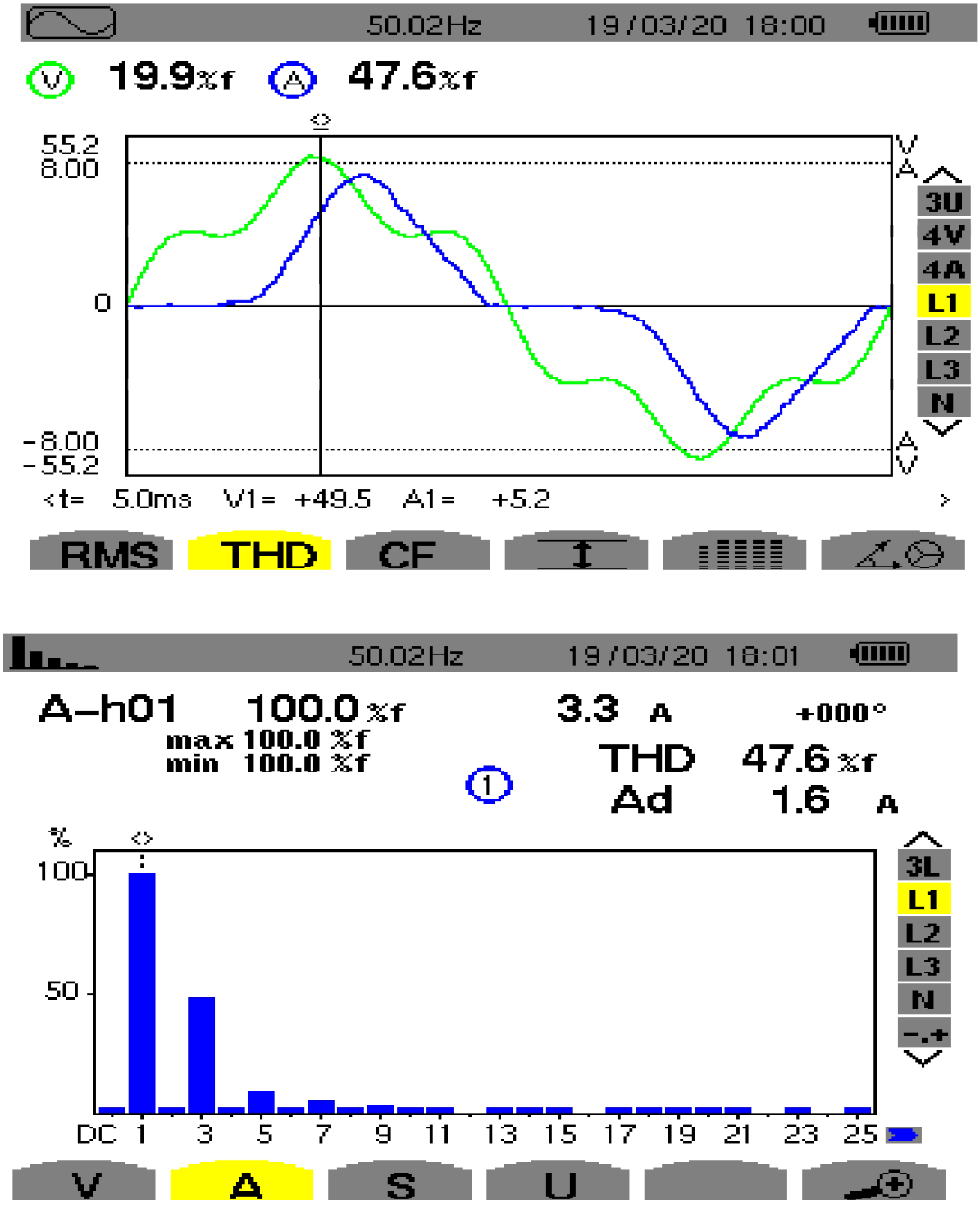

Figure.5.20: THD without **SP-SAPF** under distorted source voltage condition

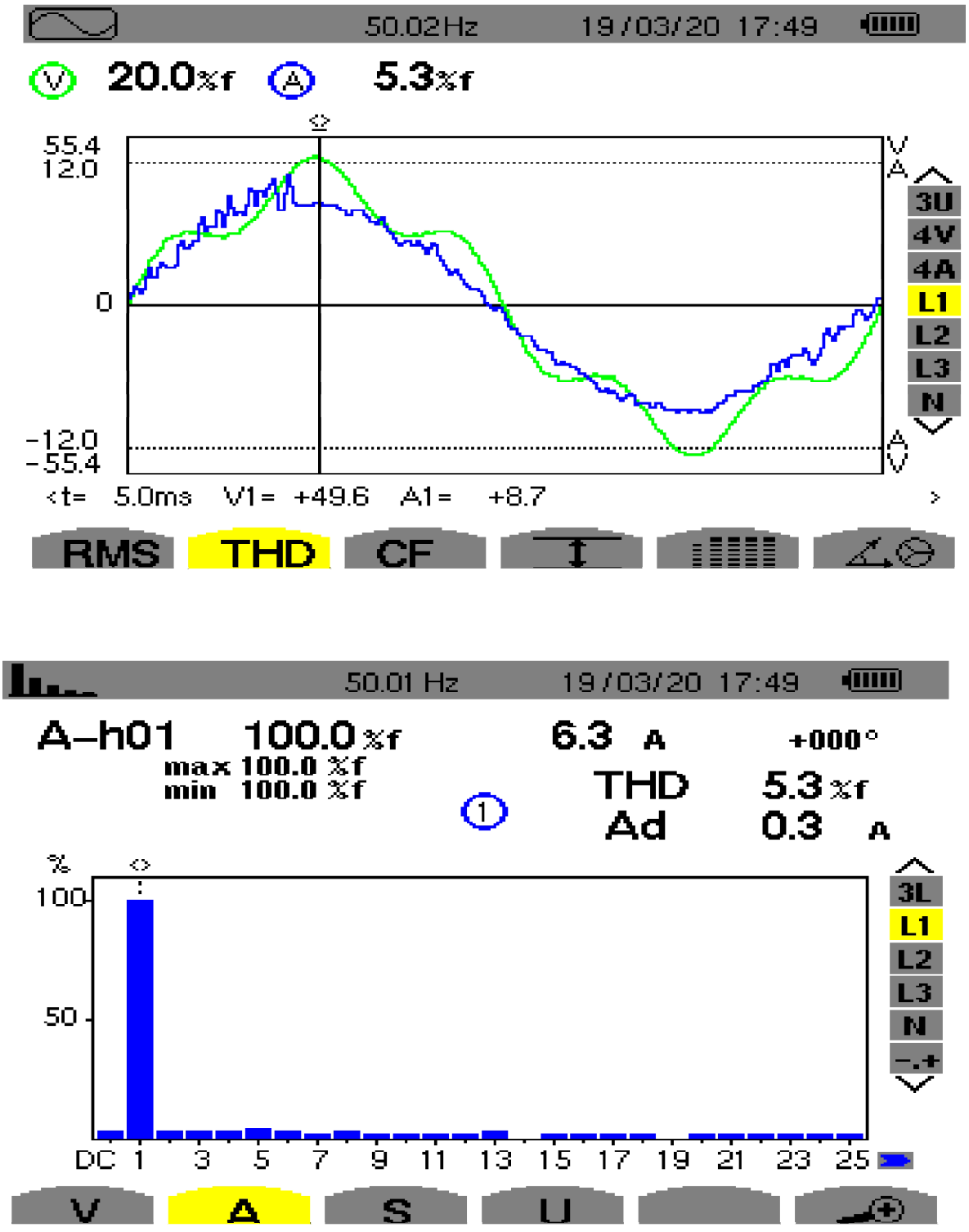

Figure.5.21: THD of i_s with **SP-SAPF** controlled by **SC-PSO** strategy under distorted source voltage condition.

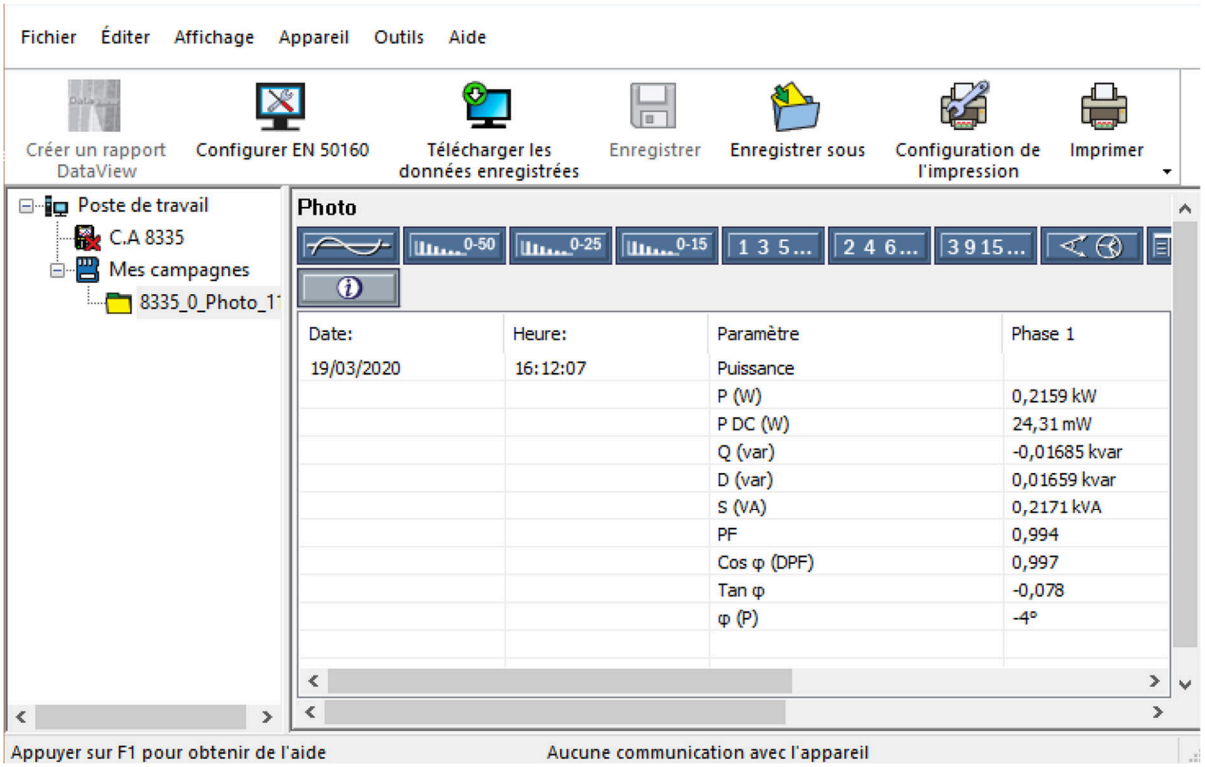

Figure.5.22: Power parameter (CA8335 - Power Quality Analyzer)

5.5 Conclusions

This chapter presents the simulation and experimental validation of the **SP-SAPF** control strategy based on the **SC** technique optimized by the **PSO** algorithm (**SC-PSO)**. The two parameters T and λ which previously were imposed arbitrarily by the designer are this time determined by the **PSO**. The proposed command was able to effectively control the DC bus voltage as well as the current of the single-phase source through the better mastery of the filtering device switches. The evaluation of the optimized synergistic control was performed by **MATLAB/Simulink** software and practically confirmed by the **dSPACE 1104** card.

The simulation in the case of the application of the optimized synergistic technique allowed us to have a better waveform of the source current (THD = 2.35%) compared to the quality of the currents obtained when using the classical hysteresis method (THD = 3.63%) and the non-optimized synergistic control (THD = 2.82%). These simulation

results show the positive impact of the optimized synergistic control on the power quality of the single-phase source feeding the non-linear load.

The feasibility of the command developed was confirmed in practice by the dSPACE 1104 card under different operating modes of the **SP-SAPF** affecting the DC link voltage reference, the non-linear load and the quality of the single-phase electrical network. The optimized synergistic control has confirmed its success through the obtained practical results. The recorded source current is sinusoidal and in phase with the input voltage with a THD of 3.3% for an unpolluted voltage source. In the case of a polluted voltage source, a source current THD of 5.3% is saved. These practical results largely meet the international standard of the IEEE.

Finally, the strategy of optimized synergistic control applied to the single-phase filtering system can effectively contribute to improve the power quality in the tertiary sector.

References:

[82] S. Biricik, S. Redif, O. C. Ozerdem and M. Basu, "Control of the shunt Active Power Filter under non-ideal grid voltage and unbalanced load conditions," Power Engineering Conference (UPEC), 2013 48th International Universities, Dublin, Ireland, 2013, pp. 1-5.
[83] S. Biricik, S. Redif, Ö C. Ozerdem, S. K. Khadem and M. Basu, "Real-time control of shunt active power filter under distorted grid voltage and unbalanced load condition using self-tuning filter," IET Power Electronics, vol. 7, no. 7, pp. 1895-1905, July 2014.
[84] Ghamri, A., M. T. Benchouia, and A. Golea. "Sliding-mode control based three-phase shunt active power filter: Simulation and experimentation." Electric Power Components and Systems 40.4 (2012): 383-398.
[85] Afghoul, H., Krim, F., Chikouche, D., & Beddar, A. (2015). Design and real time implementation of fuzzy switched controller for single phase active power filter. ISA Transactions, 58, 614–621.
[86]Aissa, O., Moulahoum, S., Colak, I., Babes, B., & Kabache, N. (2017). Analysis and experimental evaluation of shunt active power filter for power quality improvement based on predictive direct power control. Environmental Science and Pollution Research, 25(25), 24548–24560.
[87] Zerroug, N., Harmas, M. N., Benaggoune, S., Bouchama, Z., & Zehar, K. (2018). DSP-based implementation of fast terminal synergetic control for a DC–DC Buck converter. Journal of the Franklin Institute, 355(5), 2329–2343.
[88] Ouchen, S., Gaubert, J.-P., Steinhart, H., & Betka, A. (2019). Energy quality improvement of three-phase shunt active power filter under different voltage conditions based on predictive direct power control with disturbance rejection principle. Mathematics and Computers in Simulation, 158, 506–519.

General Conclusion and Future Works

6.1. General Conclusion:

Classical control laws perform well for linear systems with fixed parameters. However, in contrast to complex and nonlinear systems, the results of these controllers can be unsatisfactory because they are not robust. It is necessary to require control laws that are insensitive to parameter changes for disturbances and uncertainties. Therefore, non-linear controllers were found to overcome these obstacles.

In this dissertation, a novel and advanced approach based on incorporating **A**rtificial **I**ntelligence (**AI**) for adjusting control parameters is proposed, in order to improve the stability and robustness against disturbances and uncertainties. This non-linear approach is a **S**ynergetic **C**ontrol (**SC**) based on **P**article **S**warm **O**ptimization (**SC-PSO**) technique. This strategy has been adopted in order to get efficient control even though the under-actuation property is still present. The **SC-PSO** technique is chosen due to its useful advantages, i.e., it guarantees robustness versus parameter fluctuations, model uncertainties, and random external disturbances. To ensure the robustness of the controller, the proposed approach was experimentally tested on two different industrial systems an **U**nmanned **A**erial **V**ehicle (**UAV**) Quadrotor and **S**ingle-**P**hase **S**hunt **A**ctive **P**ower **F**ilter (**SP-SAPF**). We addressed the control problems for the steering of a quadrotor to achieve the desired position and attitude in the first part, and solve the disturbance in power quality especially harmonics using SP-SAPF in the second part.

As illustrated in the second chapter the mathematical model of the quadrotor system is complex with a Six-**D**egree-**O**f-**F**reedom (6-**DOF**) and its dynamics are under-actuated, this model allows us to perform simulations and study the behavior of the vehicle by applying control approaches.

In the third chapter, the autopilot design method for full quadrotor control was clarified, which consists of 6 different control units, each unit contains a controller. On the other hand, the **PID** and **SMC** controllers were used to compare it with the proposed **SC-PSO** controller in the vertical takeoff and landing trajectory tracking cases using MATLAB/Simulink® environment.

The major advantage performances of the suggested **SC-PSO** approach compared to PID and SMC techniques respectively are: zero overshoot and omitting chattering. Also, the following criterion: dynamic response (Rise time, settling time) and steady state error are improved by **SC-PSO**. Then, these performances are experimentally validated in Real-Time testing method **HIL** under various scenarios.

In the fourth chapter, we have presented the state of the art of several traditional and modern devices in order to solve the power quality problems. Moreover, the advantages and disadvantages are illustrated for the several filtering devices (passive, active, and hybrid). The shunt filter is one of the most useful active filtering devices, and it is the best solution which could possible to compensate for the disturbances.

In the fifth chapter, the **HC, SMC** and **SC** controllers are used in order to demonstrate the robust performances of the approaches **SC-PSO**. The comparative study have been applied for the **SP-SAPF** under hard work conditions and different scenarios in transient and steady states. The experimental results prove the superiority of the **SC-PSO** versus others controllers in terms: power quality (**IEEE 519 standard,** respecting **THD<5%**).

Since the use of the proposed **SC-PSO** algorithm gave very high performance for quadrotor systems, for that this type of algorithm was adapted for the first time (**original contribution**) to control Shunt Active Power Filter based Single phase.

We conclude from this thesis that the controller **SC** supported by artificial intelligence (**AI**) Performs significantly and robust better than conventional controllers regardless the type of industrial system (robots, power electronics).

6.2. Perspectives and Future works

The following future research works are suggested as an extension to the knowledge presented in this dissertation:

- This thesis validates the control performance of quadrotor system on a test bench with **HIL**. True experimental validation and integration in real quadrotor system is still required.
- Investigation of quadrotor system behavior under the faults effects. The extension of proposed control design for quadrotor system to the application fault-tolerant control designs will be considered for future.
- The adaptive-fuzzy controller can be also applied on DC-Bus voltage regulation of **SAPF** for reducing the voltage fluctuations and losses and improving the quality of the source current.
- For the developed controllers, a more detailed study of robustness and stability would be interesting to guarantee the theoretical global stability.
- Beside the proposed **PSO** algorithm, other evolutionary optimization methods can be used for further investigation.
- The synergetic control approach presented in this thesis can be extended to a specific application for solution of complex problems of control of nonlinear systems: flying apparatus, turbo-generators, robots, electric drives, magnetic levitation systems etc.
- The proposed idea of **s**ingle-**p**hase **SAPF** can be implemented in three-phase SAPF and the features of the proposed topology can be analyzed for high power applications.
- For the **SAPF** system, the next step should consider how to integrate the renewable energy sources (wind turbine and photovoltaic generator, fuel cell etc) for the purpose of increasing the reliability of the SAPF system.

ملخص:
لهدف الرئيسي من هذه الأطروحة هو تصميم وحدة تحكم جديدة قوية تعتمد على الذكاء الاصطناعي لتحسين استقرار ومتانة النظام ضد الاضطراب وعدم اليقين المطابقين. يتم تقديم SC-PSO التحكم التآزري (SC) استنادًا على خوارزمية تحسين حشد الجسيمات (PSO) لضمان متانة الأنظمة الصناعية. تم استغلال تقنية PSO لضبط معلماتSC.
تم استخدام وحدة التحكم الجديدة هذه لأول مرة للتحكم في النظامين التاليين: أحدهما هو مركبة جوية بدون طيار (UAV) رباعية الحركة بها ست درجات من الحرية-6) (DOFوتحتاج إلى ستة وحدات تحكم للتحكم الكامل، الثاني هو مرشح الطاقة النشط التحويلة أحادي الطور.(SP-SAPF)
على الرغم من أن هذا النهج المقترح SC-PSO لم يتم تطبيقه مسبقًا على المحرك الرباعي وSP-SAPF ، إلا أنه أظهر خصائص قوية جيدة مشابهة لنظرية التحكم في الوضع الانزلاقي (SMC) وبدون إدخال تأثير الثرثرة المستقر الذي يمكن أن يسبب التآكل والتمزق في نظام التشغيل، وهاذا يعطيها ميزة كبيرة على المتحكمات التقليدية [المشتق التكاملي النسبي (PID) ، جهاز التحكم في التباطؤ (HC أو HY)، SMC] .
تتكون الأطروحة بشكل أساسي من جزأين:
1 (في القسم الأول، باستخدام بيئة MATLAB / Simulink® , تم اقتراح دراسة مقارنة تعتمد على ثلاث تقنيات تحكم PID و SMC و SC-PSO ، لتوضيح سلوكيات وحدات التحكم تحت ظروف عمل شاقة. توضح النتائج التي تم الحصول عليها الأداء العالي (تتبع المسار) للرباعي بناءً على وحدة التحكم SC-PSO في حالات عابرة وثابتة، تم استخدام طريقة اختبار الوقت الفعلي للأجهزة داخل الحلقة (HIL) لإثبات نتائج التقنية المقترحة .SC- PSO تم إثبات الاختبار بواسطة جهازي كمبيوتر (بيئة MATLAB /Simulink®) وواثنين من بطاقات dSPACE 1104 للعديد من ظروف التشغيل.
2) في القسم الثاني، دراسة مقارنة تستند إلى وحدات تحكم HC وSMC وSC لإثبات الأداء المتميز (٪5> THD) لـ SC-PSO لمرشح الطاقة النشط أحادي الطور (التحكم الحالي). تم إثبات فعالية نهج SC-PSO المقترح من خلال المحاكاة وأخيرًا تم تنفيذ الاختبارات التجريبية في الوقت الفعلي بنجاح باستخدام الكمبيوتر (بيئة MATLAB / Simulink®) وبطاقة dSPACE 1104 والعناصر الكهربائية للعديد من ظروف التشغيل.
كلمات مفتاحية: لتحكم في الوضع الانزلاقي، التحكم التآزري (SC)، تحسين حشد الجسيمات (PSO) ، المحرك الرباعي لمركبة جوية بدون طيار (UAV) ، مرشح الطاقة النشط التحويلي أحادي الطور (SP-SAPF) ، وحدة التحكم في التخلف (HC).

Abstract:
The main objective of this thesis is to design a novel robust controller based on Artificial intelligence to improve the stability and robustness of system against matching disturbation and uncertainties. **SC-PSO** a **S**ynergetic **C**ontrol (**SC**) based on Particle Swarm Optimization (PSO) algorithme is being presented to ensure the robustness of industrial systems. The **PSO** technique has been exploited to adjust the **SC** parameters. This novel controller has been used for the first time to control the following two systems: one an **U**nmanned **A**erial **V**ehicle (**UAV**) Quadrotor which has a Six-**D**egree-**O**f-**F**reedom (6-**DOF**) and need six controllers for full control, the second is the **S**ingle-**P**hase **S**hunt **A**ctive **P**ower **F**ilter (**SP-SAPF**).
Although this proposed **SC-PSO** approach has not been previously applied for the quadrotor and the **SP-SAPF**, but it showed good robust characteristics similar to **S**liding **M**ode **C**ontrol (**SMC**) theory and without introducing steady state chattering effect which can cause wear and tear in actuating system, giving a significant advantage over conventional controller [**P**roportional **I**ntegrative **D**erivative (**PID**), **Hy**steresis **C**ontroller (**HC** or **HY**), **SMC**]
This thesis apparatus consists essentially of two parts:
1) In section one, using MATLAB/Simulink® environment; a comparative study based on three control techniques: PID, SMC and SC-PSO, is proposed to illustrate the behaviors of the controllers against work hard conditions. The obtained results demonstrate the high performances (trajectory tracking) of the quadrotor based on the **SC-PSO** controller in transient and steady states, a **H**ardware-**I**n-the-**L**oop (**HIL**)Real-Time testing method was used to prove results of the proposed technique SC-PSO. The teste has been proved by two **PC (MATLAB/Simulink® environment)** and two **dSPACE 1104 card** for several operating conditions.
2) In the second section, a comparative study based on **HC**, **SMC** and **SC** controllers to demonstrate the outstanding performance (THD<5%) of **SC-PSO** for single-phase active power filter (current control). The effectiveness of the suggested SC-PSO approach has been proved by simulation and finally real time experimental tests executed successfully using **PC (MATLAB/Simulink® environment)**, **dSPACE 1104 card** and electrical elements for several operating conditions.
Keywords: Sliding Mode Control, Synergetic Control (SC), Particle Swarm Optimization (PSO), Unmanned Aerial Vehicle (UAV) Quadrotor , Single-Phase Shunt Active Power Filter (SP-SAPF), Hysteresis Controller (HC).

Résumé:
L'objectif principal de cette thèse est de concevoir un nouveau contrôleur robuste basé sur l'intelligence artificielle pour améliorer la stabilité et la robustesse du système contre les perturbations et les incertitudes correspondantes. SC-PSO une commande Synergetique (SC) basé sur l'algorithme L'optimisation par essaims particulaires est présenté pour assurer la robustesse des systèmes industriels. La technique PSO a été exploitée pour ajuster les paramètres SC.
Ce nouveau contrôleur a été utilisé pour la première fois pour contrôler les deux systèmes suivants : un quadrirotor de véhicule aérien sans pilote (UAV) doté d'un six degrés de liberté (6-DOF) et nécessitant six contrôleurs pour un contrôle total, le le deuxième est le filtre de puissance active shunt monophasé (SP-SAPF).
Bien que cette approche SC-PSO proposée n'ait pas été appliquée auparavant pour le quadrirotor et le SP-SAPF, elle a montré de bonnes caractéristiques robustes similaires à la théorie du contrôle en mode glissant (SMC) et sans introduire d'effet de broutage en régime permanent qui peut provoquer une usure système d'actionnement, donnant un avantage significatif par rapport au contrôleur conventionnel [Proportionnel Intégratif Dérivé (PID), Contrôleur d'Hystérésis (HC ou HY), SMC]
Ce dispositif de thèse se compose essentiellement de deux parties :
1) Dans la première section, en utilisant l'environnement MATLAB/Simulink® ; une étude comparative basée sur trois techniques de contrôle : PID, SMC et SC-PSO, est proposée pour illustrer les comportements des contrôleurs face aux conditions de travail intensif. Les résultats obtenus démontrent les hautes performances (suivi de trajectoire) du quadrirotor basé sur le contrôleur SC-PSO en régime transitoire et en régime permanent, une méthode de test Hardware-In-the-Loop (HIL)Real-Time a été utilisée pour prouver les résultats de la technique proposée SC- OSP. Le test a été prouvé par deux PC (environnement MATLAB/Simulink®) et deux cartes dSPACE 1104 pour plusieurs conditions de fonctionnement.
2) Dans la deuxième section, une étude comparative basée sur les contrôleurs HC, SMC et SC pour démontrer les performances exceptionnelles (THD <5٪) du SC-PSO pour le filtre de puissance active monophasé (contrôle du courant). L'efficacité de l'approche SC-PSO suggérée a été prouvée par des simulations et enfin des tests expérimentaux en temps réel exécutés avec succès à l'aide d'un PC (environnement MATLAB/Simulink®), d'une carte dSPACE 1104 et d'éléments électriques pour plusieurs conditions de fonctionnement.
Mots-clés: Sliding Mode Control (SMC), Synergetic Control (SC), Particle Swarm Optimization (PSO), Unmanned Aerial Vehicle (UAV) Quadrotor , Single-Phase Shunt Active Power Filter (SP-SAPF), Hysteresis Controller (HC).